# Achieving Drag Reduction Through Polymer-Surfactant Interaction

by

Anosh Mevawalla

A thesis
presented to the University of Waterloo
in fulfillment of the
thesis requirement for the degree of
Master of Applied Science
in
Chemical Engineering

Waterloo, Ontario, Canada, 2013

## Author's Declaration

I hereby declare that I am the sole author of this thesis. This is a true copy of the thesis, including any required final revisions, as accepted by my examiners.

I understand that my thesis may be made electronically available to the public.

# Abstract

Drag reduction is a well-observed phenomenon, it was first observed by the British chemist Toms in 1946, yet its mechanism is still unknown to this day. Polymer Drag reduction has found application in reducing pumping costs for oil pipelines (its use in the Trans Alaska Pipeline has resulted in an increase from 1.44 million bbl./day to 2.1356 million bbl./day), increasing the flow rate in firefighting equipment , and in supporting irrigation and drainage systems. Surfactant drag reducers are used industrially in district heating and cooling systems. Though the fields of Surfactant Drag Reduction and Polymer Drag Reduction are each independently well-developed the effect of their interaction on drag reduction is a less explored phenomenon. Through a well chosen pairing of surfactant and polymer, drag reduction can be maximized while minimizing surfactant and polymer concentrations cutting down on cost and environmental impact.

The focus of this work was to determine if there was any positive interaction between the polymers Polyethylene Oxide (PEO) and Anionic PolyAcrylAmide (PAM) and the surfactant Amphosol CG (Cocamidopropyl Betaine) as well as any interaction between the polymers themselves. Both polymers are popular drag reducers while Amphosol is a practically nontoxic ($LD_{50}$=5g/kg) zwitterionic surfactant and is readily biodegradable. In order to determine if any interaction was present and at what concentration was this most notable 4 techniques were used: Surface tension, Conductivity, Relative Viscosity and Shear Viscosity measurement. From this analysis the polymer Saturation point (PSP), Critical aggregation concentration (CAC) and Critical micelle concentration (CMC) were found as well as the concentrations that optimized the viscosity for the pilot plant runs. The bench scale results were used to pick the optimum concentrations for the polymer surfactant solutions. Pressure readings and flowrate measurements were used to plot the Fanning Friction Factor against the Generalized Reynolds Number for the surfactant polymer mixtures and compared to their pure polymer and surfactant counterparts. The Blasius line was found to hold for water measurements taken and is the base to determine percentage drag reduction. The effect of the presence of amphosol on degradation and overall drag reduction were noted. Other factors considered were pipe diameter and the effect of ionic impurities in the solvent.

# Acknowledgements

# Table of Contents

# List of Figures

# List of Tables

# Chapter 1  Introduction

## 1.1 Brief Overview of Previous Studies on Polymer/Surfactant Interaction

Polymers and surfactants have an expansive range for application and this has lead to a great deal of research effort in the field of characterizing polymer and surfactant solutions. Polymer solubility plays an important role in the solution's rheology and is determined by factors such as temperature, polarity, molecular weight, cross-linking, branching and crystallinity. Solubility tends to decrease with increasing molecular weight and high cross-linking. Highly cross linked polymers inhibit the solvent molecules from interacting with the polymer chains. Polymers tend to increase in solubility with an increase in branching although the rate of solubility depends on the type of branching. We note that long branched polymers entangle with one another which negatively impacts solvent penetration and slows down dissolution. Surfactant solutions rheology is primarily affected by surfactant aggregation. Surfactant aggregation is affected by factors such as length of the hydrocarbon chain, number of branched chains, temperature, head group area, presence of counter ions or oppositely charged surfactant, head group charge and the type of solvent.

The way in which pure polymer and pure surfactant affect solution rheology is exceedingly complex and polymer/surfactant mixtures posses just as much complexity. The two general interactions that occur between polymer and surfactant are hydrophobic interaction and electrostatic interaction which occurs between charged ionic polymers and surfactants. Factors that influence polymer/surfactant interaction include polymer charge density, backbone rigidity, surfactant chain length, concentrations of polymer and surfactant (Trabelsi, Raspaud et al. 2007).

## 1.2 Polymers

A polymer is a large macromolecule made up of smaller units known as monomers. For example the polymer polyethylene oxide is made up of ethylene oxide monomers and polyacrylamide is made up of acryl amide monomers.

| Polyethylene oxide | Polyacrylamide |
|---|---|
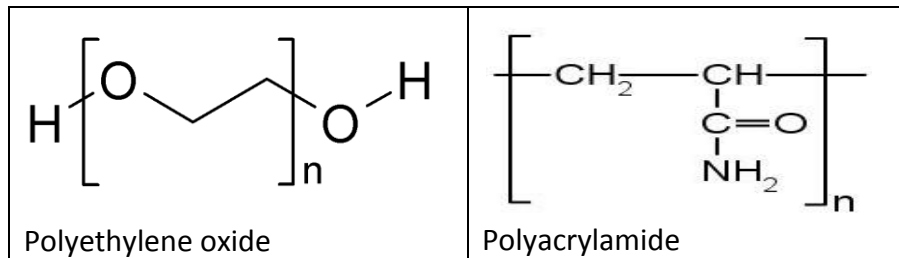
Table 1.1 Monomers for Polyethylene oxide and Polyacrylamide respectively
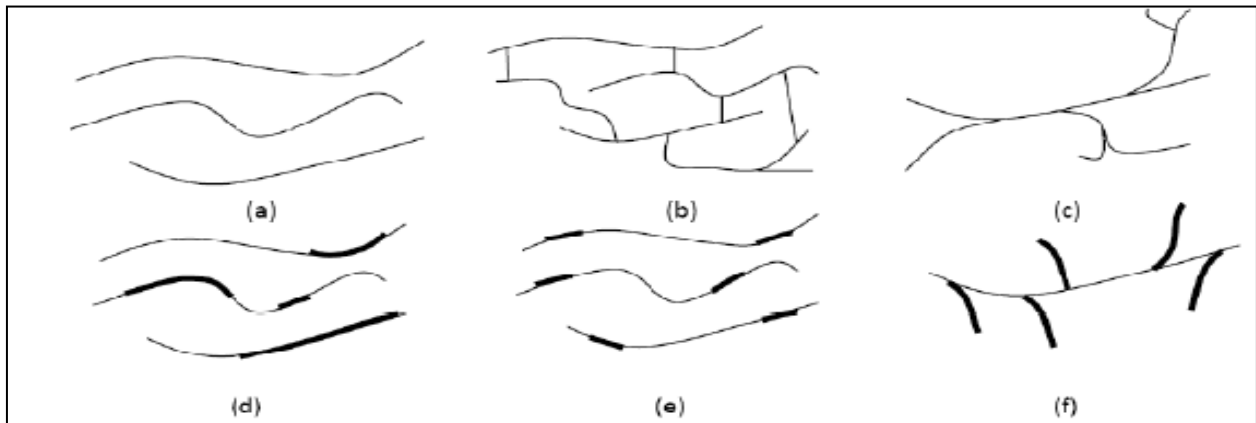


Figure 1.1 (a) Linear (b) Crosslinked (c) Branched polymers (d)Randomly Distributed (e) Block (f) Grafted Copolymers

Polymers can be linear, branched or cross-linked. Polymers can contain more than one type of monomer in which case they are known as copolymers. The distribution of the monomers determines whether they are categorized as either grafted or block copolymer.

Polymers can be nonionic (PEO), anionic (polyacrylic acid) or cationic (polyquaterniums).

The polymer configuration in solution heavily influences its rheology. Polymer conformation depends on the interaction of the monomer blocks with each other and with the solvent. Conformations range from random coil, extended configuration or a helix. Expanded polymers lead to an increase in viscosity. The solution viscosity also depends on the type of polymer, the charge density for ionic polymers, the molecular weight and the polymer concentration.

## 1.3 Surfactants

Surfactants possess hydrophobic tails and hydrophilic heads in one molecule and are thus amphiphilic compounds. Surfactants lower the free energy of the phase boundary by adsorbing at the surface. For a 2D system the fundamental equations pressure-volume term is replaced with a surface tension-interfacial area term and is show below:

$$dU = TdS + \gamma dA + \sum \mu_i dN_i \qquad \text{1.1}$$

Where U is the internal energy of the system, T is the bulk temperature, $\gamma$ is the surface tension, A is the interfacial area, $\mu_i$ is the chemical potential of component i, and $N_i$ is the number of moles of component i. The $\gamma dA$ term thus represents the work done in generating an interfacial area increment dA and the Gibbs Free energy of a surface at constant temperature and pressure is given by:

$$dG = \gamma dA + \sum \mu_i dN_i \qquad \text{1.2}$$

where G is the Gibbs free energy. Two ways to minimize the Gibbs free energy are by decreasing the surface area for example by forming a sphere or by decreasing the surface tension ($\gamma$) accomplished by changing the surface concentration. Both these phenomenon occur with surfactants as discussed below.

The surface tension of water is largely reduced when surfactant is added. Surface tension falls with surfactant addition till the surfactant molecules begin to form micelles in bulk solution; this point is known as the critical micelle concentration (CMC).
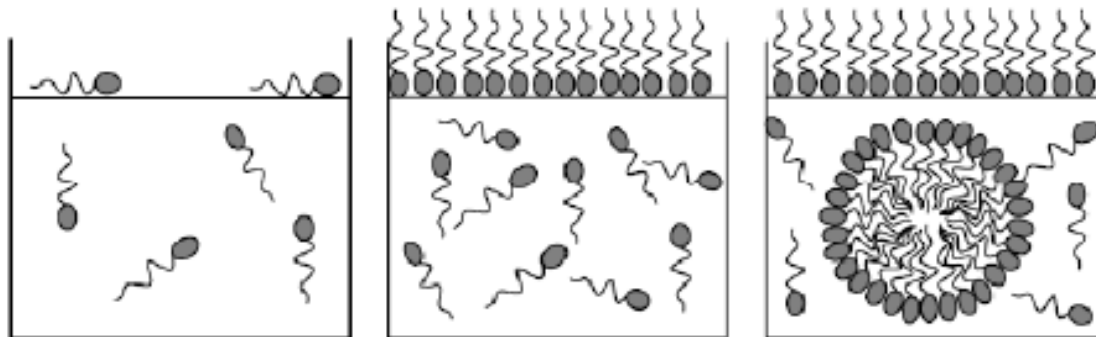


Figure 1.2 Shows Surfactant solutions with concentrations below the CMC, at the onset of the CMC and above the CMC

Surfactants consist of two parts one soluble in solvent and one insoluble in solvent. Typically the surfactant contains a hydrophobic tail of 8-18 carbon atoms of linear alkyl which may be branched. Physiochemical properties depend on the degree of branching, polar group position, length of alkyl chain, ionic charge of polar group and size of the head group.

Surfactants can be classified as

- Nonionic
- Cationic
- Anionic
- Zwitterionic

## 1.4 Applications

Polymers and surfactants are used in a wide variety of products and industries including cosmetics, paints, detergents, foods, polymer synthesis, formulation of drugs and pesticides, enhanced oil recovery, waste water treatment, firefighting and in heating and cooling loops.

## 1.5 Drag Reduction

Polymers and surfactants reduce the wall friction in turbulent pipe flow and this allows us to increase the pumping capacity or to decrease the power required. Comparison table between surfactants and polymers is presented below:

| Polymers | Surfactants |
|---|---|
| Polymers start showing drag reduction at very low concentrations and have no minimum concentration requirement | Surfactant concentration must be high enough to produce large rod-like micelles |
| Not significantly affected by temperature | Drag Reduction only occurs in a specific temperature range as micelle formation is sensitive to the temperature |
| Mechanical degradation of polymer is permanent , high shear zones leads to irreversible polymer chain scission | Mechanical degradation of surfactant is temporary, micelles break apart in high shear zones and reassemble below the critical shear stress |

Table 1.2 Comparison table between polymer drag reduction and surfactant drag reduction

Through the appropriate combination of polymer and surfactant one can produce a mixture with improved long-term stability, larger effective temperature range and larger effective Reynolds number range.

## 1.5.1 Polymer Drag Reduction

Adding long chain flexible polymer at very low concentration in the ppm range can lead to up to 80% drag reduction. It is widely believed that drag reduction in the presence of polymer is caused by the suppression of both eddy growth and eddy formation. Harder and Tiederman 1991 and Wei and Willmarth 1992 have shown that in the presence of polymer the turbulent energy production is decreased. The energy in the stream-wise (parallel to flow) velocity component is increased while the energy in the span-wise velocity fluctuation (normal to

flow) is decreased Willmarth 1992. The overall turbulent energy production decrease can be attributed to polymers changing the pressure-strain correlation or polymers essentially changing the energy budget through the introduction of non-newtonian terms such as in the stress balance.

### 1.5.2 Surfactant Drag Reduction

At concentrations sufficiently higher than the CMC surfactant molecules form worm like structures in turbulent flow. Worm-like micellar structures are crucial for drag reduction in turbulent flow. Small angle neutron scattering of surfactant induced drag reducing solution reveals anisotropic conditions where rodlike micelles align and orient themselves parallel to the direction of flow above the critical shear stress. Below the critical shear stress we observe freely rotating micelles with no ordered orientation (Bewersdorff 1986).

## 1.6 Research Objectives

The objectives of this paper were to determine if any interaction exists between the combinations Amphosol/PEO, Amphosol/PAM and PEO/PAM as well as the effect of this interaction on drag reduction and degradation. Other factors considered were the effect of pipe diameter and the presence of counterions for the case of anionic PAM.

To achieve the goal of determining if an interaction takes place in the mixtures, they were analyzed using surface tension, viscosity and conductivity measurements. From this data we determine if any interaction occurs and at what concentrations it is prevalent.

Once the appropriate concentrations of the PAM/Amphosol, PEO/Amphosol and PAM/PEO mixtures were determined they were run through the flow loop. The mass flowrate along with the pressure drop were measured and from this data the drag reduction was calculated and compared to the drag reduction achieved by the pure polymer mixtures in the same setup. The mixtures were compared to find if they were more stable (slower degradation times), had a larger effective Reynolds range, and if they achieved higher levels of drag reduction than the pure polymer solutions.

## 1.7 Outline

In the subsequent chapters the effect of polymer-surfactant interaction on drag reduction is explored further. Chapter 2 is a literature review of relevant papers in fluid flow, polymer drag reduction, surfactant drag reduction and polymer-surfactant interaction. Chapter 3 presents the Experimental procedure carried out in the thesis along with the materials studied. Chapter 4 discusses the interaction between amphosol and PAM and its effect on drag reduction and degradation. In this chapter the effect of ionized water on PAM is also explored. Chapter 5 investigates the interaction between PEO and amphosol and its effect on Drag reduction and degradation. Chapter 6 examines the PAM/PEO mixtures and how varying compositions affect the solutions rheology and drag reducing ability and stability. Finally Chapter 7 presents the main conclusions of the work and recommendations for future experiments.

# Chapter 2   Literature Survey

## 2.1 Polymer Drag Reduction

The frictional drag in pipe or channel turbulent flow can be considerably decreased through the addition of a small amount of polymer; up to 80% drag reduction can be achieved with a few ppm of polymer. Though this phenomenon was first identified in 1946 by British Chemist Toms its exact mechanism is still unknown to this day. 3 common proposed mechanisms are an increase in effective extensional viscosity, an anisotropic effect caused by the extended polymers, and the effect of elasticity introduced by the presence of polymer. Before delving any further we will restate what is known about polymer drag reduction is that the skin friction is reduced which modifies the velocity profile and shear stress distribution in the boundary layer. This affects the nature and formation of the vortices formed resulting in significantly modified near-wall structures in the boundary layer. However, the exact mechanism relating the near-wall structures and the skin friction is still unknown.

Principles of Drag Reduction have been successfully applied to transportation of crude oil in both the Alaska and Norwegian pipelines. Other areas of application include oil well fracturing operations, closed-circuit pumping installations (i.e. central heating systems). Drag Reducing agents can also be used to prevent over flooding of sewage systems in heavy rains, in hydraulic transportation of solid particle suspensions and to increase water output in firefighting and water supply irrigation systems. Drag reducing agents can also be introduced into the blood stream allowing for improved blood circulation and is an innovative way of dealing with cardiovascular disorders. PEO (one of the polymers covered in the thesis) is a blood compatible polymer meaning it can be in the presence of living cells and is a prospective candidate for tissue engineering. Tests on animals have shown beneficial effects on the blood circulation system. However PEO is easily degradable when subjected to high shear. Thus an alternative blood compatible polymer-surfactant drag reducing agent that was more mechanically stable would present greater prospective solutions.

The addition of polymer causes the following changes: The buffer layer is thickened offsetting the logarithmic region, and the slope of the velocity profile in logarithmic region at low Reynolds numbers is also slightly increased. Using direct numerical simulation (DNS) models focused on the high extensional viscosity mechanism shows a small amount of drag reduction but many of the predicted changes in the turbulence structure are not in accordance with experimental measurements. Models that focused on anisotropic effects show significant drag reduction while the turbulent statistic changes are in agreement with laser doppler anemometry (LDA) measurements. Finally numerical simulations focused on solution

elasticity show less drag reduction compared to the anisotropic model and the mean velocity profile produced differs from experimental profiles. Thus the key property for polymer drag reduction appears to be the viscous anisotropic stress introduced by extended polymers.

### 2.1.1 Turbulence:

Turbulence is a fluctuating chaotic state of fluid motion where nonlinear inertial effects overwhelm viscous effects. The nonlinear equations governing turbulent flow are difficult to analyze; and because of this turbulence is usually studied from a statistical view point. Through the use of visualization techniques large scale organized structures known as coherent structures have been discovered in turbulence flows. These coherent structures are thought to play a significant role in turbulence dynamics. Direct Numerical Simulation (DNS) is based on numerically solving the nonlinear equations and allows us to obtain information that is difficult or impossible to obtain experimentally (information such as high order statistics near the wall). It should be noted that DNS requires a large computational effort and as such is limited to simple flows and low Reynolds numbers.

### 2.1.2 Rheology:

Rheology is the study of non-newtonian fluids, fluids where the stress is not linearly dependent on the rate of deformation. Typical rheological measurements on polymer solutions are taken using conventional rheometers in which the fluid is subjected to steady flow. Thus they are only valid for weak or slow deformations and not as useful for turbulent flow.

### 2.1.3 Navier Stokes Equation:

The Navier stokes equation describes the motion of fluid substances. It is derived by applying Newton's Second Law to fluid motion and is essentially a force balance. In almost any real situation the Navier Stokes Equations are Nonlinear Partial Differential equations. The general Navier stokes Equation is:

$$\rho \frac{Dv}{Dt} = -\nabla p + \nabla \cdot T + F$$

Or

**2.1**

$$\rho \left( \frac{\partial v}{\partial t} + v \cdot \nabla v \right) = -\nabla p + \nabla \cdot T + F$$

where v is the velocity flow field, $\rho$ is the density, T is the stress tensor, f represents body forces acting on the fluid and $\nabla$ is the del operator. The left side of the equation describes the acceleration while the right side is the summation of body forces. The Navier Stokes Equation deals strictly with the conservation of momentum and usually a statement on the conservation of mass is also needed. The Mass continuity Equation is:

$$\frac{\partial \rho}{\partial t} + \nabla \cdot (\rho v) = 0$$

2.2

For incompressible Newtonian fluids the Navier Stokes equation simplifies to:

$$\rho \frac{Dv}{Dt} = -\nabla p + \mu \nabla^2 v + F$$

2.3

and the continuity equation simplifies to:

$$\nabla \cdot v = 0$$

2.4

Now we will consider dilute polymer solutions where the solvent is Newtonian. Applying the Navier- Stokes from equations 2.1 and 2.4 above we have:

$$\rho \frac{Dv}{Dt} = -\nabla p + \nabla \cdot \tau$$

$$\nabla \cdot v = 0$$

We can split the stress tensor into 2 parts:

$$\tau = \tau_N + \tau_P$$

2.5

where $\tau_N$ is the tensor on the Newtonian fluid and $\tau_P$ is the tensor for the polymer. Thus

$$\rho \frac{Dv}{Dt} = -\nabla p + \mu \nabla^2 v + \nabla \cdot \tau_P$$

2.6

Turbulence can be described by decomposing quantities into a mean and fluctuating part. The average used is the ensemble average denoted by <…>:

9

$$v = \langle v \rangle + v' = V + v' \qquad \text{2.7}$$
$$p = \langle p \rangle + p' = P + p' \qquad \text{2.8}$$
$$\tau_P = \langle \tau_P \rangle + \tau_P' = \mathrm{T_P} + \tau_P' \qquad \text{2.9}$$

and the relevant equations become:

$$\nabla \cdot v = 0 \qquad \text{2.10}$$
$$\rho\left(\frac{\partial V}{\partial t} + V \cdot \nabla V + \nabla \cdot \langle v'v' \rangle\right) = -\nabla P + \mu \nabla^2 V + \nabla \cdot \mathrm{T_P} \qquad \text{2.11}$$

## 2.1.4 Factors affecting Polymer Drag Reduction

At low Reynolds number where the viscous forces dominate over the inertial ones the presence of a small amount of polymer has no effect on the flow as it does not affect the shear viscosity. Thus the Hagen-Poiseuille equation is valid and describes fluid flow. After the transition to turbulence dilute amounts of polymer additive does affect the flow, and flow will not necessarily follow the Blasius or Von Karman lines. It has been observed on occasion that polymer solutions follow the Blasius equation up to a certain drag reduction onset Reynolds number past which the friction factor is lower than that of the solvent. Drag reduction is affected by many parameters such as polymer concentration, type of solvent, type of polymer (polymer flexibility, molecular weight, chemical composition) and pipe diameter. Qualitatively drag reduction is seen to increase with increasing molecular weight, polymer concentration, polymer chain flexibility, flow rate and with decreasing pipe diameter. This is especially true for small pipe diameters with the diameter effect being negligible at larger diameters. Experimentally it was found that an asymptote for maximum polymer drag reduction exists (VIRK, MERRILL et al. 1967) and is known as Virks asymptote:

$$\frac{1}{\sqrt{f}} = 19.0 log\left(Re\sqrt{f}\right) - 32.4 \qquad \text{2.12}$$

This asymptote is both polymer and pipe independent.
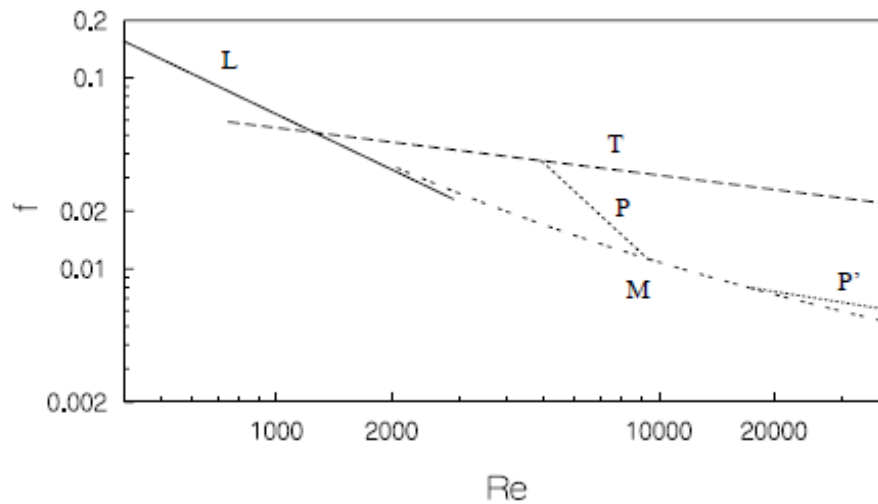
Figure 2.1 Possible Transitions from Laminar to Turbulent flow for Polymer Drag Reducing Systems

The figure shows possible fanning friction curves for drag reducing polymer solutions in a pipe. The plot shows L laminar friction law, T turbulent friction law, M Virks asymptote, P and P' possible behavior of 2 specific polymer solutions. Possible trajectories are L:T (Newtonian fluids), L:T:P:M, L:M, L:M:P'. P and P' positions depend on the parameters mentioned previously. 2 details that characterize the fanning friction factor relation are thus the wall shear stress at the onset of drag reduction and the slope of its profile compared to that of the Newtonian.

Linear, high molecular weight polymers are the most effective drag reducers. Experiments have shown that the initial polymer conformation also plays a major part in drag reduction (Virk, Wagger 1990). By varying the salinity of the solvent the initial polymer conformation can be changed from elongated to randomly coiled. Initially coiled polymers typically follow an L:T:P:M path while initially extended polymers follow the L:M:P' path. Thus for initially extended polymers there is no onset Reynolds number and the flow is drag reducing as soon as it is turbulent. (Sasaki 1991) studying xanthan polysacharide solution under varying salinity claims drag reduction decreases with increased polymer flexibility yet other studies have shown the opposite to be the case. Direct Numerical simulations by (Gillissen 2008) were carried out on rigid and flexible polymer structures. Both simulations showed an equal amount of drag reduction suggesting that polymer flexibility plays only a marginal role in drag reduction. It is this author's hypothesis that the observed differences in Drag reduction by (Sasaki 1991) are due to polymer length fluctuation through varying salinity and not due to polymer flexibility changes. It was also found experimentally through the addition of microgel to polymer solution that increasing the elasticity of a fluid decreases the drag reduction and does not enhance drag reducing properties (Sasaki 1991).

11

## 2.1.5 Velocity profiles:

The turbulent flow velocity profile is split into 3 separate parts the viscous sublayer, buffer layer, turbulent core.

1) Viscous Sublayer ($0<y^+<5$)

$$u^+=y^+ \qquad\qquad \text{2.13}$$

2) Buffer layer ($5<y^+<30$)

$$u^+=5.0\ln(y^+)-3.05 \qquad\qquad \text{2.14}$$

3) Core($y^+>30$)

$$u^+ = \frac{1}{\kappa}\ln(y^+) + C^+ \qquad\qquad \text{2.15}$$

and for smooth pipes we have

$$u^+ = 2.5\ln(y^+) + 5.5 \qquad\qquad \text{2.16}$$

where $u^+ = \frac{u}{u^S}$ , $y^+ = \frac{u^S y}{\nu}$ , $u^S = \sqrt{\frac{\tau_W}{\rho}}$

u is the time averaged local mean velocity, y is the distance from the wall, $\nu$ is the kinematic viscosity, $u^S$ is the shear velocity, $\tau_W$ is the shear stress and $\rho$ is the fluid density.

Dilute polymer solutions show no change in the viscous sublayer but the buffer layer thickens and this offsets the logarithmic region. Hence when $y^+>30$, $u^+$ is above the value predicted for the Newtonian equation and this is in accordance with drag reduction. Most experiments show the shift results in a parallel profile (Virk 1975) resulting in:

$$u^+ = A\ln(y^+) + B + \Delta B \qquad\qquad \text{2.17}$$

Careful inspection has shown that there is also an increase in slope and the velocity profile is not merely offset by $\Delta$B(Pinho, Whitelaw 1990, HARDER, TIEDERMAN 1991, WEI, WILLMARTH 1992). (Virk 1975) proposed the following ultimate profile which occurs at maximum drag reduction conditions:

$$u^+ = 11.7\ln(y^+) - 17.0 \qquad\qquad \text{2.18}$$

Notice that the slope is approximately 5 times that of the Newtonian Wall Law of 2.5. Figure 2.2 below shows this proposed velocity profile:
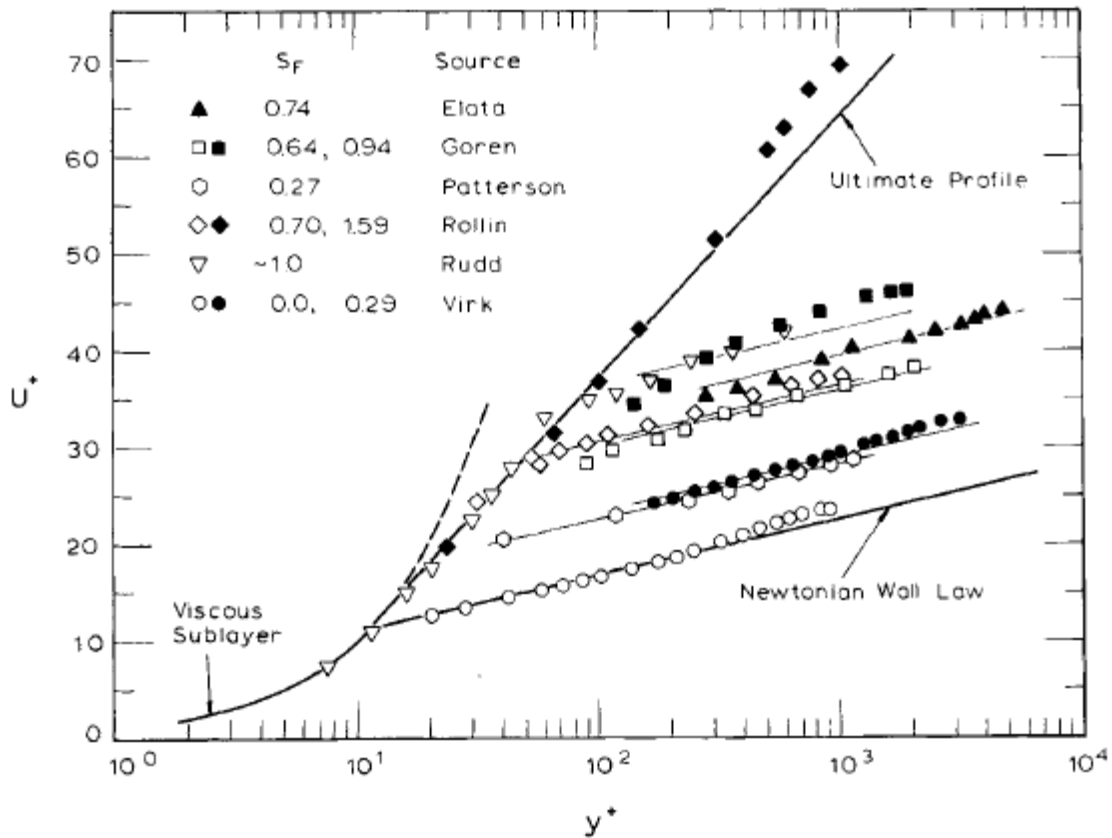
Figure 2.2 Experimental Data with respect to Newtonian Wall Law, Viscous Sublayer and Ultimate Profile (Virk 1975)

As previously mentioned most of the experimental data shows profiles parallel to but offset by some $\triangle B$ from the Newtonian Wall Law's profile. We also note the increased slope at maximum drag reduction conditions.

### 2.1.6 Mechanism of Polymer Drag Reduction:

Injection experiments allow us to test the dependence of drag reduction on the position of polymer in the flow by injecting the polymer at certain locations in the flow then measuring the appearance of polymer as it spread out downstream. Injection experiments have found that the polymer interacts with the turbulence in an annulus near but not at the wall $15<y^+<100$ (Mccomb, Rabie 1982) $10<y^+<100$ (Tiederman, Luchik et al. 1985). It is clear that the viscous sublayer does not actively participate in the drag reduction mechanism.

As mentioned in the previous section experimental data has shown that drag reduction can occur at some onset critical shear stress/ Reynold number. 2 common explanations for this

are polymer stretching and polymer aggregation due to the increase in shear stress with flow rate.
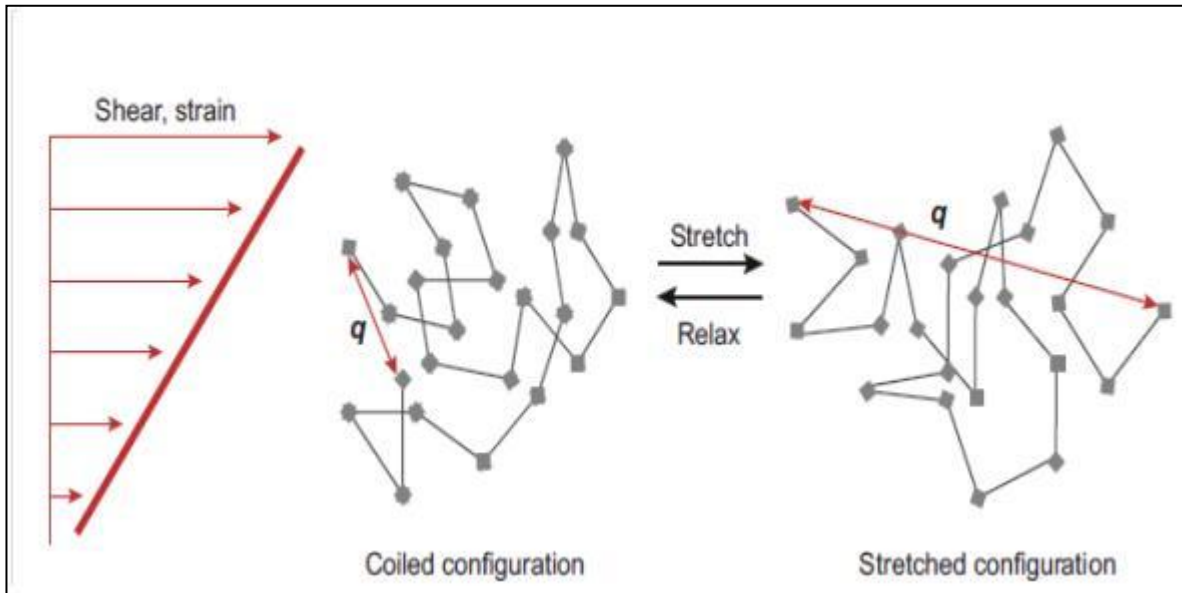


Figure 2.3 Schematic of Polymer Stretching/Relaxation of PEO in Shear Flow. q is The Vector Representation of End-End Distance. The Change in q Represents the Quantative Polymer Stretch (White, Mungal 2008)

Two experimental observations that simply justify that drag reduction is caused by an interaction between turbulence and polymer dynamics are that drag reduction is not seen until the transition from laminar to turbulent regime and secondly the onset of drag reduction at a fixed pipe diameter is determined by the number of monomers in the polymer chain. For non-polymer drag reducing solutions the turbulent structure is completely defined by the Reynolds number, but in polymer drag reduction the polymer chain length and its dynamics play a role, thus the cause of drag reduction must be due to an interaction between polymer dynamics and turbulence. Molecular extension plays an important role in drag reduction, and for extension to occur the elongation rate has to exceed the rotation rate which occurs in the buffer and core layers but not in the viscous sublayer.

(Hershey, Zakin 1967) have shown that for drag reduction to occur the polymer relaxation time must be larger than some representative time scale of the near wall turbulence. Specifically $T_z > \frac{\mu_s}{\rho u_\tau^2}$ where $T_z$ is the average time it takes for the stretched polymer to return to its coiled state, $\mu_s$ is the solvent viscosity, $\rho$ is the solution density, $u_\tau = \sqrt{\frac{\tau_w}{\rho}}$ is the wall friction velocity, and $\tau_w$ is the wall shear stress. For flexible linear polymers in solution $T_z$ increases with increasing monomer number, monomer length, solution viscosity and with

decreasing temperature. The ratio of $T_z$ to the near-wall turbulence time scale is defined as the Weissenburg number:

$$We_\tau = \frac{T_z \rho u_\tau{}^2}{\mu_s}$$

**2.19**

Experimental data has shown Weissenburg numbers of approximately 1 before the onset of drag reduction. The omission of polymer concentration from the calculation prevents its practical use for predictive purposes.

Numerical simulation of polymer drag reducing flows is a relatively new field of research that allows for the access of information (such as high order turbulence statistics near the wall) not available through experimental techniques. Most simulations involve modeling the polymer as a dumbbell whereby the polymer is modeled as 2 beads connected by an elastic spring. The most common model is known as the FENE-P model. The FENE-P model account for the finite polymer extension and uses a second-order closure model for the polymer stress tensor which cuts down on computation costs. Limitations arise from the second-order approximation and the simplification of the polymer of typically $10^5$ monomers to a simple dumbbell. In addition to this the model does not count for polymer-polymer interaction in flow.

An alternate form of drag reduction known as heterogeneous drag reduction has been observed experimentally by injecting highly concentrated polymer solution in pipe or channel flow. It is sometimes observed that the injected polymer forms a stable thread in the flow yet significant drag reduction is still measured. This is in contradiction to the homogenous drag reduction finding where polymer had to be present in the buffer layer to be effective, thus a different mechanism must be at play (Hoyt, Sellin 1991, Vleggaar, J., & Tels, M. 1973). Some studies show that a significant part of this drag reduction originates from a dissolving process and consequently from the same mechanism as homogenous drag reduction (Smith, Tiederman 1991, Bewersdorff, Gyr et al. 1993).

Finally it should be noted that the addition of polymer not only results in drag reduction but a reduction in heat transfer as well (Matthys 1991).

## 2.2 Surfactant Drag Reduction

Polymers degrade when they are subjected to the high shear stress and elongation often seen in pumps. This degradation causes the polymer chains to be broken into smaller chains which are not effective as drag reducing agents. The degradation of polymers increases with temperature and is irreversible. The district heating and cooling sectors require constant recirculation of water and pumping energy costs play an important role. Drag reducing agents that are non-degrading or rapidly repairable which can be used for long times would greatly decrease these pumping costs. Surfactant drag reducers are great candidates for this role. The surfactant micelle microstructure necessary for drag reduction can repair itself in a timescale of seconds after passing through high shear regions.

Surfactants possess hydrophobic tails and hydrophilic heads in one molecule; and as such are known to be amphiphilic compounds. Generally the hydrophobic tail is a long chain alkyl group and the hydrophilic head is ionizable, polar, polarizable or is suitable for forming hydrogen bridges. For the hydrophobic phase to avoid contact with water the surfactant molecules orient themselves such that the hydrophobic groups are in a non-polar phase such as a gas phase, non-polar solid, hydrophobic liquid; thus they typically accumulate in interfacial regions. Another method to avoid water contact is self association, surfactant molecules form assemblies known as micelles in which non-polar groups concentrate in the center while polar ends lie on the outside in contact with the water. Micellization occurs in surfactant solution above the critical micelle concentration (CMC). Above the CMC micelles are in thermodynamic equilibrium with monomer molecules.
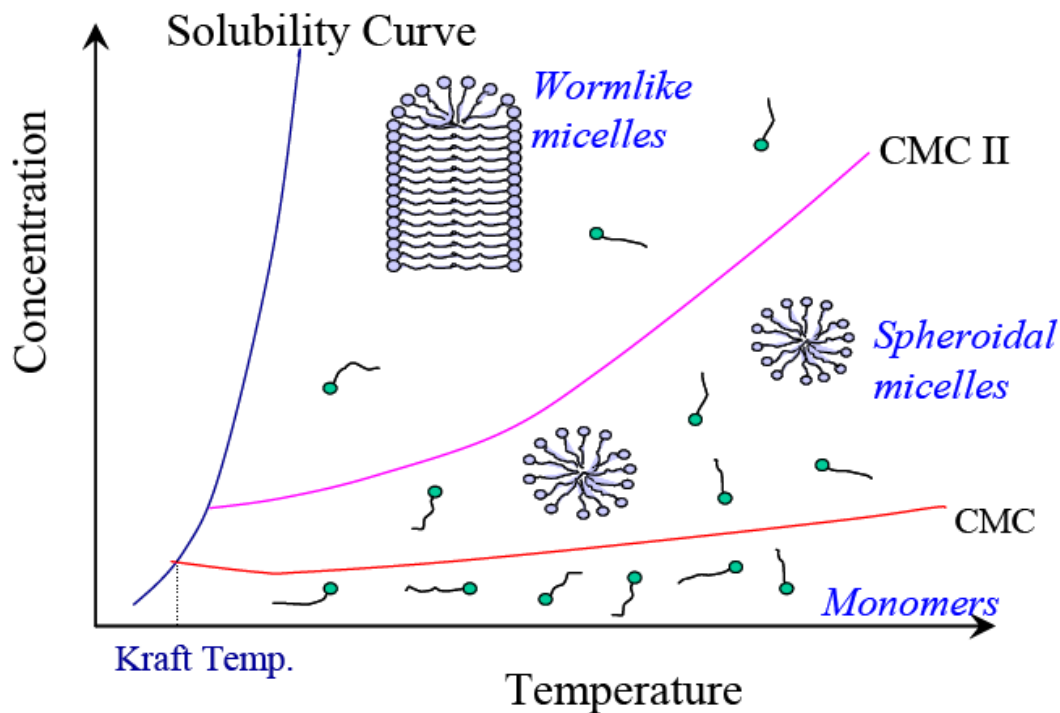
Figure 2.4 Solubility Curve, CMC and CMC II Plots Showcasing Surfactant and Temperature Dependence

When the temperature is below the Kraft point the surfactant is partially in crystal or gel form in solution. For temperatures above the kraft point micelles can form if the surfactant concentration is above the CMC and rod like micelles can form if above the $CMC_{II}$ concentration. Note that the CMC is almost independent of temperature while the $CMC_{II}$ increases with temperature.

| Surfactants | Ionic | Cationic |
| --- | --- | --- |
| | | Anionic |
| | | Zwitterionic/Amphoteric |
| | | |
| | Non-ionic | Semi-polar |
| | | Single bond |

Table 2.1 Surfactant Categorization based on Head Group Charge

### 2.2.1 Micelle shape:

1. Spherical
2. Rodlike
3. Lamellar
4. Vesicles

At the CMC concentration micelles are believed to be spherical. (TANFORD 1972) suggested ellipsoid shape over spherical shape. Regardless of the shape at the CMC when the concentration is increased to $CMC_{II}$ rod-like micelles form. Static light scattering, magnetic birefringence, quasi elastic light scattering spectra and NMR measurements all used to test shape of micelles (Porte, G., J. Appell and Y. Poggi 1980).

CryoElectron microscopy allows for the direct observation of micellar structure without alteration in sample preparation. Rod-like or worm like micelles with entangled micellar networks were observed for drag reducing cationic surfactants while only spherical micelles were observed for non-drag reducing surfactant systems (Lu, B.,X. Li, Y. Talmon and J.L. Zakin, 1996, Lu, B., Y. Talmon and J.L. Zakin, June 9-13 1996, Lu, B.,X. Li, Y. Talmon and J.L. Zakin, Novermber 10-15 1996, Lu, B., Y. Talmon and J.L. Zakin, 1996).

Consider surfactant with chain length L, volume of alkyl chain in micelle core per molecule V, and a cross-sectional area of head group per molecule a, the packing parameter is then defined as:

$$\frac{V}{La} \qquad \textbf{2.20}$$

If N is the number of carbon atoms on alkyl chain embedded in hydrocarbon core then V is given by:

$$V = 27.4 + 26.9N \qquad (\hat{A}^3) \qquad \textbf{2.21}$$

and $L_{max}$ the maximum possible extension of hydrocarbon tail is given by:

$$L_{max} = 1.5 + 1.265N \qquad (\hat{A}) \qquad \textbf{2.22}$$

| Value of packing parameter $\frac{V}{La}$ | Shape of Micelle |
|---|---|
| 0 – 1/3 | Spherical |
| 1/3 – ½ | Rod-like |
| ½ - 1 | Lamellar |
| > 1 | Reversed Micelles in non-polar media |

Table 2.2 Micelle Shape Related to Packing Parameter Value

The Critical Packing Parameter can be increased by:

1. Lengthening hydrocarbon chain
2. Using a branched chain
3. Addition of long chain alcohol (medium chain alcohols solubilize in vicinity of the head group increasing its cross-sectional area, a, and thus decrease packing parameter value
4. Addition of oppositely charged surfactant
5. Addition of salt

Regardless of the shape of the micelle no point within micelle can be further from micelle surface than $L_{max}$. This means that at least one of the 3 dimensions of the micelle is less than $2L_{max}$. Thus for spherical and rod-like micelles the radius is approximately $L_{max}$. The actual extension length of the hydrocarbon tail (L) is usually less than $L_{max}$ due to packing in the core. The addition of salts, co-surfactants or counter ions can induce the formation of rod-like micelles and promote the formation of large micelles.

### 2.2.2 Micelle Size:

Micelle size depends on many factors such as chain structure, head group, counter-ions, added salts, temperature. From a geometrical stand point we expect that the aggregation number (the number of surfactant molecules present in a single micelle) of spherical micelles increases with an increase in chain length and decreases with an increase in head group size, in fact this is what is observed. If the head group area is larger than the cross section of the hydro carbon chain the system will form convex curvature, if they are about the same size planar structures are formed. If the cross-section of the hydrocarbon is greater than that of the head group then inverse micelles are formed.

The length of rod-like micelles increases with an increase in surfactant concentration or a decrease in temperature. Rod-like micelles are longest and strongest around the surfactant kraft point (Elson, Garside 1983). Rod length was observed to increase linearly with surfactant concentration to a peak past which the length begins to decrease (Zakin, Bewersdorff 1998).

Maximum rod length concentration was noted as $C^*$. It is believed that at $C^*$ the rod length approaches the mean distance between the rods. $C^*$ increases with decreasing alkyl chain length.

Salts that can neutralize the charge of cationic surfactants head groups favoring micelle growth and formation. Rod length of cationic surfactant was observed to increase with salt concentration to a peak then decrease with further increase in salt concentration (Ohlendorf, Interthal et al. 1986). The higher the valence of the salt's anionic ions the more effective the salt was at increasing rod length. Generally the effectiveness of the salt on aggregation number increases with increasing lyotropic number of the anion (purely electrostatic ranking with no dependence on size or geometry of the anion). Micellar growth is induced by 2 processes: the first being a change in the packing parameter area to volume ratio and the second being the reduction of micellar surface charge. This was determined through the use of aromatic acid anion (particularly benzoate); as aromatic acids are known to dissolve on the micellar surface with the degree of penetration depending on the nature and position of the substituent groups on the phenyl ring (Rehage, Hoffmann 1991).

### 2.2.3 Drag Reduction:

#### *2.2.3.1 Overall*
Our consideration of surfactant drag reduction is split into 4 different sections anionic, cationic, nonionic, zwitterionic. Anionic surfactants are good drag reducers and mechanically stable though they are limited in application as they precipitate with magnesium ($Mg^{+2}$) and calcium ($Ca^{+2}$) ions typically found in tap and sea water. Anionic surfactants also tend to form foams with air. Nonionic and cationic surfactants are less sensitive to cations; nonionic surfactants however are generally only effective drag reducers in a narrow temperature range around the cloud point (Zakin, Lui 1983). Cationic surfactants have a broader temperature range.

#### *2.2.3.2 Concepts of Drag Reduction*
By a force balance wall shear stress is related to pressure drop as follows:

$$\Delta P(\pi r^2) = \tau_W(2\pi rL) \rightarrow \tau_W = \frac{\Delta PD}{4L} \qquad \textbf{2.23}$$

Where $\triangle P$ is the pressure drop, r is the pipe radius, $\tau_W$ is the wall shear stress, D is the pipe diameter and L is the pipe length. The fanning friction factor (f) is then defined as:

$$f = \frac{\tau_W}{\frac{1}{2}\rho V^2} = \frac{\triangle P D}{2\rho V^2 L} \qquad \text{2.24}$$

Polymers such as polyethylene oxide and polyacrylamide experience drag reduction at such low concentrations that deviations in shear viscosity are usually neglected. Some drag reducing surfactants exhibit significant increase in viscosity and this cannot be neglected. Drag reduction is said to occur with the addition of an additive to turbulent flow if at the same flowrate the pressure drop is reduced or if at the same pressure drop flow rate is increased. One common method to measure drag reduction is defined as:

$$\%DR = \frac{f_s - f}{f_s} \times 100 \qquad \text{2.25}$$

Where %DR is percentage drag reduction, f is the fanning friction factor of the solution and $f_s$ is the fanning friction factor of the solvent at the same flow rate. $f_s$ can be calculated directly by either von karman equation or Blasius equation or directly measured in system for the solvent. The Von Karman Equation describes friction loss in a smooth pipe for Newtonian fluids and is valid for Reynolds numbers between 5*10^3 to 5*10^6:

$$\frac{1}{\sqrt{f}} = 4.0 \log(Re\sqrt{f}) - 0.4 \qquad \text{2.26}$$

The Blasius Equation describes Newtonian fluids in smooth pipes with a Reynolds range from 5000 to 10^5:

$$f = \frac{0.079}{Re^{0.25}} \qquad \text{2.27}$$

A fluid is drag reducing if the percent drag reduction is positive with larger values indicating more effective drag reduction. To measure %DR we need to measure the pressure drop and flowrate of the flowing solution. The three major methods of representing data are

1. %DR vs. log(Re)
2. log(f) vs. log(Re)
3. f^-1/2 vs. log(Ref^1/2)

The von karman or Blasius line is used in the latter 2 representations for comparison.

### 2.2.3.3 Drag Reduction of Anionic Surfactants:

Savins (1967-1968) obtained percent drag reduction values greater than 80% using sodium oleate in water with potassium chloride (KCl). Increasing the KCl concentration from 3.5% to 10% increased the percent drag reduction from 45% to 82%. He suggested that with an increase in electrolyte concentration spherical micelles rearrange into cylindrical micelles, forming a network of interlaced rod-like elements. Drag reduction dropped to zero when the wall shear stress exceeded the critical stress but the process was reversible. This sudden decrease in drag reduction is attributed to the breakup of micelle structure at high shear stresses. At high stress the rate of micelle break up is larger than the rate of micelle reformation while below the critical stress the opposite situation occurs. Major limitations of anionic surfactants include precipitation with magnesium and calcium ions as well as the formation of foams in the presence of air.

### 2.2.3.4 Drag Reduction of Nonionic Surfactants:

As nonionic surfactants possess no charge they are less affected by ions. Nonionic surfactants have unique upper coacervation temperatures (cloud points) at and above which surfactant-water systems separate into 2 phases. Nonionic surfactants with straight chain alkyl groups ($C_xH_y$-$(OCH_2$-$CH_2)_z$-OH where x is 12 to 18, y is 2x+1 to 2x-1 and z is approximately 0.5x) are effective drag reducers while alkyl phenyl surfactants are not (Zakin, Lui 1983). Nonionic surfactants were found to be effective drag reducers just above and below the cloud point. Through the addition of sodium sulfate or phenol the cloud point could be lowered and the drag reducing abilities were enhanced at lower temperatures. Nonionic surfactants are found to be mechanically stable and regain their drag reducing abilities after passing through regions of high shear. (DeRoussel 1993) found maximum drag reduction to occur at the cloud point with at least 20% DR 10-25 ˚C of the cloud point using saturated and unsaturated $C_{12}$-$C_{18}$ alkyl groups with 4-23 ethylene oxide groups. The cloud point temperature as well as the effective temperature range could be decreased by lengthening the alkyl group or decreasing the number of ethylene oxides present. It was also found that mixed nonionic surfactant

systems had cloud points in between the pure ones. Minor adjustments to the cloud point temperature can be made changing the unsaturation level on the alkyl chain where an increase in unsaturation leads to an increase in the cloud point temperature. All these factors can be used for screening and influencing the effective temperature range.

### 2.2.3.5 Drag Reduction of Zwitterionic Surfactants:

Zwitterionic surfactants have both positive and negative charges on the same surfactant molecule. The betaines (one type of zwitterionic surfactant) are considered readily biodegradable and less toxic to marine organisms than many cationic surfactants. As these surfactants possess both a positive and negative charge they may be sensitive to ions and their long-term stability needs to be investigated.

### 2.2.3.6 Drag Reduction of Cationic Surfactants:

Drag reduction of nonionics is limited to its narrow effective temperature range while anionics tend to foam and precipitate in the presence of ions. Generally cationic surfactants have a wide temperature range and are not sensitive to magnesium or calcium ions being present.

#### 2.2.3.6.1 Drag Reduction of Cationics: Surfactant structure effects:

Quaternary ammonium surfactants and similar structures are known to be excellent drag reducers. Cetyl trimethyl ammonium bromide (CTAB) and 1-Napthol at equimolar concentrations of 508 ppm were observed to have no onset phenomenon but rather a gradual departure from the laminar line (Zakin, Bewersdorff 1998). Drag reduction was also found to terminate at a fixed wall shear stress independent of pipe diameter. This maximum stress limit is known as the critical wall shear stress. A similar explanation to the one for anionic surfactants was proposed where by past the critical shear stress the shear force overwhelms the forces causes soap aggregation and the aggregates are broken down into smaller particles which cannot produce drag reduction. Other studies have found that the upper temperature limit is dependent on alkyl chain length with larger chains having higher maximum temperatures and that the effective temperature range is independent of pipe diameter (Zakin, Bewersdorff 1998). Above the maximum temperature no drag reduction is observed but drag reduction ability is regained when the solution is cooled. The lower temperature limit is dependent on surfactant solubility; the more soluble the surfactant the lower the minimum effective temperature. By increasing the degree of unsaturation the surfactant's solubility will increase thus decreasing the effective drag reduction temperature.

(Chou, L.C. and J.L. Zakin 1991) showed that for their surfactant system the effective drag reduction temperature went to high temperatures for long chains and to low drag reduction temperatures for short chains. Through the addition of a minimum amount of small chains the system can maintain its upper temperature limit while drastically decreasing its lower temperature limit allowing for wide effective temperature ranges.

*2.2.3.6.2 Drag Reduction of Cationics: Counterion Effects:*

Generally at low concentrations (concentrations below 1%) cationic surfactants do not from the rod-like micelles necessary for drag reduction without the presence of counterion or other additives. (Chou, L.C. and J.L. Zakin 1991) noted the decrease of Drag reduction efficiency with excess counterion for hydroxynaphtoates. He suggested that the rod-like micelles become rigid in the presence of excess counterion and this negatively impact drag reduction.

*2.2.3.6.3 Drag Reduction of Cationics: Stability*

(Linder, P., H.W. Bewersdordd, R. Heen, P. Sittart, H. Thiel, J. Langowski and R, Oberthur 1990) used small angle neutron scattering on unstressed and stressed solutions of $C_{14}TASal$ in heavy water and found that for unstressed solutions the neutron scattering curve fit model calculations which assumed homogenous cylindrical micelles, but this was not the case after stressing the solution in turbulent flow for several hours. The largest deviations were occurred above the critical wall shear stress increasing the mean radius of gyration. The new micellar form was observed to persist even after months of storage at rest at room temperature. A decreasing active temperature range with time has been reported. This decrease was unavoidable in the presence of oxygen, indicating that oxidation of surfactant was the cause.

## 2.2.4 Diameter Effects:

For Newtonian fluids a plot of fanning friction factor versus Reynolds number is independent of the pipe diameter but this is not the case for drag reducing fluids. For drag reducing fluids the fanning friction factor is a function of both the Reynolds number and the pipe diameter. Drag reduction terminates at a fixed wall shear stress independent of pipe diameter however (Elson, Garside 1983).

(HOYT 1991) developed a simple scale-up technique for polymer drag reduction where $\triangle B$ the negative roughness is independent of pipe diameter. This technique requires no iteration or graphing and is successful for pipes with diameters greater than 10mm. Below 10mm the stronger effect of the viscous sublayer is believed to invalidate the scale-up technique.

(Gasljevic, K. amd E.F. Matthys 1995) studying an ethoquad/NaSal system in 2, 10, 20 and 52 mm pipes found that in the subcritical region (where the shear stress is lower than critical shear stress) drag reduction is a function of the bulk flow velocity and independent of pipe diameter for all but the smallest pipe diameter of 2mm. In the supercritical region the shear stress is the determining factor over pipe diameter or bulk flow velocity.

(Pollert, J., P. Komrzy, K. Svejkovsky, J. Pollert Jun, B. Lu and J.L. Zakin 1996) found that drag reduction increased with pipe size studying 500ppm Habon G at diameters above 4 mm.

(Park, S.P., H.S. Suh, S.H. Moon and H.K. Yoon 1996) also found drag reduction to increase with pipe size from 4.65 mm to 10.85 mm for the surfactant sytems CTAC/NaSal, STAC/NaSal and Habon G systems at varying concentrations of 100, 250 and 500 ppm. Drag reduction was also observed to increase with surfactant concentration.

## 2.2.5 Heat Transfer Reduction in Drag Reducing Flows:

Drag reduction also results in a decreased heat transfer coefficient (Monti 1972, Rose, G.D., K.L. Foster, V.L., Slocum and J.G, Lenhart July 1984). The decrease in heat transfer coefficient is explained due to the increased thickness of the boundary layer that accompanies drag reduction. This increased thickness causes an increase in thermal resistance between the wall and bulk fluid and hampers heat transfer.

Above the critical shear stress or critical temperature both drag reduction is lost and the heat transfer coefficient returns to that of the solvent; as such heat exchangers must be designed with this in mind. Plate heat exchangers have winding tortuous paths which prevent the formation of thick viscous layers and thus have higher heat-transfer rates than their tube in tube counterparts (Christensen, R.N. and J.L. Zakin June 1991). The reduction in heat transfer coefficients decreases with an increase in fluid velocity or a decrease in surfactant concentration. Sometimes the reduction in heat transfer coefficient is advantageous as in the transporting of heating or cooling water over long distances.

## 2.2.6 Maximum Drag Reduction Asymptote:

For polymer drag reduction there is a maximum asymptote. Virk's asymptote is believed to be valid:

$$f^{\frac{-1}{2}} = 19.0 \log\left(Re\ f^{\frac{1}{2}}\right) - 32.4$$

Or

**2.28**

$$f = 0.58 Re^{-0.58}$$

For Reynolds 4000-40000

Surfactant drag reducers can have fanning friction factors lower than those predicted by virks asymptote (McMillan 1970, HERSHEY, KUO et al. 1975, CHARA, ZAKIN et al. 1993). (Zakin, Myska et al. 1996) proposed a new asymptote for non-polymeric drag reduction:

$$f = 0.32Re^{-0.55}$$

**2.29**

Zakin's asymptotes values are significantly lower than Virks and the fanning friction factor is simply a function of the Reynolds number.

### 2.2.7 Mechanism of Surfactant Drag Reduction:

Many theories have been proposed for drag reduction but none of them provides a detailed mechanism for drag reduction. Turbulence measurements, rheology measurements and small angle light scattering measurements have all been used to elucidate the nature of this mechanism.

We note the significant difference in maximum drag reduction asymptote and velocity profiles between high molecular weight polymers and aluminum disoap surfactant solutions. This strongly suggests that the mechanism for surfactant drag reduction is different from that of polymer drag reduction. Though the reasons for this difference are not clear one proposed explanation is the formation of Shear induced structures (SIS) which are discussed in further detail in the following sections. These SIS may be more effective than MDRA polymer solutions at reducing turbulent energy production and turbulent eddy formation.

Small angle neutron scattering experiments (SANS) showed no anisotropy in scattering pattern meaning that below the onset of drag reduction there is no orientation of the micelles and they rotate freely (Bewersdorff, Dohmann et al. 1989, Linder, P., H.W. Bewersdordd, R. Heen, P. Sittart, H. Thiel, J. Langowski and R, Oberthur 1990). After drag reduction occurs the micelles align and as Virks asymptote is approached nearly complete alignment of micelle in flow direction. Measurements have shown that during drag reduction the micelles are oriented such that their long axis is parallel to the flow direction (Porte, G., J. Appell and Y. Poggi 1980). Above the second critical shear stress both drag reduction and micelle alignment are lost and the micelles rotate and are dissalligned in the turbulent flow. The mechanism of drag reduction is thought to be from the interaction of the turbulence with the non-Newtonian fluid properties of the viscoelastic surfactant solution. Thus the rheology of the solution may give some insight on the mechanism of drag reduction.

## 2.2.8 Rheology:

The consideration of the solutions rheology on its drag reduction has been split into 4 sections: shear viscosity, viscoelasticity, network/ shear induced structures and extensional viscosity.

### *2.2.8.1 Rheology: Shear Viscosity:*

Additives have been found to change the shear viscosity of solution in many Drag reducing systems. These viscosity changes have been attributed to a change in micellar structure. The viscosity of dilute rod-like micellar solutions can be modeled by (Doi, Edwards 1978, Doi, Edwards 1978) equation:

$$\eta_0 = \eta_s\left(1 + \hat{C}L^3\right)$$

2.30

where $\eta_0$ is the viscosity of surfactant at 0 shear rate, $\eta_s$ is the viscosity of the pure solution, Ĉ is number of rods per unit volume, L is rod length. Ĉ calculated using the equation:

$$\hat{C} = \frac{C_m M}{\pi \rho r^2 L}$$

2.31

$C_m$ is the surfactant concentration, M is the molecular weight of the surfactant monomer, r is the radius of the rod like micelle and $\rho$ is the density of the solution. Substituting the equation for Ĉ in the original equation for shear viscosity yields:

$$\eta_0 = \eta_s\left(1 + \frac{C_m M}{\pi \rho r^2}L^2\right)$$

2.32

We can see that the shear viscosity increases with the square of the rod length. When Ĉ is much greater than $\frac{1}{L^3}$ the rods begin to overlap and the equation is no longer valid (the solution is no longer considered to be dilute). For such systems (Doi, Edwards 1978, Doi, Edwards 1978) proposed a new equation:

$$\eta_0 = \eta_s\left(1 + \left(\hat{C}L^3\right)^3\right)$$

2.33

Substituting the equation for Ĉ we get:

$$\eta_0 = \eta_s \left( 1 + \left( \frac{C_m M}{\pi \rho r^2} \right)^3 L^6 \right)$$
<div align="right">2.34</div>

Thus at these concentrations there is a much larger viscosity increase with rod length and at high concentrations the micelles can form a 3-D network.

### *2.2.8.2 Rheology: Viscoelasticity:*

Both drag reduction and viscosity are dependent on with shear rate and additive concentration but at high shear rates the viscosity is relatively constant and is typically 2-5 times that of water. This increase in viscosity is not enough to explain the level of drag reduction observed. (Savins 1967, Gravsholt 1976, Rehage, Hoffmann et al. 1986) have suggested that viscoelastic rheological properties are responsible for drag reduction.

Viscoelasticity can be induced in surfactant system through the addition of oppositely charged surfactant, organic counterions and some uncharged compounds such as esters or aromatic hydrocarbons (Rehage, Hoffmann et al. 1986). Viscoelasticity can be measured through the swirl decay time (SDT). The SDT is the time between the stopping of swirling motion of vessel and the cessation of solution movement before recoil. Smaller SDTs imply higher viscoelasticities. (Elson, Garside 1983) studying CTAB/1-Naphtol solutions found that the critical wall shear stress at which drag reduction disappears reaches a maximum when the SDT is at a minimum meaning when the solution has maximum viscoelasticity. Another method to characterize viscoelasticity is the first normal stress difference ($N_1$).

Strong elastic forces arise from the interaction between elongated, rod-like micelles (Elson, Garside 1983). A sudden increase in viscosity and viscoelasticity is observed when the rod-length of micelles exceeds the mean separation distance between micelles. This jump is attributed to the presence of a dynamic 3D network which forms immediately after the rod length is greater than the separation distance.

(Lu, Li et al. 1997, Lu 1997) found effective drag reducing surfactant system without normal viscoelasticity characteristics. The solutions displayed zero first normal stress difference value and displayed no recoil. The solutions did possess high extensional viscosity.

### *2.2.8.3 Rheology: Network and Shear Induced Structure (SIS):*

As some surfactant solutions can increase in viscosity under shear stress it is believed that some network exists or forms under shear. (Hoffmann, M. Lobyl and H. Rehage 1985) proposed rod-like micelles can bundle together under adhesion forces that counter the electrostatic repulsion between micelles. Adhesion forces can be due to van der waals or interfacial tensions between the rods. Cryotransmission electron microscopy has been used to detect network structure but preparing cryotem samples requires significant shear; thus

the observed network may be shear induced(Bellare, Kaneko et al. 1988, Lu, B., Y. Talmon and J.L. Zakin, June 9-13 1996, Lu, B., Y. Talmon and J.L. Zakin, 1996).

Evidence for the formation of SIS includes solutions with $\hat{C}$ below $\frac{1}{L^3}$ still achieving drag reduction and affecting the flow at high shear rates (Ohlendorf, Interthal et al. 1986). Other evidence is the generally observed viscosity jump (Bewersdorff, Ohlendorf 1988, Rehage, Hoffmann et al. 1986). The viscosity was observed to be low at low shear rates followed by a sudden increase in viscosity to high values at some critical shear rate, sometimes an increase of 8 times was observed. The viscosity jump was dependent on the surfactant concentration, solution temperature, geometry of viscometer and gap width shear rate. After the jump the solutions were always shear thinning. The jump is attributed to a sudden change in microstructure. This viscosity jump is commonly found in systems with a 1:1 counterion/surfactant ratio and at higher ratio no jump is observed. This lack of viscosity jump suggests the presence of a preexisting network and not a shear induced one for solutions of higher counterion/surfactant ratio. Thus the SIS structure only exists in certain shear rate ranges above a certain shear rate to induce their formation but not above the second critical shear rate at which the network becomes unstable.

### 2.2.8.4 Rheology: Extensional Viscosity

High extensional viscosity has been proposed as the cause for polymer drag reduction (Landahl 1977, Bewersdorff, Thiel 1993). High extensional viscosity increases the resistance to vortex stretching and turbulent eddy growth decreasing energy dissipation. (Lu 1997, Lu, Li et al. 1997) found a drag reducing surfactant system lacking normal viscoelastic behavior but with high extensional viscosity. (Vissmann, Bewersdorff 1990) studying dilute CTASal solutions detected increase in elongational viscosity for solutions where the preshear rate was in the critical range for shear induced states to be present. When the preshear rate was below critical shear or above the upper critical shear rate the ratio of elongational to shear viscosity was 3 which is the typical value for Newtonian fluids. At high shear rates the SIS micelle structure is destroyed and this results in the observed ratio discrepancy.

Surfactant systems usually show shear viscosities limited to 10 times that of water but have unusually high extensional viscosity. The mechanism of drag reduction is probably due to the suppression of small scale turbulent eddies. In the bursting and growth of these eddies extensional motions dominate. A large extensional viscosity represents an increase in resistance to extensional flow curbing the formation and growth of small-scale eddies. This reduces energy loss and leads to drag reduction.

## 2.3 Polymer-Surfactant Interaction

### 2.3.1 Introduction

When water soluble polymer, surfactant and salt are mixed in aqueous solution structures known as aggregates may form. These aggregates are formed through polymer-surfactant interaction and can have a drastic effect on the solution's rheology. Many factors influence the interaction between polymer and surfactant some of which include the nature of the surfactant head group, the presence of a polar group on the polymer backbone, level polymer hydrophobicity and the polymer flexibility. The structure of these aggregates is described as polymer film is formed around surfactant micelles. In pipe flow these aggregates take on an ordered orientation that minimizes resistance to flow. At high Reynolds numbers and shear stress the aggregates elongate. Polymer-surfactant aggregates can show stronger drag reduction than the substances alone, have slower degradation and display drag reduction for a larger range of Reynolds numbers. Additionally damaged structures can be partially rebuilt, to destroy the structure the process of degradation should be carried out longer than in than in the polymer case alone. For these reasons the right combination of polymer and surfactant is advantageous to many applications and a necessary field of research.

Micellar solutions are commonly used as emulsifiers through surface tension manipulation, polymer additives can be used to enhance micelle stability and further influence rheological behavior. Polymers help to stabilize micelles by reducing the surface tension between the micelles hydrophobic cores and water. Other stabilization methods imparted by the polymer include specific interactions between polymer and surfactant headgroups and decreasing the electrostatic repulsion between charged head groups.

Polymer-surfactant solutions have found application in paints, coating fluids, inks drug-delivery systems, food stuffs, cosmetic products, laundry detergents and in tertiary oil recovery. Polymer-surfactant systems can also be used to create simple models of DNA/Protein interaction with surfactant and other biological binding processes such as those with the cell membrane. These models are valid as no significance difference in phase behavior is observed when polymer is replaced by protein. Another area of significant research is in utilizing drag reduction to alter blood flow in arteries. Drag reducing agents can be used to improve blood flow and prevent heart attacks. PEO is a blood compatible polymer but it is readily degradable under high shear. Increasing its degradation time through the use of a suitable surfactant would be key in its successful implementation for improving blood flow.

At the surfactant concentration known as the critical aggregation concentration (CAC) the interaction between polymer and surfactant begins. After the CAC further addition of

surfactant leads to polymer surfactant aggregate formation. As the surfactant concentration increases further a point known as the polymer saturation point (PSP) occurs. At the PSP polymer molecules are saturated with surfactant and further addition of surfactant leads to free surfactant in solution and rapid decrease in surface tension until the point of free surfactant micelle formation in solution there after surface tension is constant.

Many studies have been performed on nonionic polymers and anionic polymers which have frequently shown strong interaction. Nonionic polymers and cationic surfactants were originally thought to not form aggregates due to the bulky cationic head groups which prevents strong interaction with the polymer solvation shell. Recent studies have shown this is not the case and many nonionic polymers do form aggregates with cationic surfactants. The accumulation of these relatively weak forces between nonionic polymer and cationic surfactant can influence the rheology considerably. The interaction between nonionic polymer and surfactant is generally attributed to the non covalent bonding between surfactant and polymer. Past the CAC surfactant micelles begin to form on the polymer chains and this causes changes in the polymer coil conformation. Hydrophobic interaction between the micelle interior and the polymer is the reason for micelle adsorption onto the polymer backbone. The bulkiness of large surfactant head groups can reduce this interaction. Polymer-surfactant aggregates have improved micelle stabilization by shielding the micelles hydrophobic core from water and by decreasing the electrostatic headgroup repulsion. The increased stability leads to more efficient internal stress transfer and suppresses the first appearance of turbulent eddies as shown in figure 2.8.

### 2.3.2 Effect of Counter-ions on aggregation

Salt aids in the formation of surfactant-polymer aggregates. Counterions can screen electrostatic repulsion between surfactant head groups decreasing the distance between them leading to a decrease in head group area. In addition some bulky aromatic salts such as sodium Salicylate (NaSal) increase the lyphophilic volume of the surfactant. Thus counter ions can increase the critical packing parameter allowing for the formation of worm-like micelles. Counter ions also aid in the formation of aggregates by decreasing polymer hydrophilicity increasing the hydrophobic interactions with surfactant. In general an increase in salt ionic strength leads to a decrease in the CAC, increased micelle size and an increase in the number of micelles attached to polymer.

## 2.3.3 Polymer-Surfactant Interaction Measurement Techniques

The 2 primary methods of polymer-surfactant interaction are electrostatic interaction and hydrophobic interaction. Electrostatic interaction occurs when the polymer and surfactant are of opposite charge while hydrophobic interaction occurs between the hydrophobic parts of the polymer and surfactant. Electrostatic interaction is usually much stronger than a hydrophobic interaction. There are many methods to measure Polymer-surfactant interaction including:

- Conductivity
- Surface Tension
- Viscometry
- Dye Solubilization
- Calorimetry
- Chromatography
- Spectroscopic methods (NMR, IR, Light-scattering, SANS)

In this thesis conductivity, surface tension and viscometry were used to measure polymer-surfactant interaction.

### *2.3.3.1 Surface Tension*
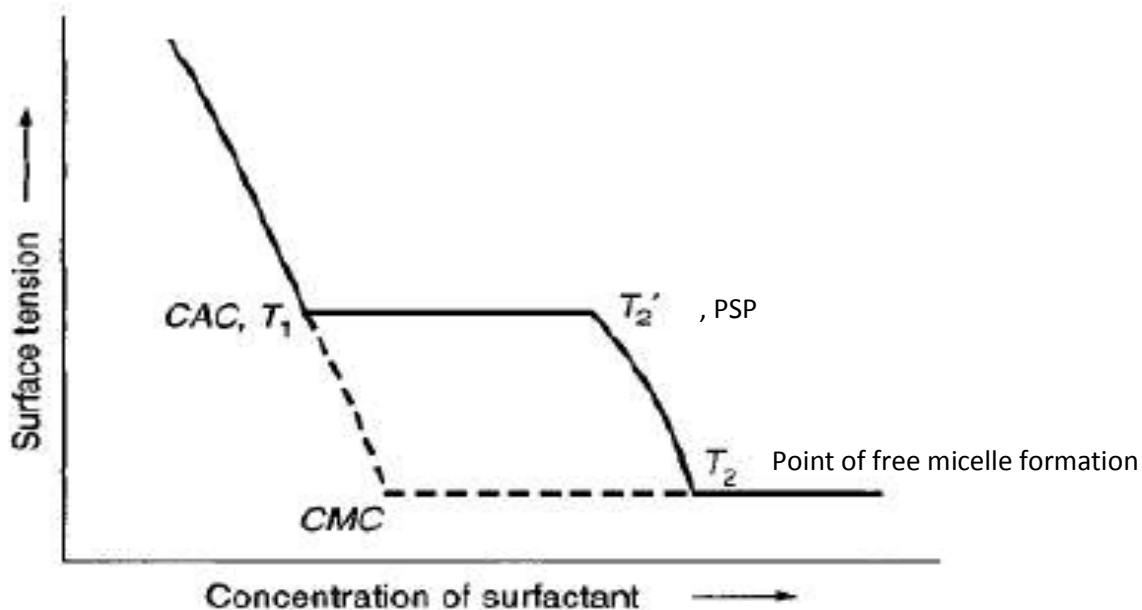


Figure 2.5 Idealized Surface Tension Plot showing Strong Polymer-Surfactant Interaction versus Pure Surfactant Surface Tension Plot

Figure 2.5 above shows the idealized behavior of polymer surfactant interaction. When no polymer is present the surface tension is seen to decrease with increase in surfactant concentration. At the point known as the critical micelle concentration (CMC) surface tension reaches a constant value and further addition of surfactant results in micelle formation instead of free surfactant molecules accumulating at the solvent surface. It is the presence of surfactant molecules at the solvent surface that causes a decrease in surface tension. In the presence of polymer surface tension is observed to decrease with increasing surfactant concentration until a point known as the critical aggregation concentration. This is the concentration at which polymer and surfactant begin to interact and usually occurs at a surfactant concentration below the CMC. Once the polymer and surfactant begin to interact further addition of surfactant leads to a slower decrease in surface tension, thus a decreased slope on the surface tension graph. This reduced surface tension slope continues until the point known as the polymer saturation point (PSP), at this point the polymer molecules are saturated with surfactant micelles and cannot support further adhesion of micelles. Past the PSP a sudden decrease in surface tension is observed as all added surfactant is present as free surfactant in solution and will accumulate at the solvent surface drastically decreasing the surface tension. At point T2 on the figure the surface tension is that of the CMC concentration and further addition of surfactant leads to free surfactant micelles present in solution.

## 2.3.3.2 Conductivity
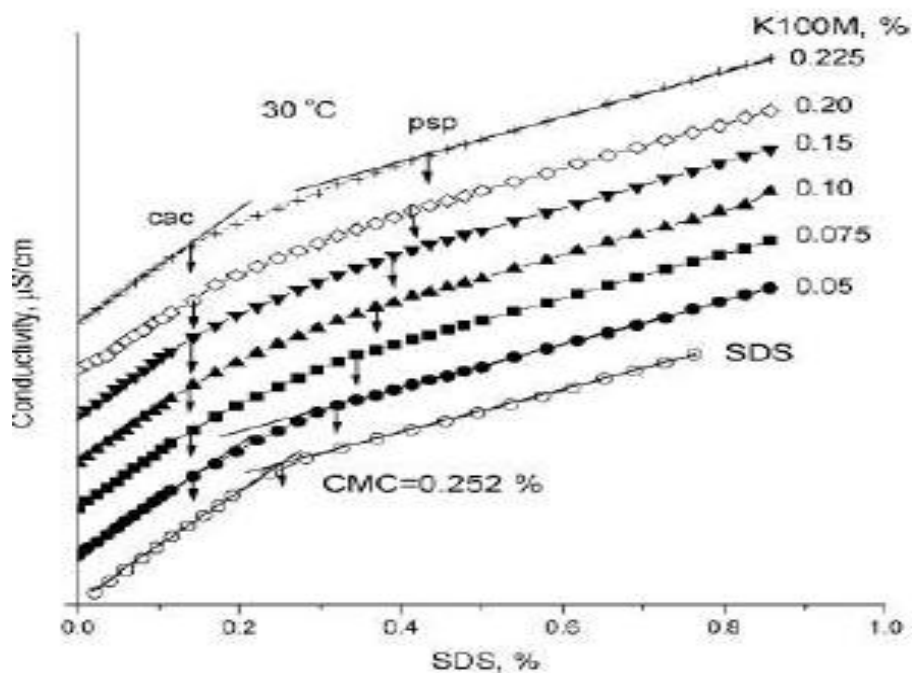


Figure 2.6 Conductivity Plot with SDS surfactant and Polymer Hydroxypropyl methylcellulose (HPMC) Indicating the CMC, CAC and PSP of solution

The CAC and PSP can also be detected through conductivity measurements. In figure 2.6 above we see the polymer Hydroxypropyl methylcellulose (HPMC) and its interaction with sodium dodecyl sulfate (SDS). When no polymer is present the usual curve for surfactant is observed. At first we observe a steep slope followed by a decrease in slope past the CMC due to decreased mobility of the bulky micelles over the highly mobile surfactant molecules. When polymer is present the change in slope does not immediately jump at a point but instead is gradual beginning at the CAC and finishing at the PSP. Conductivity is determined by charge and mobility thus when the surfactant begins to form aggregates with the polymer this negatively affects mobility and conductivity increase for a given amount of surfactant addition decreases. This trend continues till the PSP where further addition of surfactant leads to free surfactant in solution. It should be noted that the CAC is relatively independent of polymer concentration while the PSP is heavily affected by polymer concentration. High polymer concentrations mean more polymer molecules are available for binding leading to higher PSP concentrations.

## 2.3.3.3 Viscometry
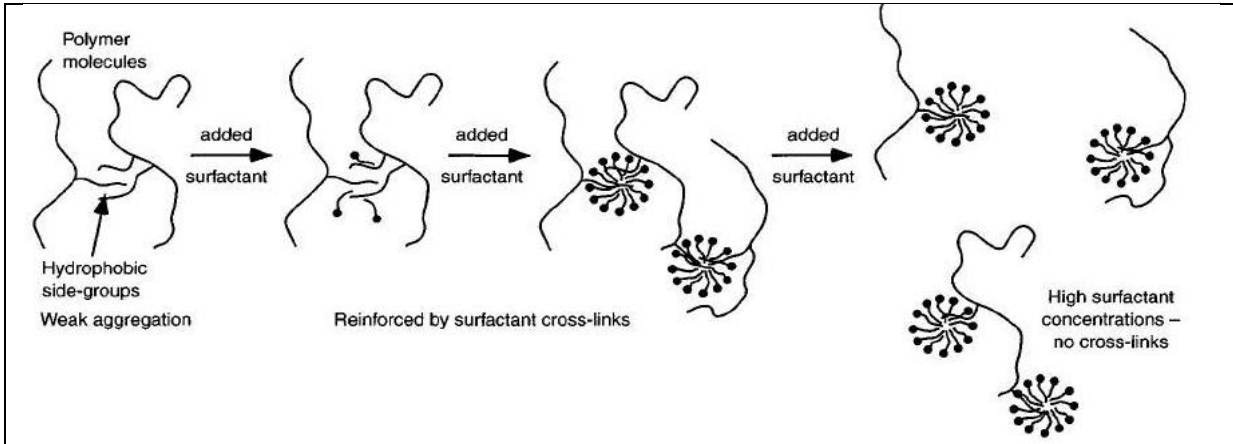


Figure 2.7a Molecular Explanation for Commonly Observed Viscosity Peak with Increase in Surfactant Concentration
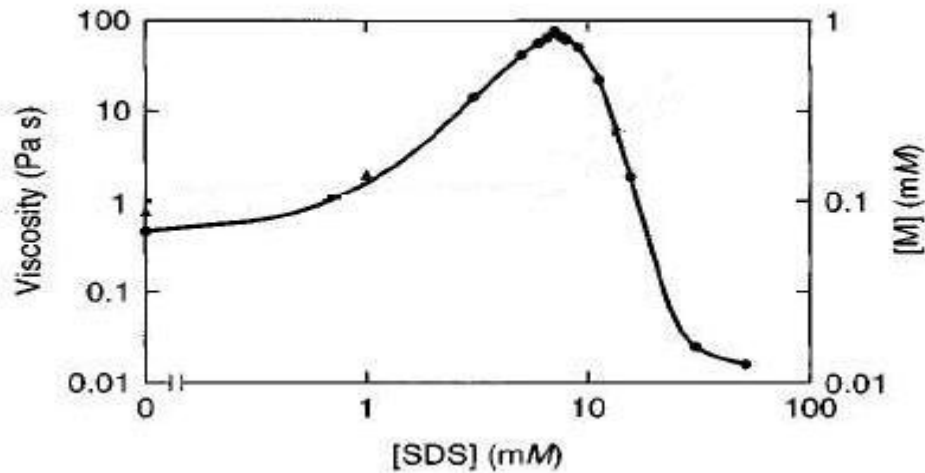


Figure 2.7b The Commonly Observed Viscosity Peak is Shown Above

Figure 2.7 Pictorial Representation of the Effect of Surfactant on Polymer-Surfactant Solution Viscosity

Figure 2.7 above shows how viscometry can be used to measure polymer-surfactant interaction. Figure 2.7a pictorially explains why the viscosity peak is usually observed in polymer surfactant solutions. When no surfactant is present polymer molecules may aggregate slightly due to hydrophobic interaction. As surfactant is added the crosslinkages between polymer molecules is reinforced and an increase in viscosity is observed. This viscosity increase continues up to a maximum value past which a viscosity decrease occurs resulting in a characteristic peak. At high surfactant concentrations the polymer is highly soluble in water and hydrophobic interaction between polymer molecules is minimized resulting in minimum cross-linking.

Polymer concentration also plays an important role on the measured viscosity. At low polymer concentrations when polymer molecules are far apart the presence of surfactant micelles on the polymer backbone cannot help in crosslinking the distant polymer molecules.

At polymer concentrations around the pure polymer crosslinking concentration the surfactant concentration plays a considerable role. At these intermediate concentrations surfactant micelles can reinforce the polymer crosslinks. Finally at high polymer concentrations the polymer molecules are already crosslinked to one another and surfactant will typically be unable to bind to the polymer molecules which have no room for further bonding. Thus surfactant will not affect solution viscosity through polymer interaction.

## 2.3.4 Drag Reduction in Polymer-Surfactant Systems
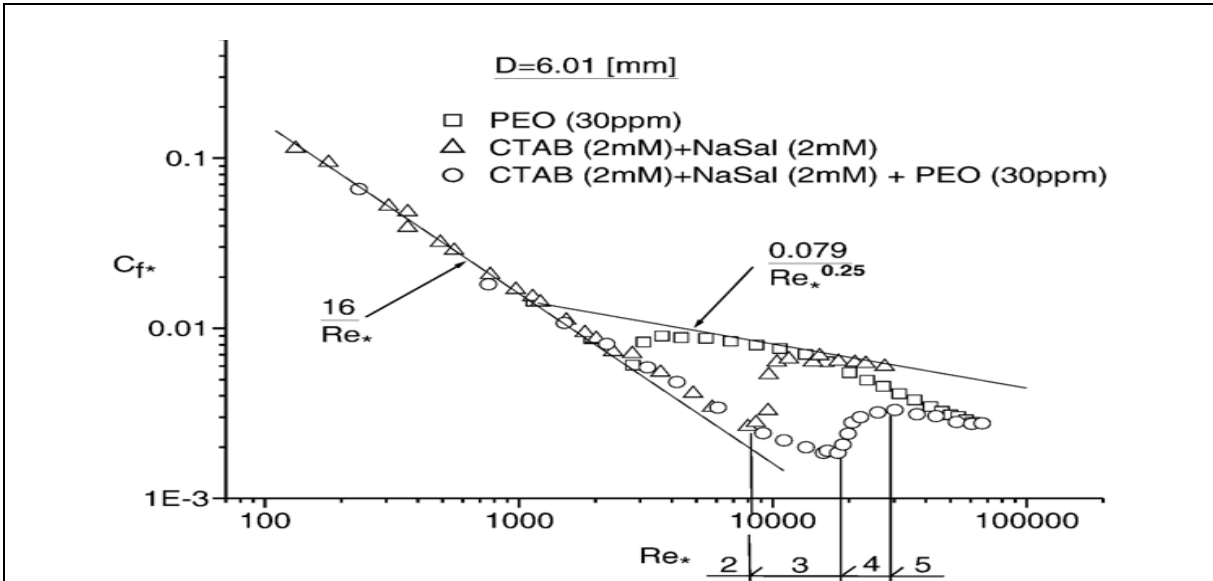


Figure 2.8a Comparison between Pure Polymer (PEO), Pure Surfactant (CTAB) and Polymer-Surfactant (PEO/CTAB) Drag Reduction Values
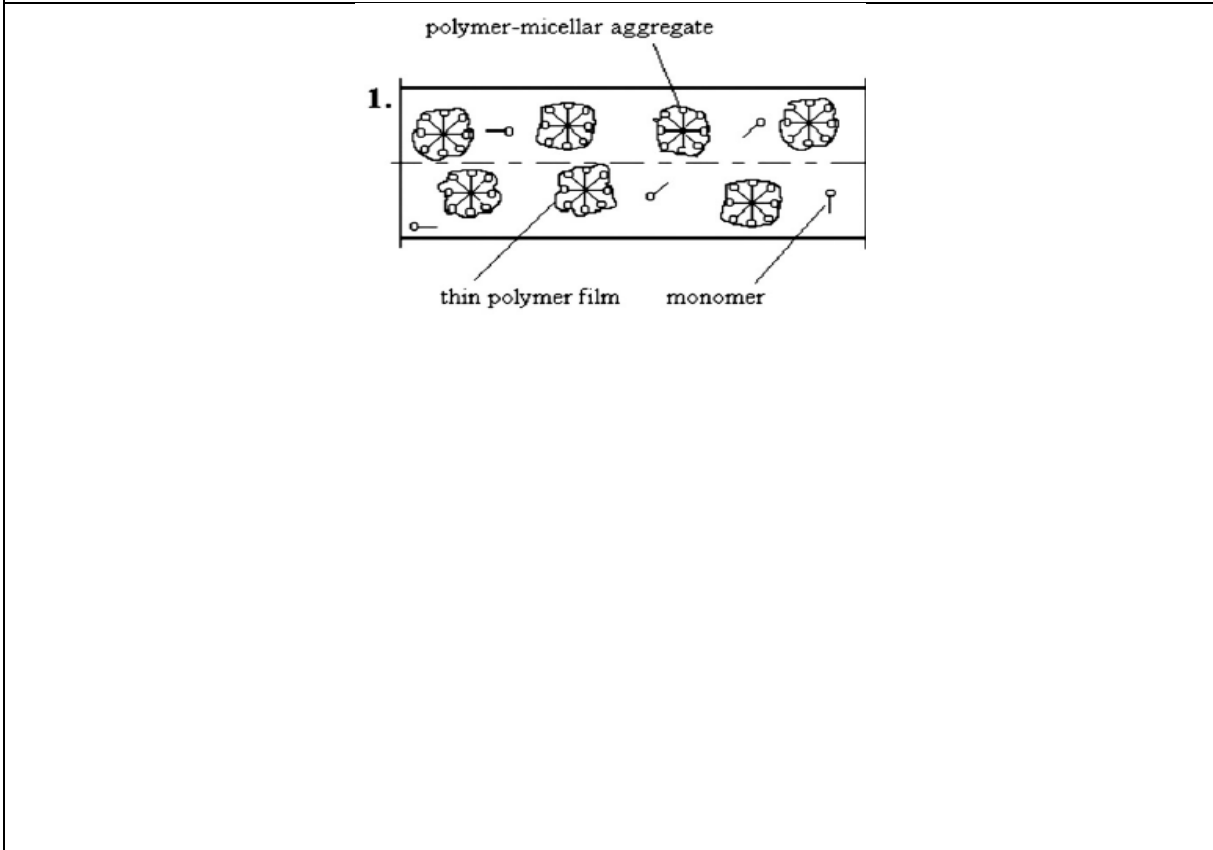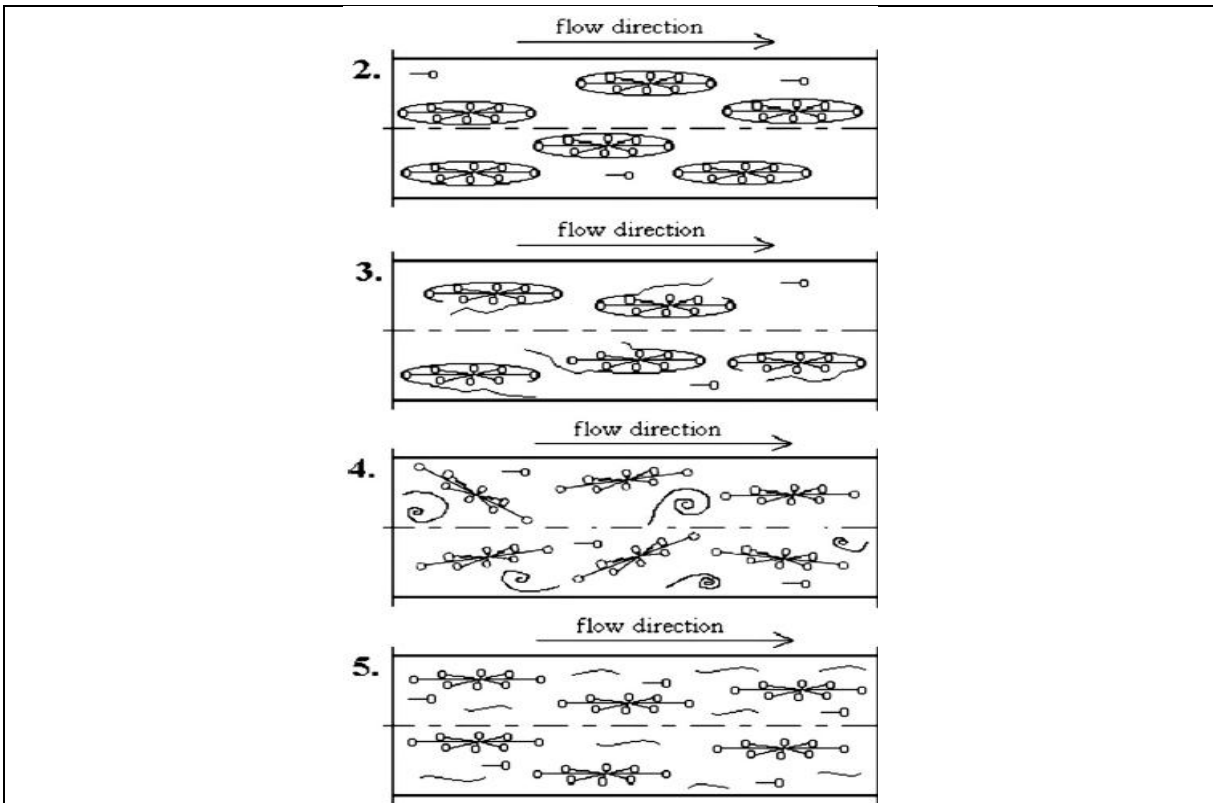
Figure 2.8b Proposed Mechanism for Polymer/Surfactant Drag Reduction and the Regions of Change Specified in 2.8a

Figure 2.8 Shows general model for polymer-surfactant aggregate Drag Reduction (Matras, Malcher et al. 2008)

Figure 2.8 proposes a mechanism for surfactant-polymer drag reduction. 2.8b1 shows the commonly accepted model for polymer-surfactant interaction in no flow conditions. 2.8b2-2.8b5 show structures corresponding to regions 2-5 labeled in figure 2.8a. In 2.8b2 aggregates are shown to take on ordered orientation to minimize resistance to flow. As the Reynolds number increases the structures elongate. These are the structures responsible for drag reduction. At a certain critical Reynolds number surfactant drag reduction ceases but polymer-surfactant drag reduction continues past this point. 2.8b3 shows polymer-surfactant aggregate disintegration. The polymer and surfactant micelles begin to influence flow individually. 2.8b4 shows the critical Reynolds number for polymer-surfactant systems at which the surfactant micelles lose orientation and the polymer coils. 2.8b5 as the Reynolds number increases so does the shear stress which causes the macromolecules to extends in the flow direction and the micelles recover ordered orientation in flow direction.

Overall we see an increase in fanning friction factor after critical shear rate is due to aggregate disintegration and loss of orientation. Also note that shear induces changes on aggregate structure thus macroscopic properties such as viscosity also depend on shear rate. Shear stress causes elongation of polymer-surfactant aggregates and these internal stresses

accumulate as elastic strain energy. Initially stresses accumulate in the polymer-surfactant aggregates but after disintegration the stresses accumulate in the polymer and surfactant elements individually. If the aggregates are slower to disintegrate than the micelles alone this will allow the transfer of greater internal stress and lead to more efficient drag reduction.

# Chapter 3   Experimental Procedure

The drag reducing polymers selected were polyethylene oxide (PEO) and anionic polyacrylamide (PAM) with cocamidopropyl betaine (Amphosol) chosen as the surfactant. Amphosol is a biodegradable, nontoxic, zwitterionic compound. Both PAM and PEO are popular drag-reducing agents. PEO is a nonionic, blood-compatible polymer with a wide range of application. PAM in its polymerized form is a non-toxic, linear chain structure but it should be noted unpolymerized acrylamide monomers are a neurotoxin.
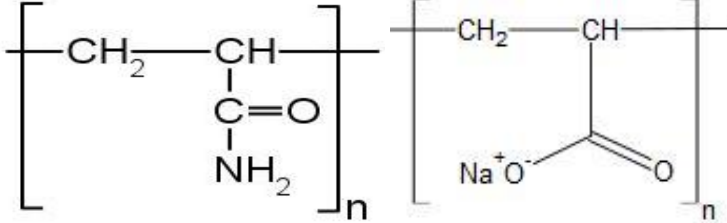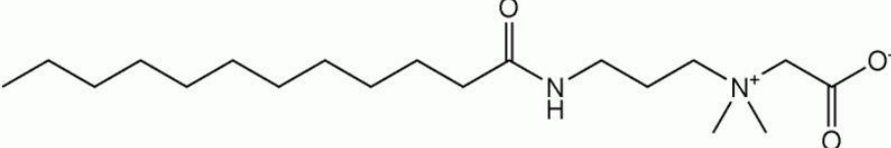


a) Polyethylene Oxide (PEO)

b) PAM is a copolymer of acrylamide shown on the left and sodium acrylate on right

c) Cocamidopropyl Betaine (Amphosol)

Table 3.1 Chemical Structure of the Polymers and Surfactants under Investigation in Thesis

Experimental analysis consisted of a bench scale analysis to determine the concentrations of maximum interaction between polymer and surfactant followed by drag reduction measurement at pilot plant level using optimized bench scale concentrations.

## 3.1 Bench Scale

### 3.1.1 Overview

The purpose of the bench scale experiments was to find the concentrations that maximized interaction between the pairs of PEO/Amphosol, PAM/Amphosol and PAM/PEO. These components are discussed in detail below.

Polyethylene oxide is a nonionic, water soluble, linear polymer made up of ethylene oxide monomer and is highly hydrophilic due to the presence of oxygen atoms in chain. Specifically Polyox WSR-301 manufactured by DOW Chemicals, USA with an average molecular weight of $4*10^6$ g/mol was used. The product is a white powder at room temperature.

The particular brand of PAM was Hyperdrill AF207 produced by Hychem, Inc. USA. This is an anionic water-soluble copolymer of acrylamide and sodium acrylate with a molecular weight range from $11\text{-}14*10^6$ g/mol and a charge density of approximately 30%. When dissolved in water sodium acrylate releases $Na^+$ ions into the water and leaves a negative charge on the polymer chains. PAM is a white powder at room temperature.

The particular brand of Amphosol used was Amphosol CG-50. It is coconut-oil based, zwitterionic, non-toxic and biodegradable with a $LD_{50}$ of 5g/kg. It is a clear, amber liquid at room temperature.

Stock solutions were prepared in deionized water at 2.0-4.0μS/cm. Polymer stock solutions were made consisting of 0.5% PEO and 0.3% PAM by weight. The polymer stock was then diluted to the required level. Amphosol stock solution was also prepared at 2 weight% and diluted to required ppm level.

The mixtures were then characterized through surface tension, viscosity and conductivity measurements. Pure Amphosol readings were taken from 0-5000ppm. For the PAM/Amphosol experiments PAM concentration was varied from 50-5000ppm while the amphosol concentration range was from 0-4000ppm. For the PEO/Amphosol analysis PEO concentration ranged from 100-1000ppm and Amphosol from 0-1000ppm. PAM/PEO procedure consisted of varying the PEO concentration from 0-1000ppm at 100ppm and 200ppm PAM. All solutions were prepared in deionized water with the average conductivity ranging from 2.0-4.0μS/cm. The 3 methods of solution characterization (surface tension, viscosity and conductivity measurement) are discussed in detail in the following sections. Table 3.2 shows the bench-scale equipment used.

(a)


(b)


(c)


(d)

Table 3.2 Table of Bench-Scale Equipment (a)Ubbelohde Viscometer (b)Coaxial Cylinder Viscometer (c)Conductometer (d)Surface Tensiometer

### 3.1.2 Viscosity Measurement

### *3.1.2.1* **Ubbelohde** *Viscometer*

The relative viscosity of solution was determined using an Ubbelohde viscometer. All measurements were taken at 25˚C. Relative Viscosity is defined as the time of flow for test solution divided by the time of flow for water through the capillary of the viscometer. The equation for relative viscosity is presented below:

$$\eta_r = \frac{t_p}{t_w}$$

3.1

Where $\eta_r$ is the relative viscosity, $t_p$ is the time the test solution takes to pass through the capillary and $t_w$ is the time water takes to flow through same capillary. We also note the specific Viscosity is defined as:

$$\eta_s = \frac{t_p - t_w}{t_w}$$

3.2

Where $\eta_s$ is the specific viscosity.

### *3.1.2.2 Coaxial Cylinder Viscometer*

A coaxial cylinder viscometer was used to measure the shear viscosity. In this device a rotor is spun at a specified shear rate while a bob measures the force exerted on the surface of the viscometer. After calibration the following equations were obtained:

Shear Stress is given by:

$$\tau = 0.0881(Dial\ Reading) - 0.3694$$

3.3

where $\tau$ is the shear stress

and the shear rate equation is:

$$\gamma = \frac{2s^2}{s^2 - 1}\Omega$$

3.4

where $\gamma$ is the shear rate, s is the ratio of rotor to bob radius (1.067546 for our setup) and $\Omega$ is defined as:

$$\Omega = \frac{2\Pi(RPM)}{60}$$
**3.5**

where RPM is the revolutions per minute.

### 3.1.3 Conductivity

The polymer saturation point (PSP) and the critical aggregation concentration (CAC) can be found from conductivity plots. This method can only be used on ionic surfactants which allowed for its use with Amphosol. A thermoscientific conductometer (Orion 3 Star) was used to perform measurements.

### 3.1.4 Surface Tension

Surface tension can be used to find the PSP, CAC and point of free micelle formation. Surface tension measurements can be used on both ionic and non-ionic surfactants to determine the mentioned quantities. We note that if both the polymer and the surfactant are surface active then the surface tension results can be misleading. In the thesis a CSC Du Nouy Ring Tensiometer (model #70535) was used. This tensiometer uses the ring method whereby a platinum-iridium ring is dipped into solution then slowly pulled out of solution. As the ring passes through the surface the liquids surface tension causes a downward force on the retreading ring and this force is measured. We should note that the Du Nouy ring has a relatively high degree of error but can be used to study the pattern of interaction between polymer and surfactant.

## 3.2 Pilot-Plant Experiments

Pilot Plant experiments were carried out in DI Water and tap water. DI conductivity ranged from 1.70-5.00 μS/cm while tap water conductivity ranged from 650-700 μS/cm. Polymer was diluted down to 0.3% and 0.5% stock solutions. Surfactant was added to diluted polymer in tank. Solution temperature was maintained at 25°C.

The bench-scale data was used to determine the concentrations of surfactant and polymer to run in the pilot-plant system (the concentrations that showed the maximum level of interaction). The purpose of the Pilot-plant experiments was to compare the drag-reduction and degradation times of PAM/Amphosol, PEO/Amphosol and PAM/PEO mixtures to the drag-reduction and degradation of pure polymers not in mixture. In addition to this the effect of counterions on the drag reduction of anionic PAM was also studied.

The solutions were run through the flow loop with the appropriate measurements being taken at specified times while being degraded within the loop.

To perform this analysis fanning friction factor versus generalized Reynolds number plots were made for the pure polymer and its mixtures. The Fanning Friction F was defined previously as:

$$f = \frac{\Delta P D}{2\rho V^2 L}$$

**3.6**

Where $\Delta P$ is the pressure drop, D is the pipe diameter, $\rho$ is the density, $V$ is the average velocity and L is the pipe length across which the pressure drop occurs. The physical meaning of the fanning friction factor is a ratio of the input energy to the output energy with lower fanning friction factors indicating more efficient energy transfer.

The Generalized Reynolds number is defined as:

$$Re_G = \frac{\rho D^n V^{2-n}}{8^{n-1} K \left(\frac{3n+1}{4n}\right)^n}$$

**3.7**

Where n and K are derived from the power law model for fluids. The Physical meaning of the generalized Reynolds number is the same as that for the Reynolds number it is the ratio of inertial forces to viscous forces. The Generalized Reynold number does not assume the fluid to be Newtonian.

To calculate these nondimensional parameters the mass flowrate and the pressure drop had to be measured experimentally within the system. In addition to this percent drag reduction versus Generalized Reynolds number plots were created where the percentage drag reduction is defined as:

$$\%DragReduction = \frac{f_{solvent} - f_{solution}}{f_{solvent}} \, X100\% \qquad \textbf{3.8}$$

where $f_{solvent}$ is the fanning friction of the solvent and $f_{solution}$ is the fanning friction factor of the tested solution. These methods provide us with a way to quantitatively compare between drag reducing solutions. PAM/Amphosol experiments consisted of a 2 hour degradation period of both 200ppm PAM and 200ppm PAM/100ppm Amphosol in the flow loop as well as a comparison of drag reduction between 250ppm PAM in tap water with 200ppm PAM in deionized water. PEO/Amphosol experiments were comprised of a 5 hour degradation period of 1000ppm PEO and 1000ppm PEO/700ppm Amphosol mixture. PAM/PEO experiments were also for 5 hours of degradation of a 100ppm PAM/500ppm PEO mixture and compared to the 200ppm pure PAM and 1000ppm pure PEO mixtures from the previous experiments.

### 3.2.1 Setup

The system was previously calibrated by Ali Mohsenipour and the calibration is included in his thesis (Mohsenipour 2011). Selected material from his work is presented below. The setup consisted of the components shown in the diagram and table below. The system consisted of a jacketed tank to prepare the solution, pump, pressure transducers, flowmeter and a flow loop. The tank temperature was maintained through a temperature controller which passed hot and cold water through the jacket to match the temperature measured within the tank with the set point temperature (25˚C). A centrifugal pump was used to circulate the test fluid. In the thesis 2 straight tubes with internal diameters of 34.8mm and 22.02mm were used. The tubes were fitted with pressure tabs which were setup to be easily connected with pressure transducers with pressure ranges of 0-5 psi and 0-10 psi. The pressure tabs were located far enough from the tube entrance to allow for the formation fully developed flow in the measurement area. The pressure drop is measured as the difference between the 2 pressure tabs (the difference between the first reference tab and the second pressure tab).
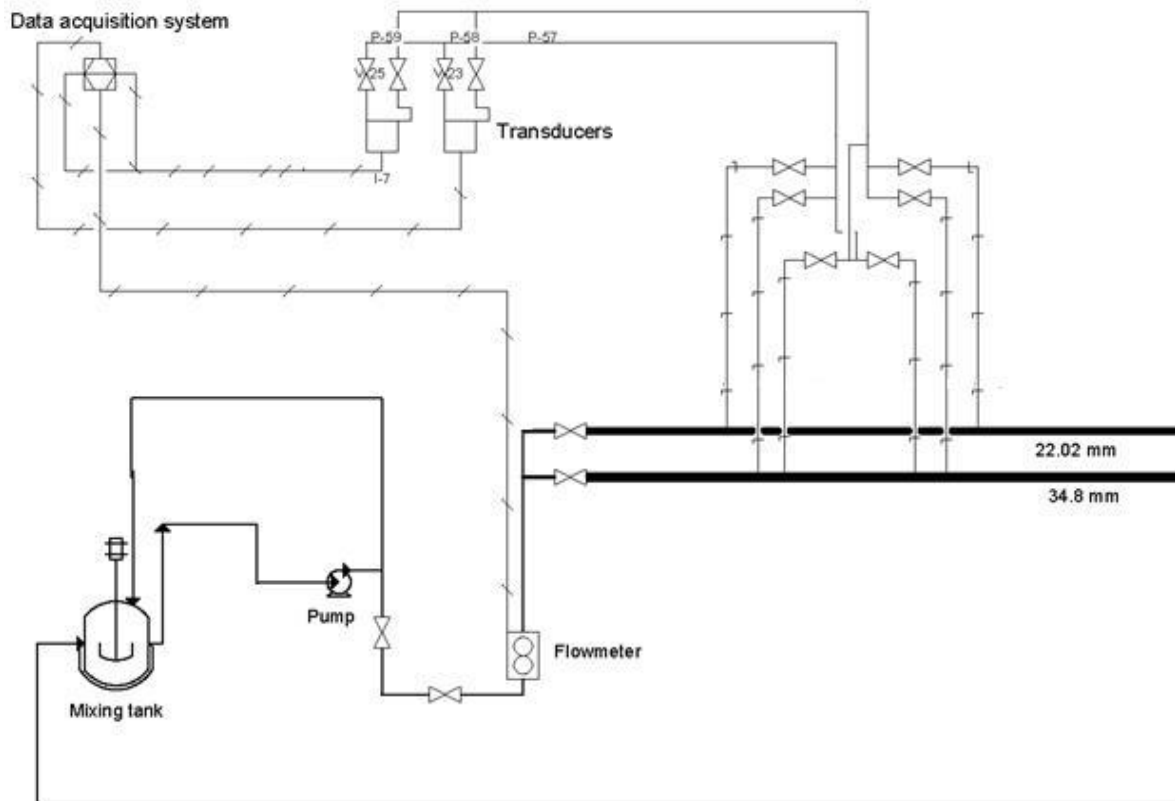
Figure 3.1 Pilot-plant System Setup

Solutions were prepared in the mixing tank and run through the flow loop. The flowmeter took the mass flowrate while the pressure transducers measure the pressure drop across the pressure tabs shown above.

|                    (a)                    |                    (b)                    |

Table 3.3 Picture showing (a) Jacketed tank, Temperature Controller and Mixer (b) Centrifugal Pump

| Item# | Equipments and test sections | Description |
|---|---|---|
| 1 | Mixing tank | Stainless still with Jacket |
| 2 | Pump | Centrifugal 7.5 HP |
| 3 | Coriolis flow meter | Krone company Optimass 7050C S25, nominal flow 1200 1b/hr |
| 4 | Straight Tube | Tube #1 stainless still tube (22.02mm ID) |
| 5 | Straight Tube | Tube #2 stainless still tube (34.8mm ID) |
| 6 | Pressure transducers | Rosemount and Cole-Parmer: 0-5, 0-10 psi |
| 7 | Control panel for transducers connection | Gives flexibility for transducer to pressure tap connections |
| 8 | Data acquisition system | Consisting of: personal computer, electronic board and software |

Table 3.4 Table of Pilot-plant Components (Mohsenipour 2011)

| Tube # | Nominal diameter (in) | I.D. Inside diameter (mm) | Entrance length (m) | Test section length (m) |
|---|---|---|---|---|
| 1 | 1.5 | 34.8 | 154.2 | 3.048 |
| 2 | 1.0 | 22.02 | 154.2 | 3.048 |

Table 3.5 Tube Specifications

### 3.2.3 Coriolis Flowmeter

A coriolis flowmeter was used to measure the mass flowrate though the system. It was calibrated by Ali Mohsenipour (Mohsenipour 2011) as follows:
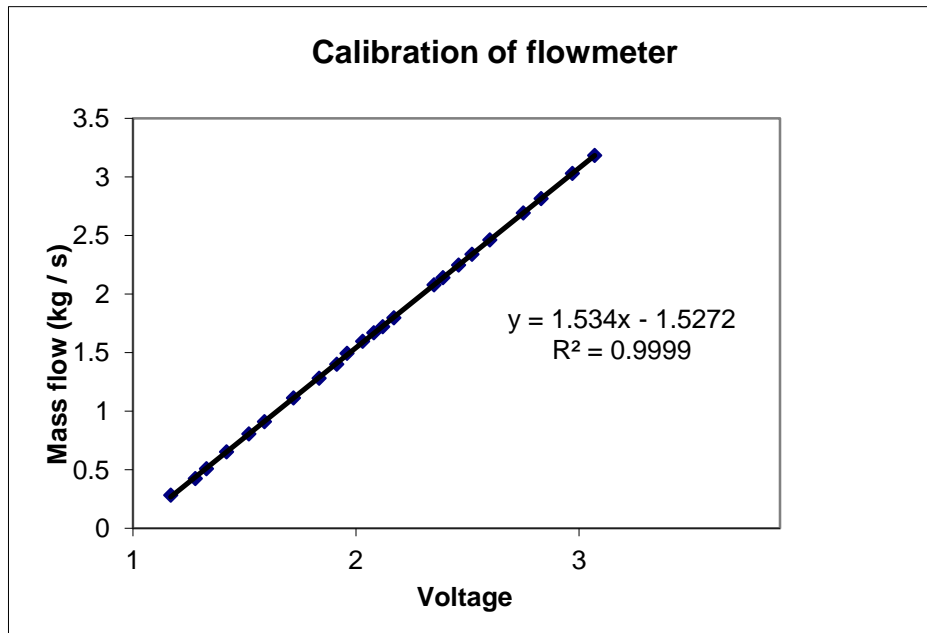


Figure 3.2 Calibration Curve of Mass Flowmeter (Mohsenipour 2011)

With the equation for mass flowrate being:

$$\textbf{Mass Flow(Kg/s)=}1.534*\textbf{(Reading Volts)}-1.5272 \qquad \textbf{3.9}$$



Figure 3.3 Picture of flow meter used

## 3.2.4 Pressure Transducer

Each Pressure transducer has 2 shut off valves and 1 bypass valve allowing the whole line to be purged with water when necessary.
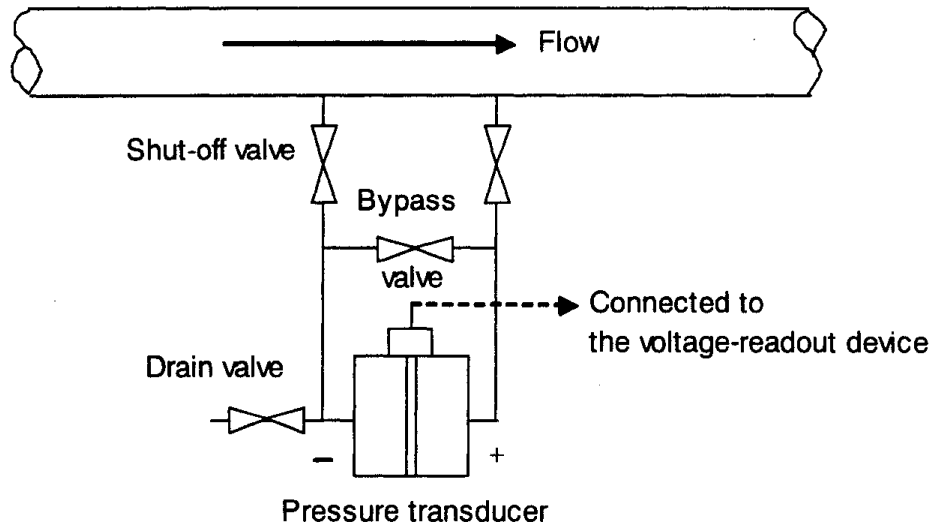


Figure 3.4 Pictorial Representation of Pressure Transducers (Mohsenipour 2011)

The pressure transducers were calibrated using a manometer by Ali Mohsenipour (Mohsenipour 2011)using the setup show below:
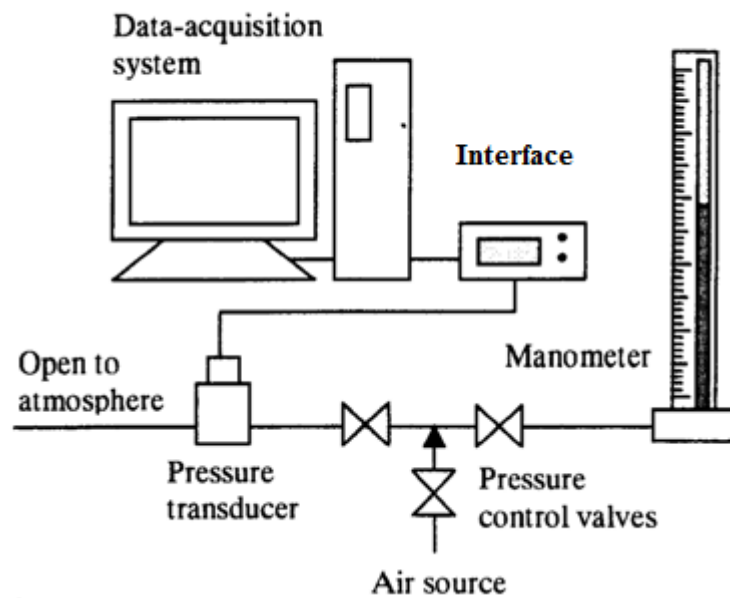


Figure 3.5 Pressure Transducer Calibration Setup(Mohsenipour 2011)

Pressure transducers relate the pressure difference to a voltage output. The pressure transducers were calibrated using a manometer and a digital pressure transducer calibrator. The air pressure was incrementally increased from atmospheric pressure to the maximum pressure the pressure transducer could measure. For each increment the corresponding voltage and pressure was measured. The calibration graphs were produced and the linear Equations were fit as show below:



$y = 2.5297x - 2.5573$
$R^2 = 0.9999$
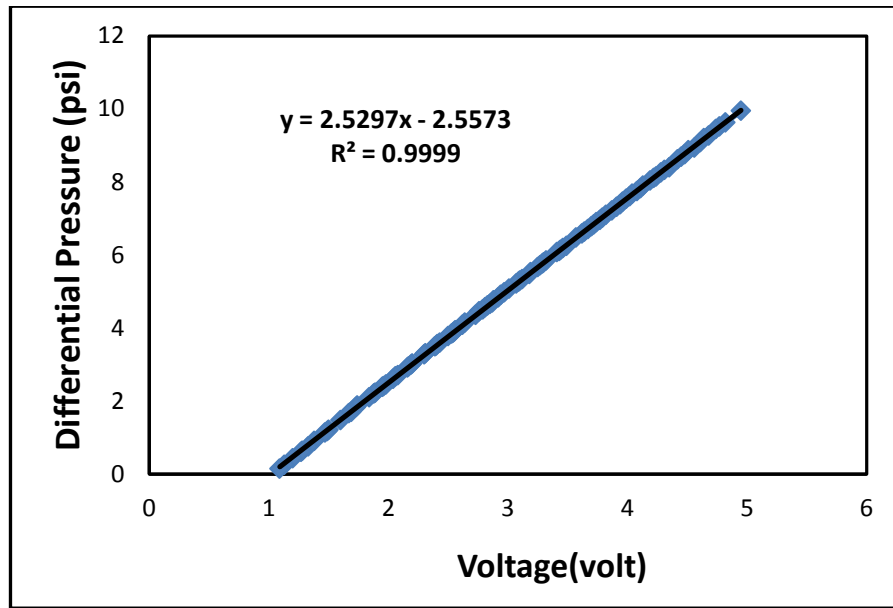
Figure 3.6: 0-10 psi Pressure Transducer Calibration (Mohsenipour 2011)



$y = 1.2556x - 1.3149$
$R^2 = 0.9999$
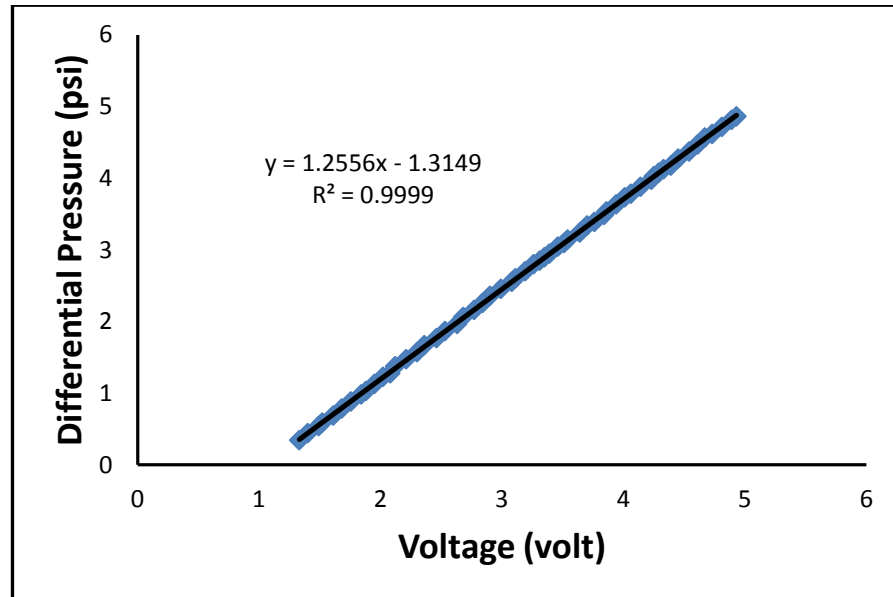
Figure 3.7: 0-5 psi Pressure Transducer Calibration (Mohsenipour 2011)

| Range | Differential Pressure Calibration |
|---|---|
| 0-10 psi | Differential pressure = 2.5297*(Reading voltage) - 2.5573 |
| 0-5 psi | Differential pressure = 1.2581*(Reading voltage) - 1.2823 |

Table 3.6 Calibration Equations for Pressure Transducers
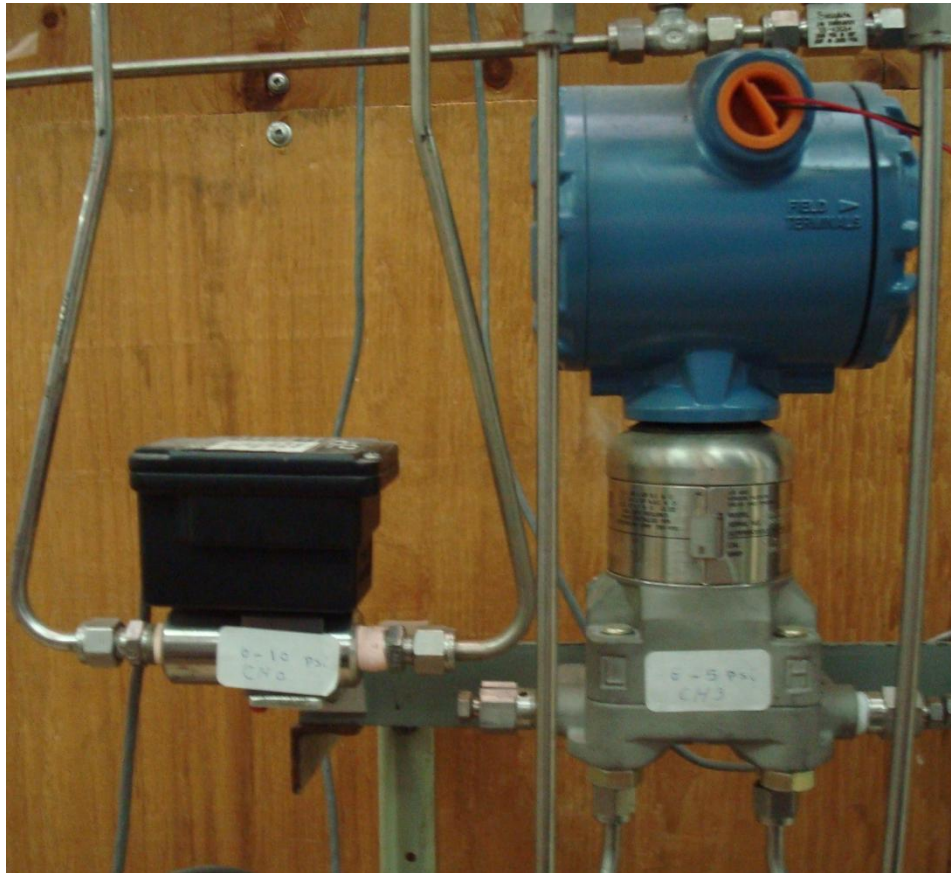


Figure 3.8 Picture of the 0-10psi Pressure Transducer on Right and 0-5psi Pressure Transducer on Left

## 3.2.5 Newtonian Fluid Flow Comparison
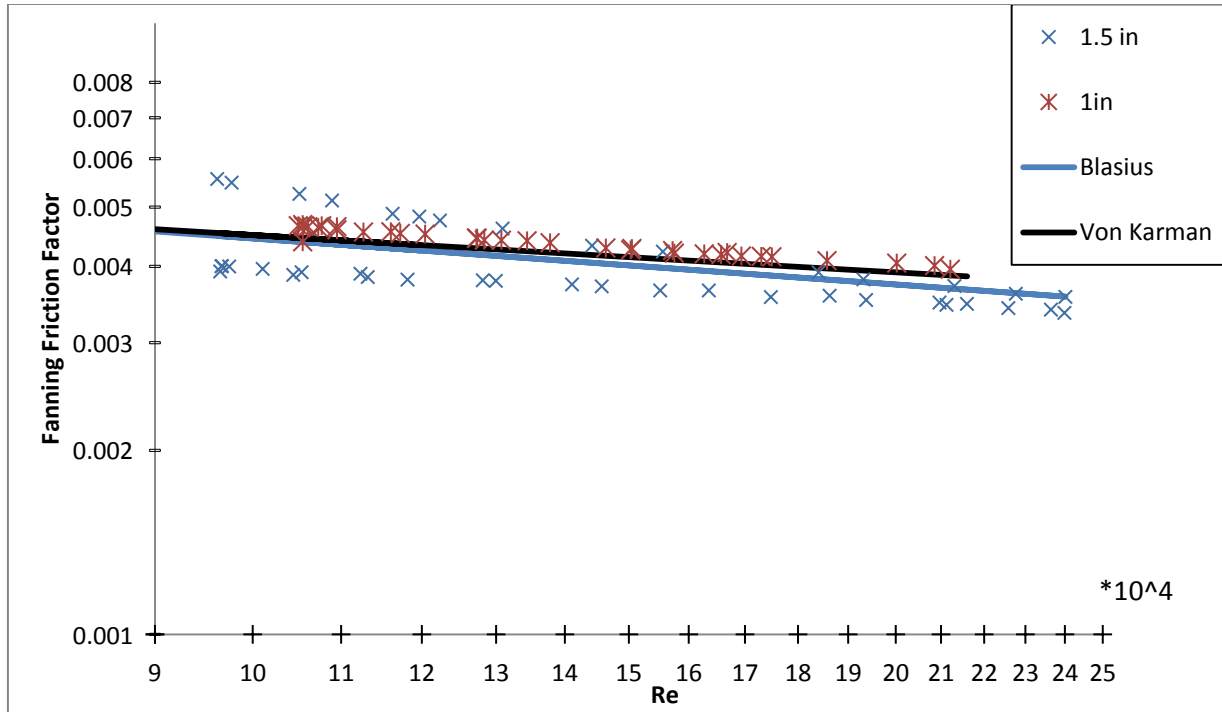


Figure 3.9 Water Measurements through Flow-Loop Fit by Blasius and Von Karman Equations

Both the Von Karman line and the Blasius line fit actual Newtonian fluid flow in our system. This shows that the system has been properly calibrated and that the Blasius equation is a good fit in the operated Reynolds number range. The Von Karman and Blasius Equations were presented earlier (Eqns 2.26 and 2.27 respectively) and are presented below.

Von Karman:

$$\frac{1}{\sqrt{f}} = 4.0 \log(Re\sqrt{f}) - 0.4 \qquad \textbf{3.10}$$

Blasius:

$$f = \frac{0.079}{Re^{0.25}} \qquad \textbf{3.11}$$

# Chapter 4   Amphosol PAM Results and Discussion:

## 4.1 Bench Scale

Bench Scale experiments were performed to determine the concentrations to be run at pilot plant scale. Surface tension, conductivity and relative viscosity measurements are presented in the following section. All bench-scale solutions were prepared in DI water with an average conductivity range of 2.0-4.0μS/cm. Please refer to Experimental Procedure (Chapter 3) for a detailed overview of the procedure.

### 4.1.1 Surface Tension:

Surface Tension measurements were taken for the PAM/Amphosol mixtures and compared to those for pure Amphosol. The PAM concentration was held constant at 50,100,200 and 500 ppm while the Amphosol concentration varied. PAM is not a surface active polymer. The results are presented below:
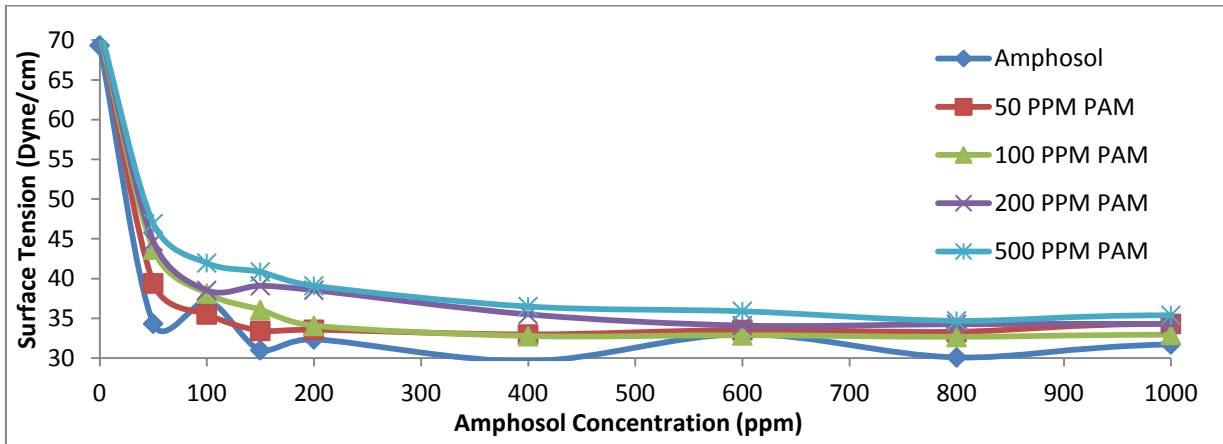


Figure 4.1 Surface Tension Vs. Amphosol concentration plots for Amphosol/PAM mixtures with pure Amphosol plot included.

Figure 4.1 above shows the CMC of pure amphosol to occur at approximately 50 ppm. The interaction between PAM and amphosol is seen to be weak and does not display the idealized curves for clear readings of the critical aggregation concentration and the polymer saturation point. A 2 factor ANOVA with replication was performed to confirm if the observed slight differences were statistically significant and the ANOVA table is presented below:

| ANOVA | | | | | | |
|---|---|---|---|---|---|---|
| *Source of Variation* | *SS* | *df* | *MS* | *F* | *P-value* | *F crit* |
| Polymer Concentration | 570.8736 | 4 | 142.7184 | 578.3039 | 7.3E-73 | 2.454213 |
| Surfactant Concentration | 18363.44 | 10 | 1836.344 | 7440.981 | 9.1E-151 | 1.917827 |
| Interaction | 305.4738 | 40 | 7.636844 | 30.94497 | 6.15E-44 | 1.504268 |
| Within | 27.14667 | 110 | 0.246788 | | | |
| | | | | | | |
| Total | 19266.93 | 164 | | | | |

Table 4.1 Table presents relevant quantities after ANOVA analysis of Surface Tension Data

Since the F value is larger than Fcritical the differences between polymer concentrations is statistically significant.
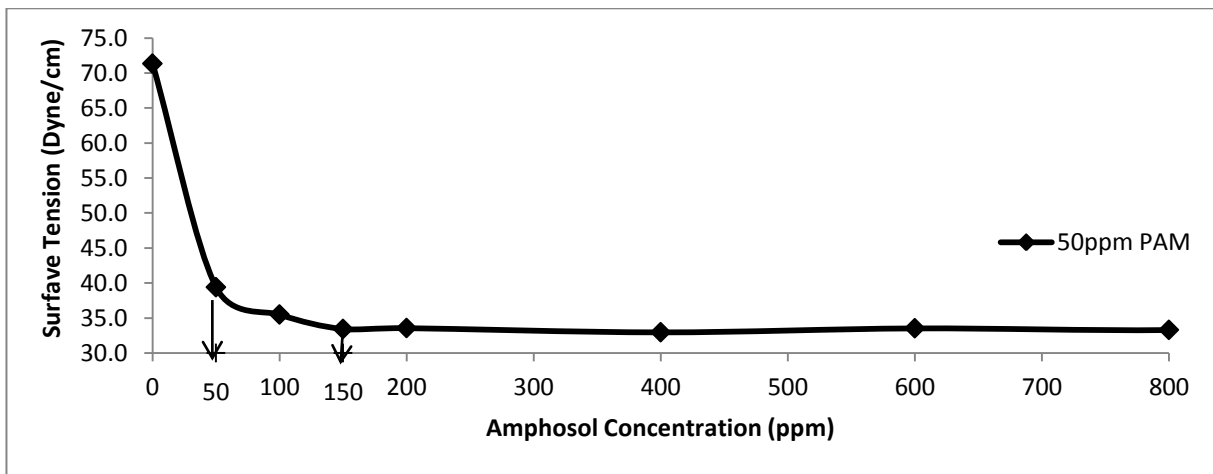


Figure 4.2 Surface Tension Vs. Amphosol concentration plot for PAM/Amphosol mixtures of 50ppm PAM and varying Amphosol concentrations
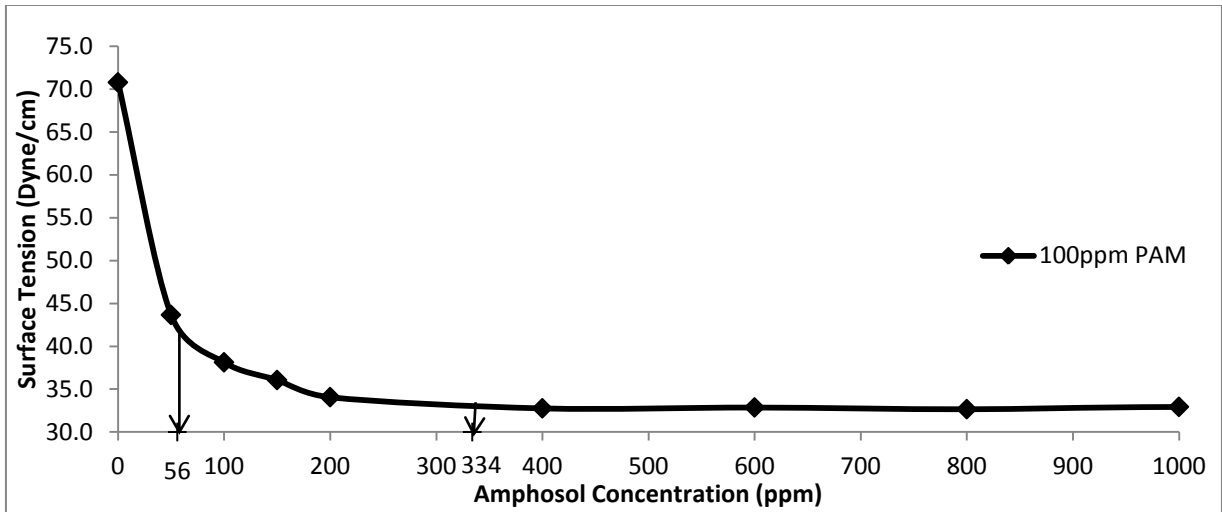
Figure 4.3 Surface Tension Vs. Amphosol concentration plot for PAM/Amphosol mixtures of 100ppm PAM and varying Amphosol concentrations
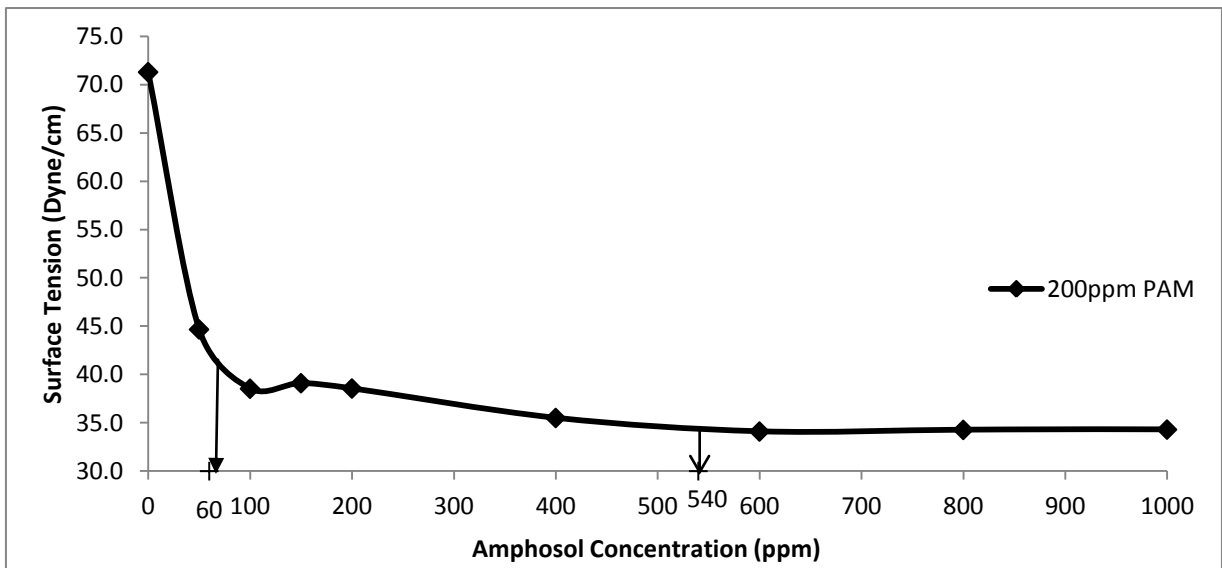


Figure 4.4 Surface Tension Vs. Amphosol concentration plot for PAM/Amphosol mixtures of 200ppm PAM and varying Amphosol concentrations
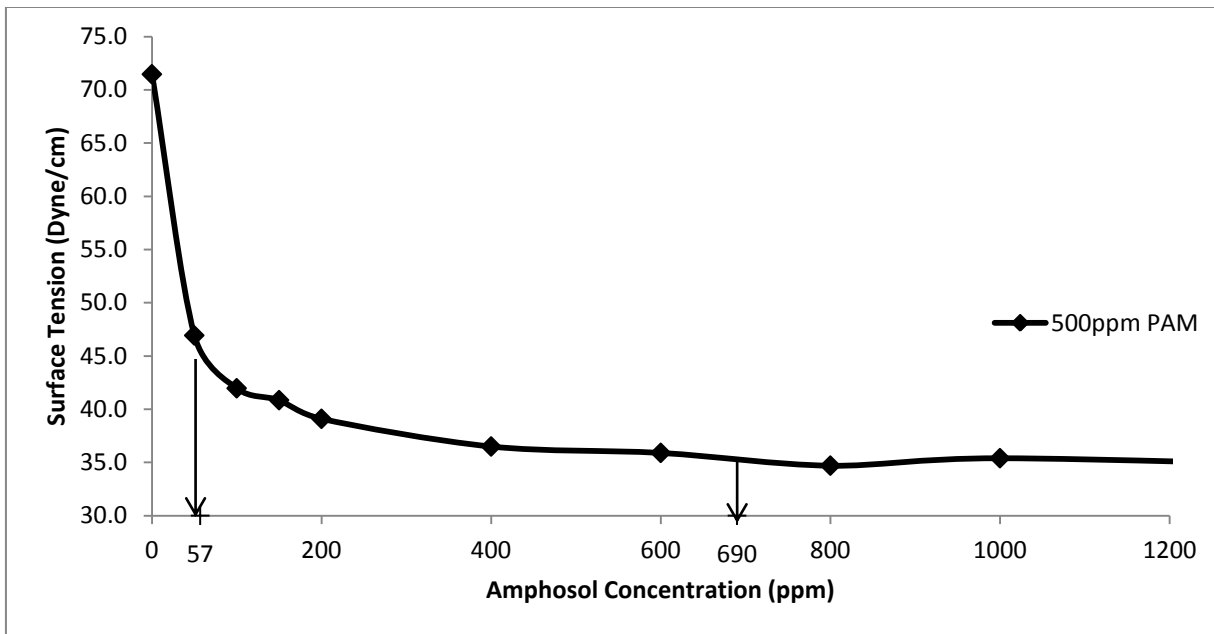
Figure 4.5 Surface Tension Vs. Amphosol concentration plot for PAM/Amphosol mixtures of 500ppm PAM and varying Amphosol concentrations

The first point marked is the critical aggregation concentration (CAC) where polymer-surfactant interaction first appears. The CAC occurs at the point of departure from the pure surfactant surface tension plots. It is the point at which the plot first diverges from that of the pure surfactant. The CAC is observed to be almost independent of the polymer concentration. From the figure we see the polymer-surfactant interaction is not strong enough to produce the plateau needed to clearly read the polymer saturation point, thus the point of free micellization formation in solution (T2) is marked instead. The point of free micellization formation (T2) occurs when surfactant forms free micelles in solution unattached to polymer. As such past this point there is no further decrease in surface tension and is clearly visible on the surface tension plots.  It is found that the point of free micelle formation is strongly dependent on polymer concentration.
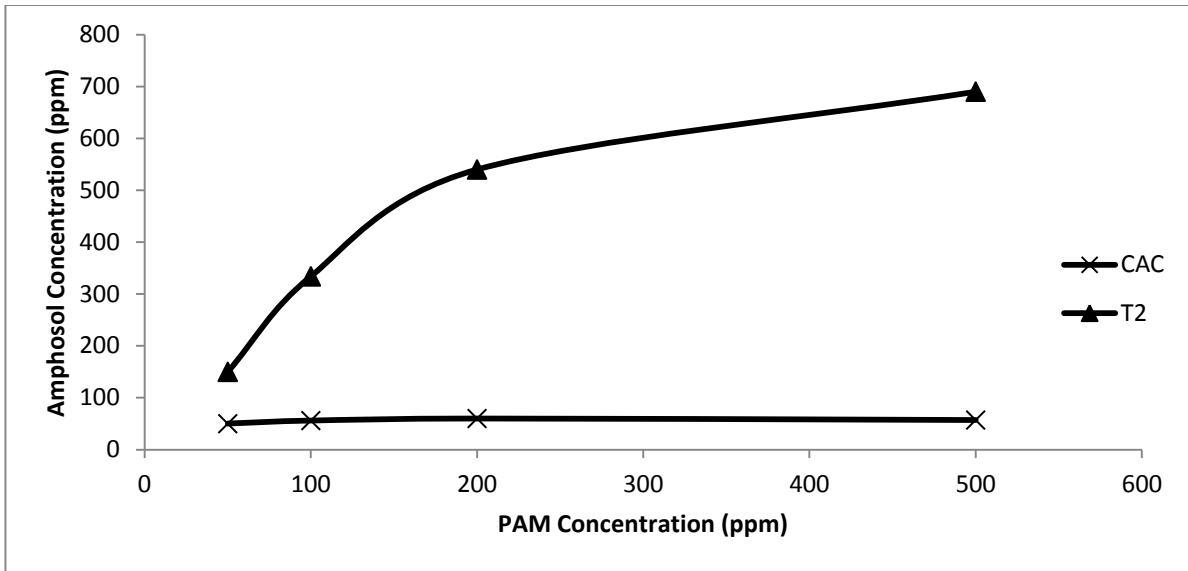
Figure 4.6 Amphosol Concentration of the CAC and Free Micellization points Vs. PAM concentration for various PAM/Amphosol mixtures

The graph shows the critical aggregation concentration to be independent of polymer concentration as previously mentioned. Also note the sudden change in slope of the free micellization point past 200 ppm PAM. This is attributed to the fact that the polymer begins to form a network at this concentration thus each polymer molecule presents less area for surfactant interaction and this decreases the slope observed.

## 4.1.2 Relative Viscosity:

As stated in the Experimental Procedure the Relative Viscosity is defined as the ratio of the time taken by tested solution through capillary viscometer to the time taken by water to pass through same section of the capillary viscometer.
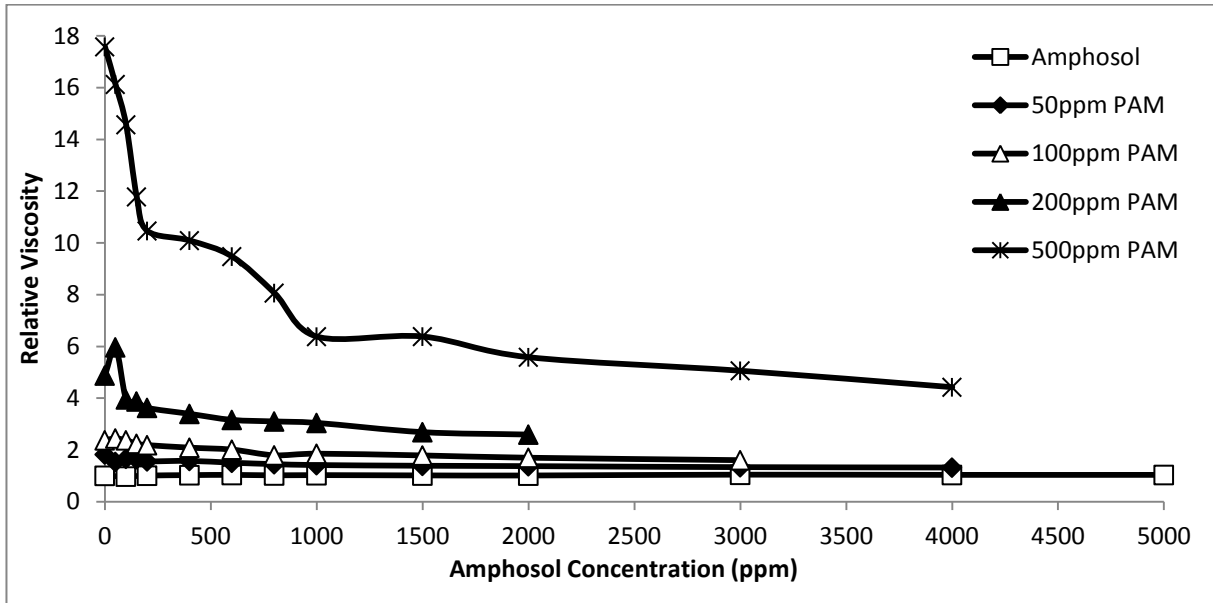


Figure 4.7 Relative Viscosity Vs. Amphosol Concentration plot for various Amphosol/PAM mixtures with pure Amphosol included
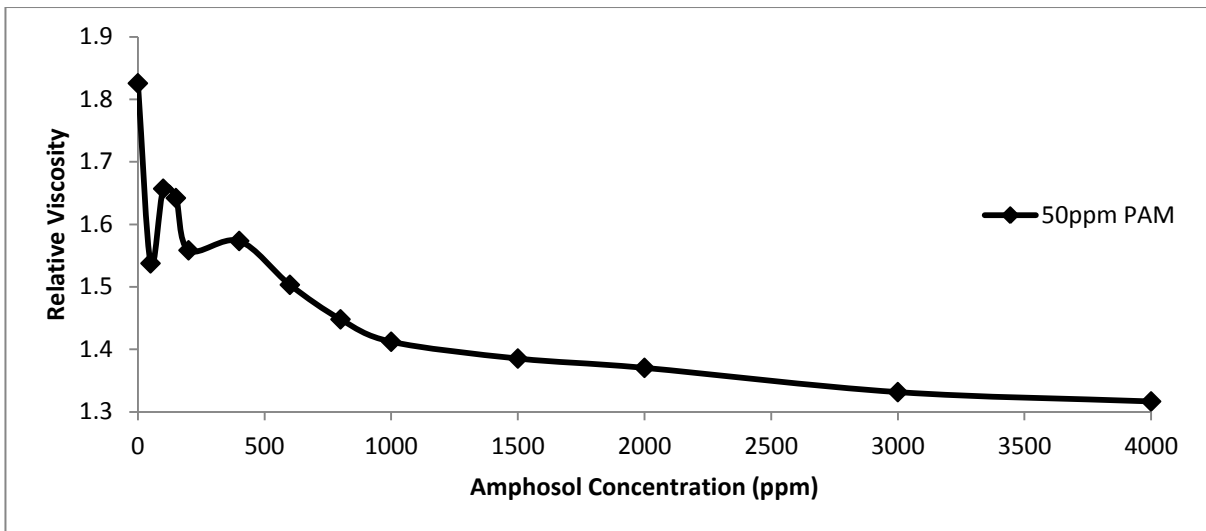


Figure 4.8 Relative Viscosity Vs. Amphosol Concentration for Amphosol/PAM mixture at 50ppm PAM and varying Amphosol concentrations

60
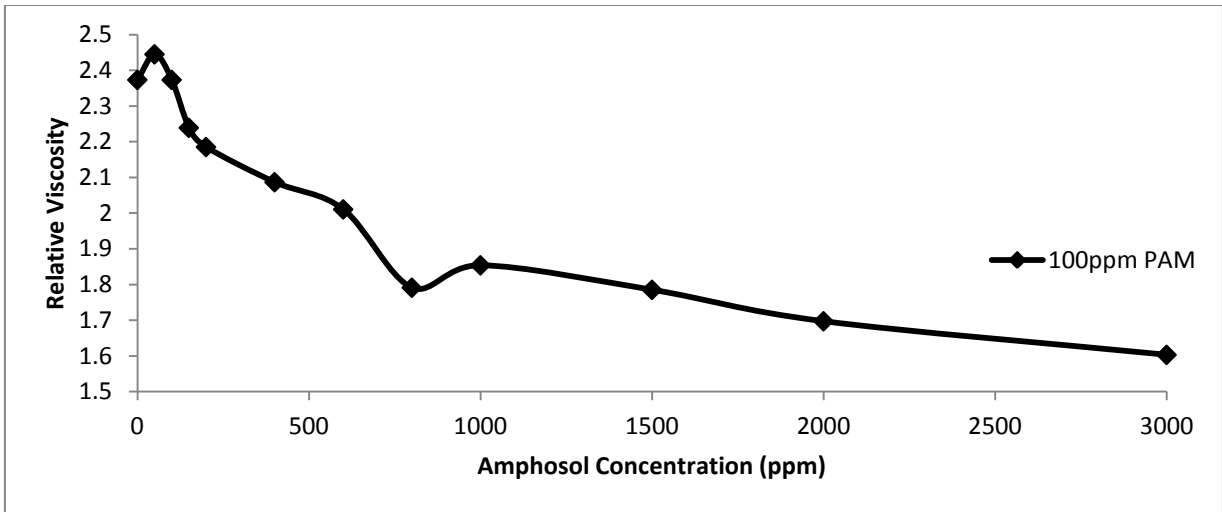
Figure 4.9 Relative Viscosity Vs. Amphosol Concentration for Amphosol/PAM mixture at 100ppm PAM and varying Amphosol concentrations
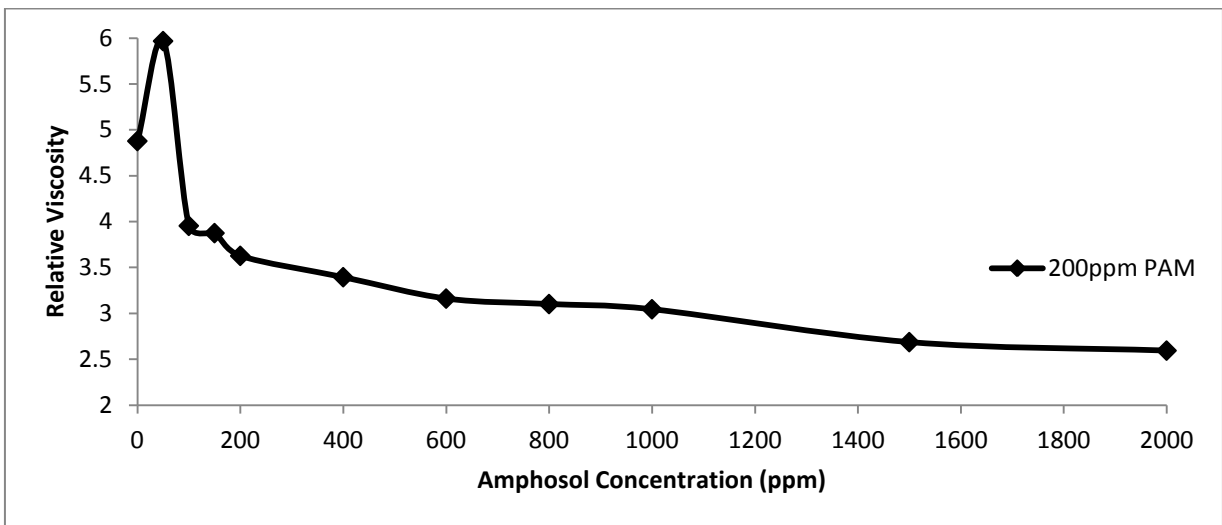


Figure 4.10 Relative Viscosity Vs. Amphosol Concentration for Amphosol/PAM mixture at 200ppm PAM and varying Amphosol concentrations
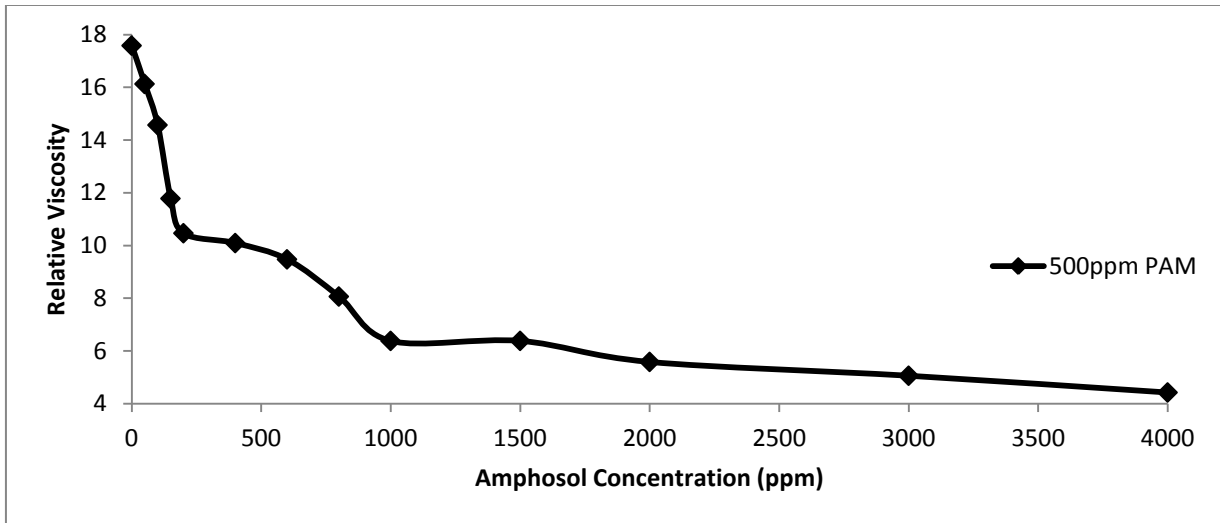
Figure 4.11 Relative Viscosity Vs. Amphosol Concentration for Amphosol/PAM mixture at 500ppm PAM and varying Amphosol concentrations

The relative viscosity of pure amphosol is not significantly affected by the amphosol concentration. The relative viscosity trend for PAM/Amphosol mixtures is separated into three groups as follows: low, intermediate and high polymer concentrations.

At low PAM concentrations (concentrations well below the network concentration of 170ppm) we observe that amphosol decreases the zero shear rate viscosity at all concentrations.

At intermediate PAM concentrations (concentrations around 170ppm) a viscosity peak is observed. The presence of amphosol seems to strengthen crosslinking between polymer molecules and increase the solution viscosity at first but this is followed by a decrease in viscosity at high surfactant concentration indicating that at high surfactant concentrations polymer crosslinking is negatively affected.

Finally at high PAM concentration (concentrations well above 170ppm) the viscosity is decreases for all levels of surfactant concentration. At high polymer concentration the polymer has already formed a network and any addition of surfactant only serves to disentangle and destroy crosslinks.

Shear Viscosity measurements were also taken, please see appendix A for further information.

### 4.1.3 Conductivity:
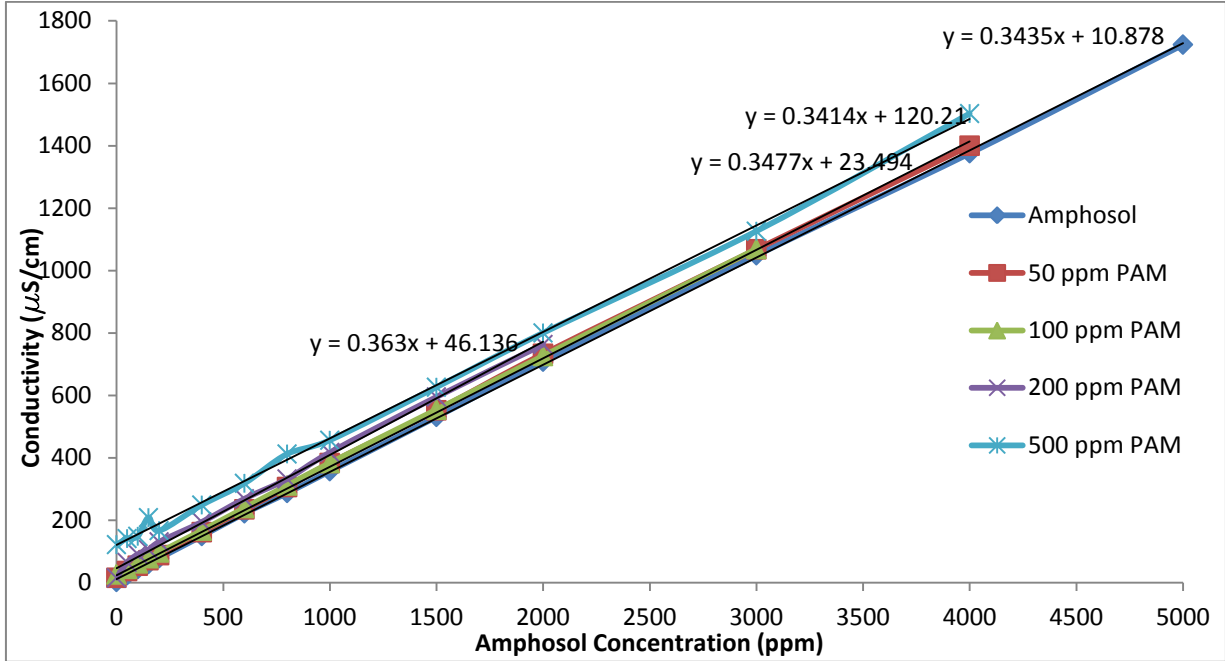


Figure 4.12 Conductivity Vs. Amphosol Concentration for Various Amphosol/PAM mixtures with pure Amphosol Included

For pure amphosol the change in slope that occurs at the CMC is not detectable. The idealized trend for polymer-surfactant interaction is not seen and the CAC or PSP are not identifiable. In fact linear trend lines are fit to the data and all have similar slopes regardless of polymer concentration with the only change between polymer groups occurring in the y intercept value.

## 4.2 Pilot-Plant Experiments

In the following section the concentrations that showed strong polymer/surfactant interaction at the bench scale are run through the flow loop to test the effect of surfactant on overall drag-reduction as well as its effect on solution degradation. In addition to this the effect of counter-ions on the drag reduction of pure PAM is tested. The Reynolds number used was the Generalized Reynolds Number defined as:

$$Re_G = \frac{\rho D^n V^{2-n}}{8^{n-1} K \left(\frac{3n+1}{4n}\right)^n} \qquad \textbf{4.1}$$

63

Where n and K are derived from the power law model for fluids. The generalized Reynolds number is used to prevent errors from assuming the solutions are Newtonian.

## 4.2.1 Effect of PAM/Amphosol Interaction on Drag Reduction

Fanning Friction Factor of PAM/Amphosol mixture and pure PAM for 2 hours of degradation against the Reynolds number are presented in figure 4.13. 100ppm Amphosol/200ppm PAM and PAM at 200 ppm were degraded in the flowloop for 2 hours results for ID 34.8mm and ID 22mm are presented.
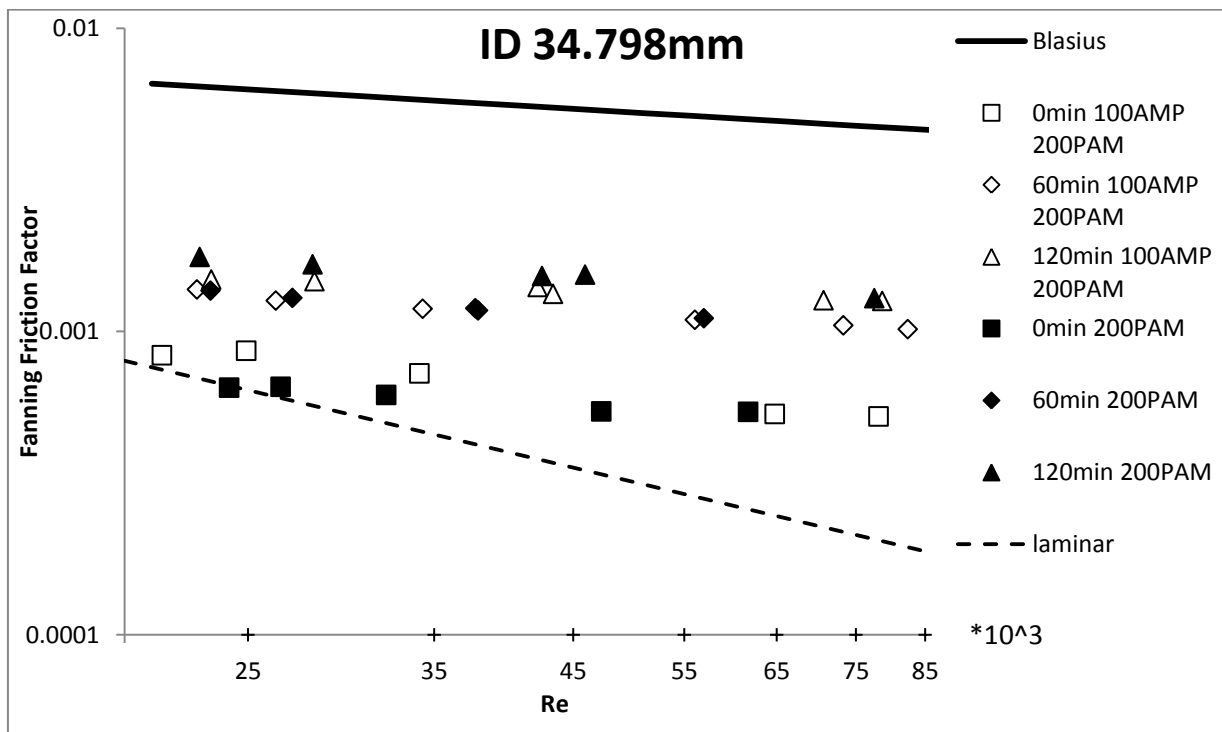


Figure 4.13 Fanning Friction Factor Vs. Generalized Reynolds number for 100ppm AMP/ 200ppm PAM mixture in 34.798mm Pipe with Measurements taken during 2 Hours of Degradation
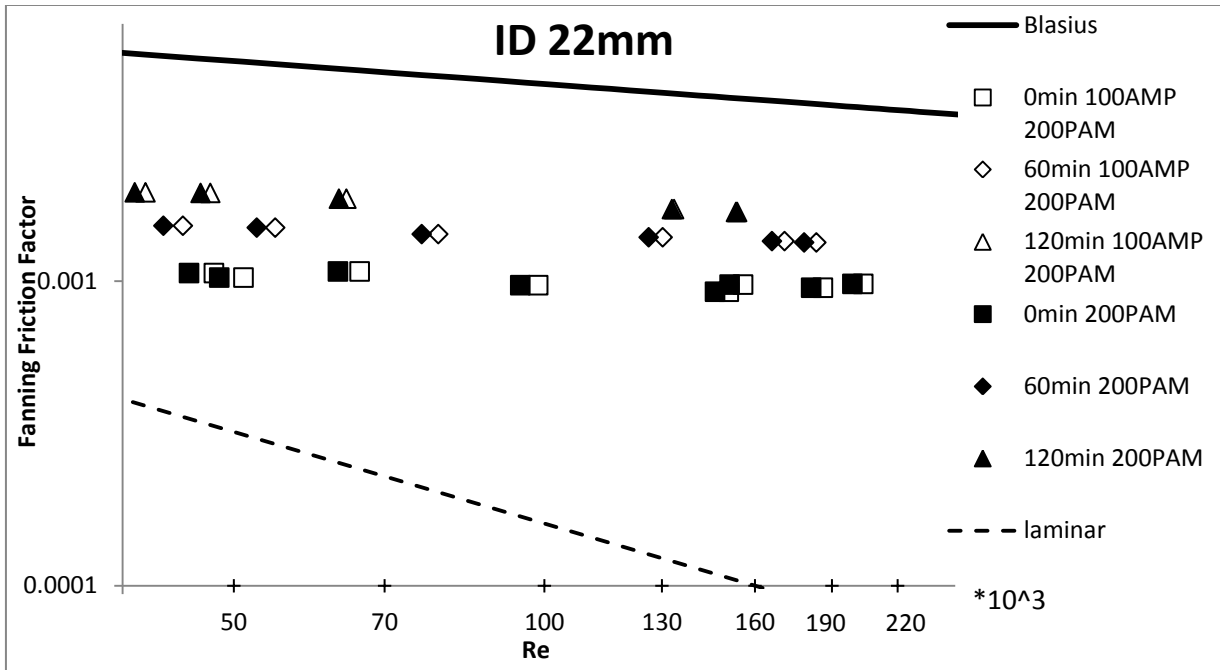
Figure 4.14 Fanning Friction Factor Vs. Generalized Reynolds number for 100ppm AMP/ 200ppm PAM mixture in 22mm Pipe with Measurements taken during 2 Hours of Degradation

Refer to Appendix A for further information on how Generalized Reynolds numbers were calculated. We observe that for pure PAM polymer the graph departs from the laminar line around 24000 Reynolds number, and this is in agreement with previous findings (Mohsenipour 2011). The polymer was degraded for 2 hours within the pump and selected data is presented above. We observe a much larger decrease in the first hour of degradation than in the subsequent hour. When Amphosol was added to solution no significant change was observed in either the initial drag reduction or to the effect degradation had on drag reduction.

## 4.2.2 Effect of Ionized water on PAM Drag Reduction

Fanning Friction Factor versus generalized Reynolds number for 200ppm PAM, 200ppm PAM/100ppm Amphosol mixture and 250 ppm PAM in Tap Water are presented below.
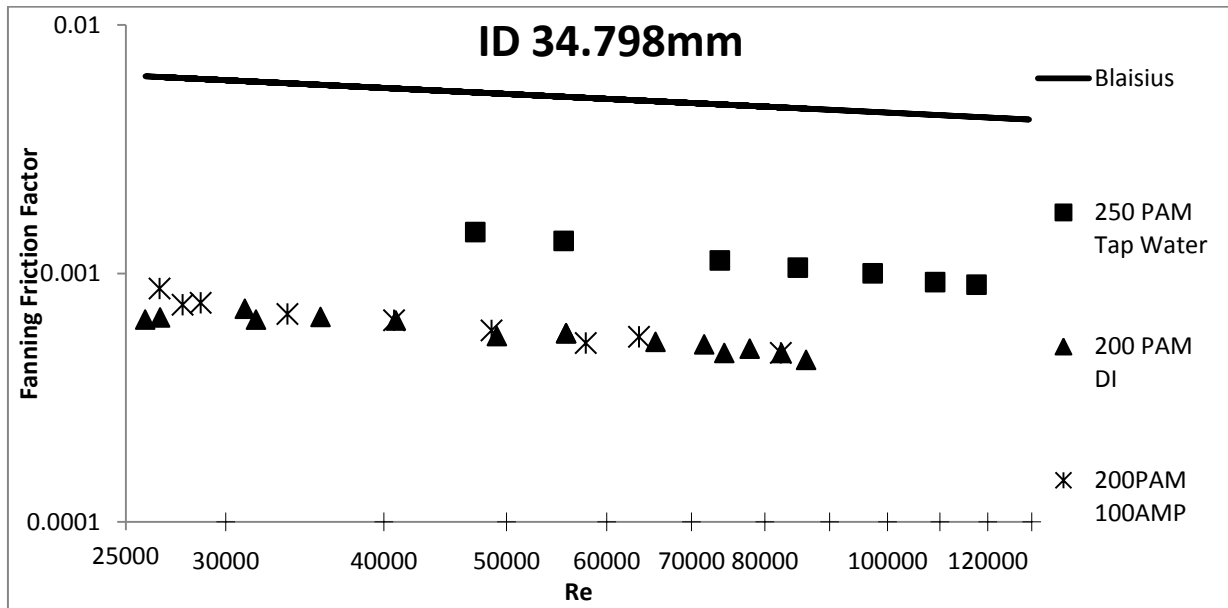


Figure 4.15 Fanning Friction Vs. Generalized Reynolds Number Comparison Between Pure 250ppm PAM in Tap water, Pure 200ppm PAM in DI Water and 200ppm PAM/100ppm Amphosol mixture in DI water in 34.798mm Internal Diameter Pipe
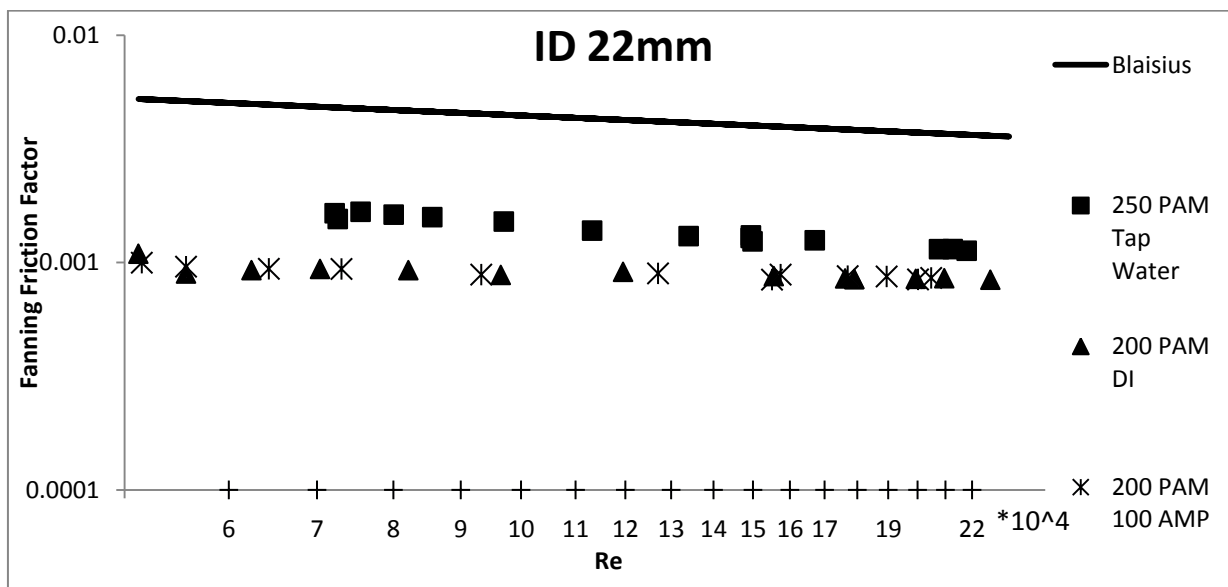


Figure 4.16 Fanning Friction Vs. Generalized Reynolds Number Comparison Between Pure 250ppm PAM in Tap water, Pure 200ppm PAM in DI Water and 200ppm PAM/100ppm Amphosol mixture in DI water in 22mm Internal Diameter Pipe

PAM at 250ppm in tap water produces less drag reduction than 200ppm PAM in deionized water. PAM molecules are believed to coil in the presence of ions in the tap water and this causes a decrease in drag reduction.

## 4.3 Conclusions

- The critical aggregation concentration for PAM/Amphosol is independent of polymer concentration
- The point of free micellization formation is strongly dependent on polymer concentration and the polymer concentration's effect decreases past the overlap concentration
- 200ppm PAM/100ppm Amphosol shows no increase in degradation time or achieved drag reduction level when compared to pure 200ppm PAM solution
- PAM and PAM/Amphosol mixtures experience larger drop in drag reduction during the first hour of degradation compared to the subsequent hour
- 250ppm PAM in tap water shows less drag reduction than 200ppm PAM in DI water.

# Chapter 5   Amphosol PEO Results and Discussion:

## 5.1 Bench-Scale PEO/Amphosol Results

Bench Scale experiments were performed to determine the strength of interaction between Amphosol and PEO. Surface tension, viscosity and conductivity measurements were performed and the results are presented below.

### 5.1.1 Surface Tension:

Surface tension measurements were taken to determine the PSP and CAC of the PEO/Amphosol mixtures. The polymer concentrations were held constant at 100,200,500 and 1000ppm PEO while varying the amphosol concentration. Though PEO is a surface active molecule this did not present any additional complexity as the minimum surface tension for PEO is approximately 62 dyne/cm while that of Amphosol is approximately 32 dyne/cm. The results are presented below:
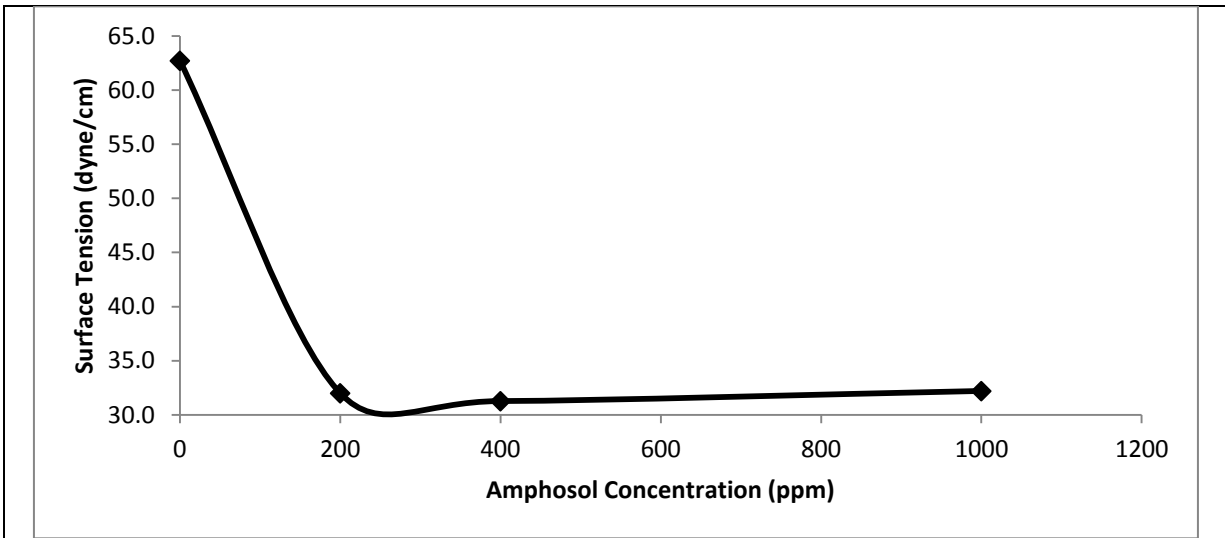
Figure 5.1 a) Surface Tension vs. Amphosol Concentration for 100 ppm PEO solution
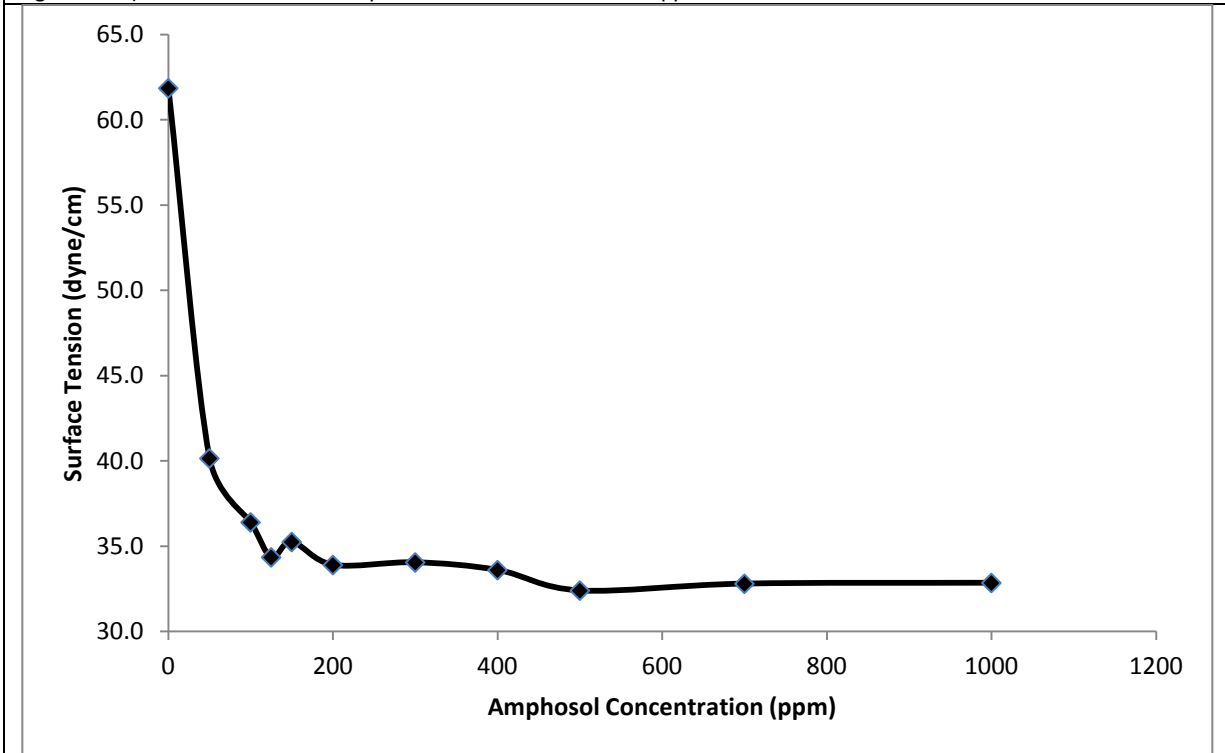


Figure 5.1 b) Surface Tension vs. Amphosol Concentration for 200 ppm PEO solution
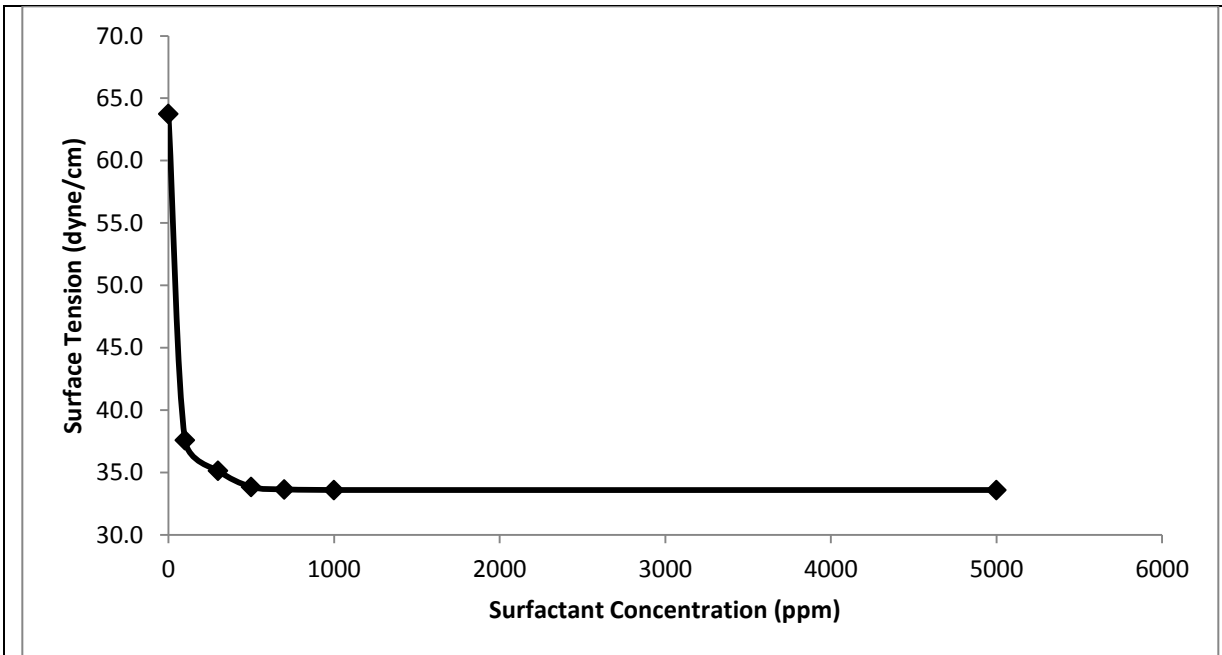
Figure 5.1 c) Surface Tension vs. Amphosol Concentration for 500 ppm PEO solution
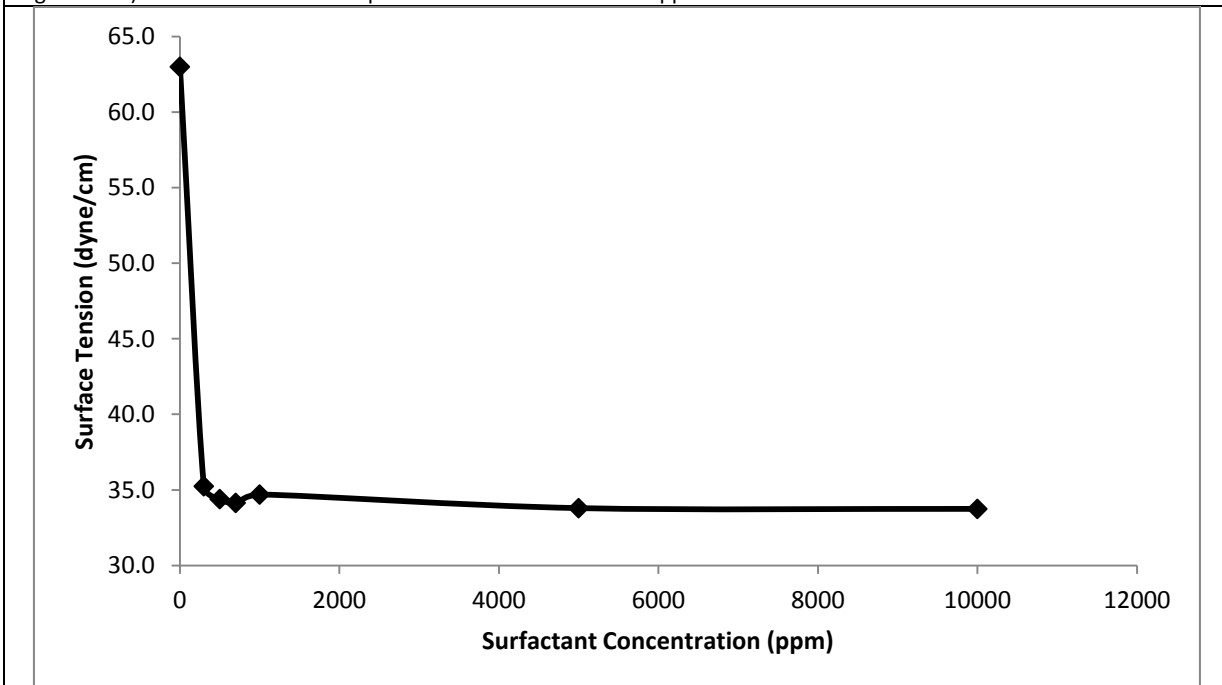


Figure 5.1 d) Surface Tension vs. Amphosol Concentration for 1000 ppm PEO solution

Figure 5.1 Surface Tension vs. Amphosol Concentration plots for various PEO concentrations

The Du Nouy ring tensiometer was incapable of picking up the PSP or the CAC of the polyethylene/amphosol mixtures for all concentrations of polymer ranging from 100 to 1000 ppm PEO. Instead we observe a sudden drop in surface tension similar to that of pure Amphosol with a new starting point of 62 dyne/cm due to the presence of PEO. No deviation

from the pure surfactant profile could be detected. This is our first indication that the interaction between polyethylene oxide and amphosol is weak.

## 5.1.2 Relative Viscosity:

Relative Viscosity measurements were performed to determine the effect of amphosol on solution viscosity, the results are presented below:
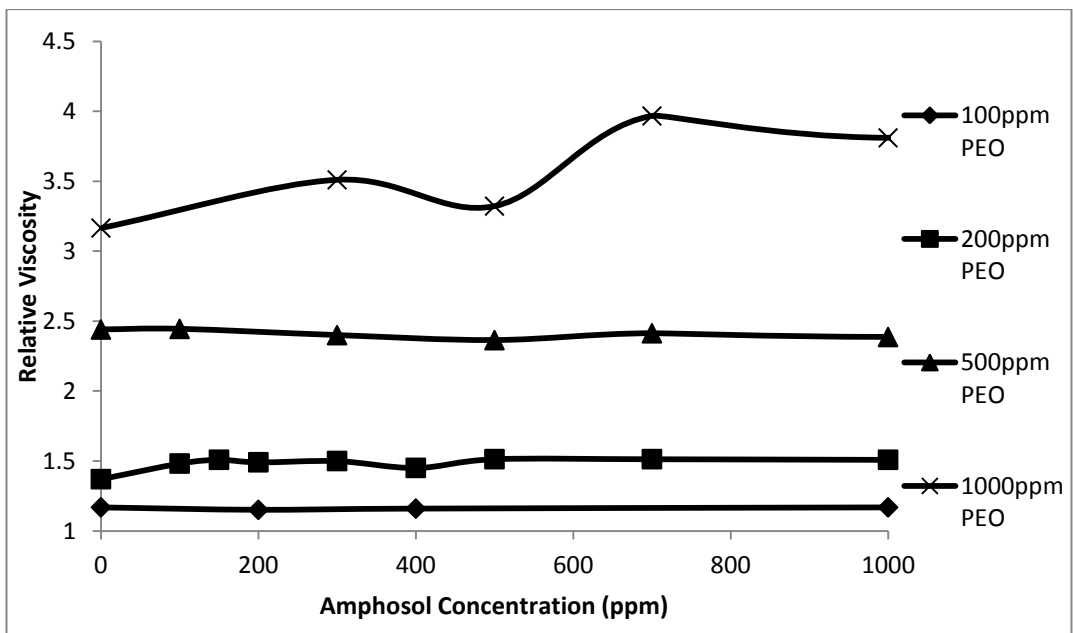


Figure 5.2 Relative Viscosity vs. Amphosol Concentration for 100ppm to 1000ppm PEO concentrations

Amphosol has no significant effect on relative viscosity for low concentrations of PEO. Since the PEO molecules are far apart at this low concentration it is unlikely any crosslinking reinforcement occurs due to the presence of surfactant.

Around the overlap concentration C* (approximately 1550ppm in deionized water (Mohsenipour 2011)) relative viscosity increases with Amphosol concentration, indicating amphosol reinforces cross linking between polymer molecules. At 1000ppm PEO in the 0ppm to 1000ppm Amphosol range no peak in relative viscosity was observed, instead a dip followed by a further increase in viscosity was observed. Refer to Appendix B for further information regarding viscosity measurements.

## 5.1.3 Conductivity

Conductivity measurements were taken for 100,200,500 and 1000ppm PEO with varying amphosol concentrations to determine if and interaction could be detected. The results are shown below:
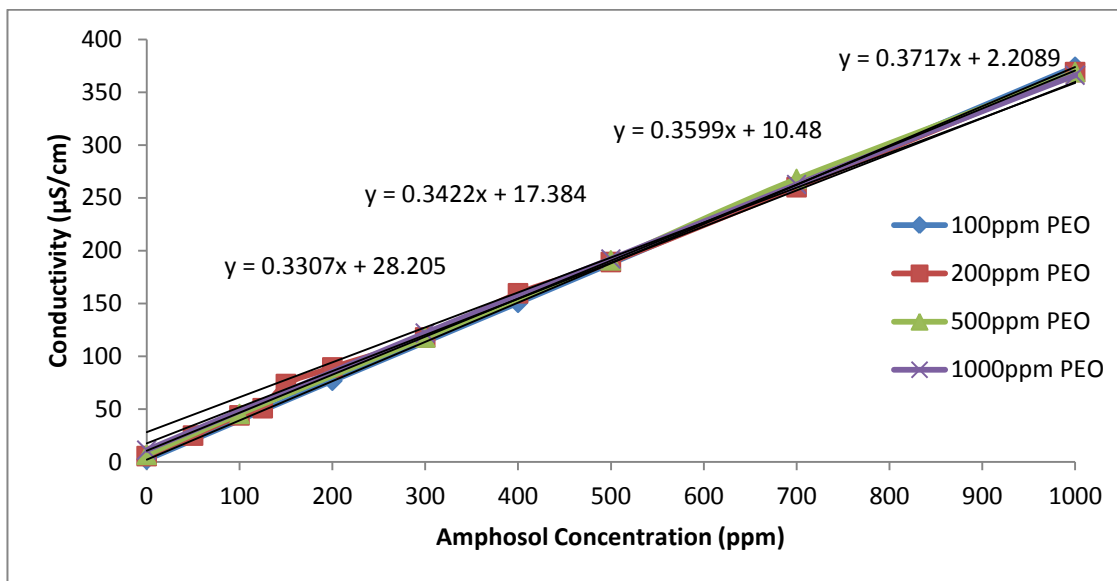


Figure 5.3 Conductivity vs. Amphosol Concentration for 100-1000ppm PEO Concentrations

Amphosol did not show a change in slope to display its PSP and CAC, instead all concentrations of PEO tested showed linear behavior of conductivity with respect to Amphosol Concentration. The slope of the conductivity graphs did decrease with increasing polymer concentration, indicating there is some interaction between polymer and surfactant. The difference in conductivity readings between polymer concentrations is minuscule however. Figure 5.4 is a graph of the conductivity slopes from figure 5.3 against the PEO concentration. The slopes physical meaning is the rate of increase of conductivity with Amphosol concentration. Smaller slopes represent less mobile amphosol which indicates polymer/surfactant interaction.
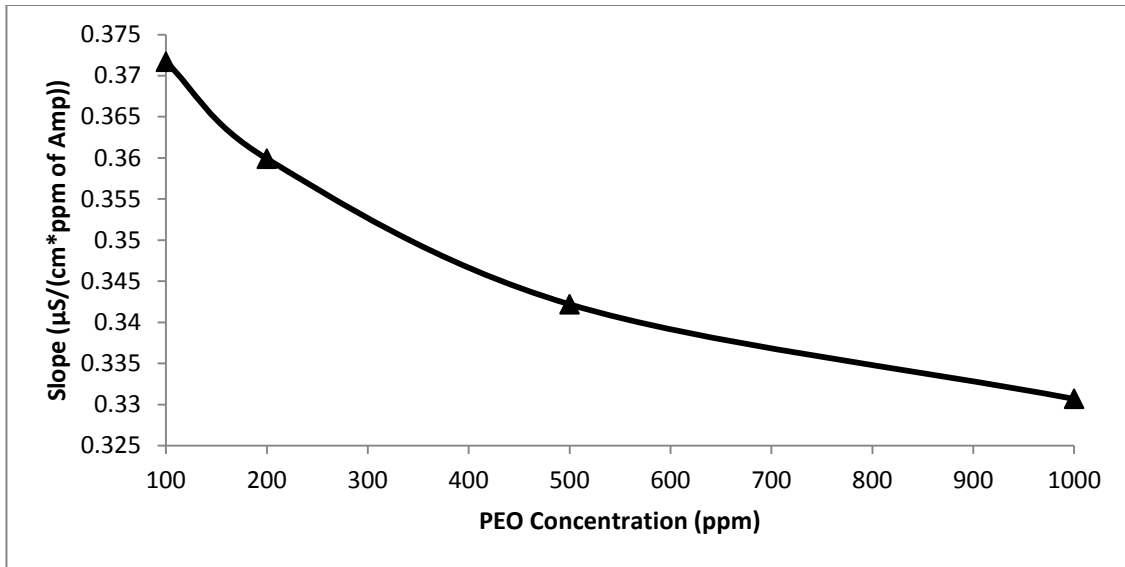
Figure 5.4 Rate of increase of conductivity with respect to Amphosol Concentration vs. PEO concentration

The graph above shows the curve of the rate of increase of conductivity with respect to Amphosol concentration versus PEO concentration, it is a plot of the slopes from figure 5.3 against PEO concentration. We observe a decrease in slope with increasing PEO concentration. This implies amphosol mobility decreases with increasing PEO concentration. Stated alternatively amphosol/PEO interaction increases with increasing PEO concentration. Note that an increase in PEO concentration has the strongest effect on the conductivity slope for low PEO values. The slope appears to reach a constant as the PEO concentration reaches its overlap concentration. This suggests that once the PEO molecules start forming a network there is less room for amphosol to attach to PEO molecules and reinforce cross-linking

## 5.2 Drag Reduction PEO/Amphosol Results

In the following section concentrations that showed possible positive interaction based off bench-scale results were run through the flow-loop. 1000ppm PEO and 1000ppm PEO/700ppm Amphosol was run through the loop and degraded for 5 hours the results are presented below.

### 5.2.1 Effect of PEO/Amphosol Interaction on Drag Reduction

In the following figures the fanning friction factor is plotted against the generalized Reynolds number for pure 1000ppm PEO and 1000ppm PEO/700 ppm Amphosol mixture with values shown before degradation after 3, 4 and 5 hrs of degradation. Consult Appendix B for further information
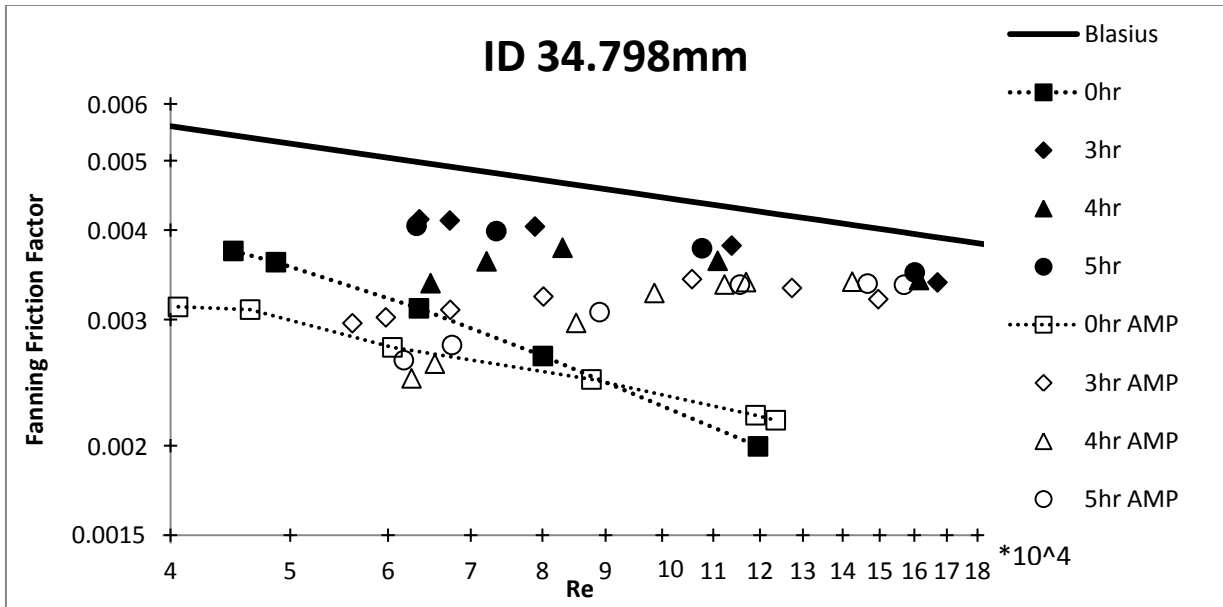
Figure 5.5 a) Fanning friction factor vs. Reynolds Number in 34.798mm inner diameter pipe for 1000ppm PEO and 1000ppm PEO/700 ppm Amphosol Solution
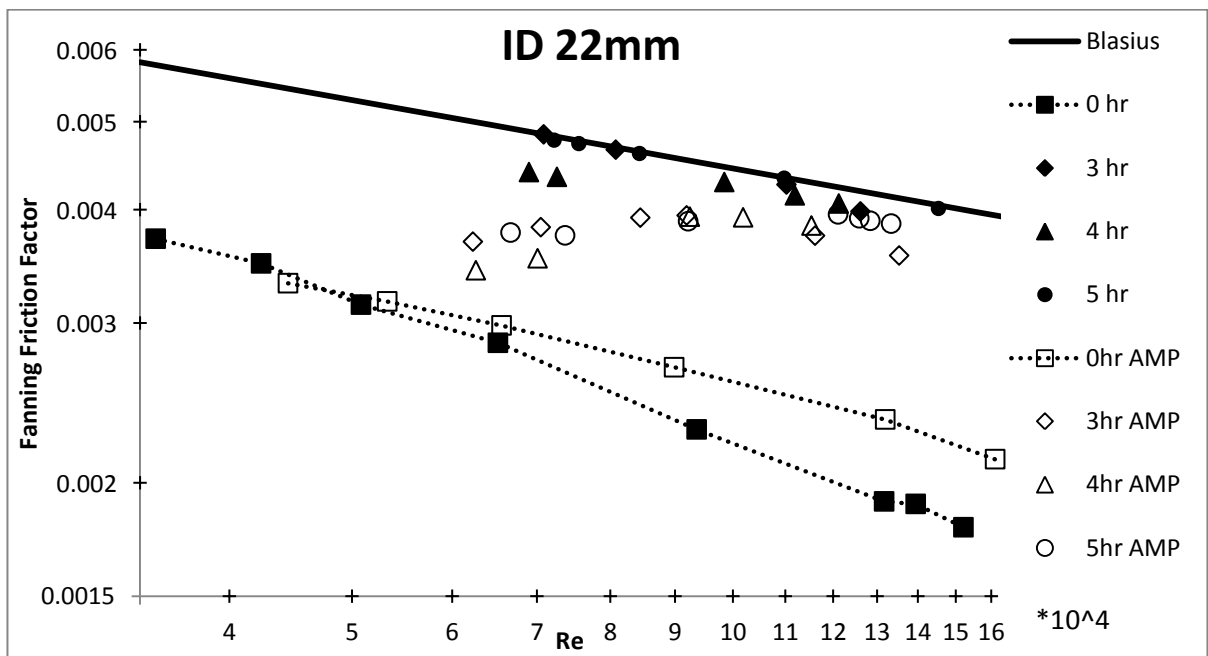


Figure 5.5 b) Fanning friction factor vs. Reynolds Number in 22mm inner diameter pipe for 1000ppm PEO and 1000ppm PEO/700 ppm Amphosol Solution

Figure 5.5 above shows the drag reduction achieved at 1000ppm PEO without and in the presence of 700ppm Amphosol as well as the effect of degradation. The bench scale showed little interaction between Amphosol and PEO at these concentrations and this is evident as the pure PEO and PEO/Amphosol mixture show similar levels of drag reduction with no degradation. However, the presence of Amphosol does have a positive effect on drag reduction after degradation. Figure 5.6 below elucidates this point
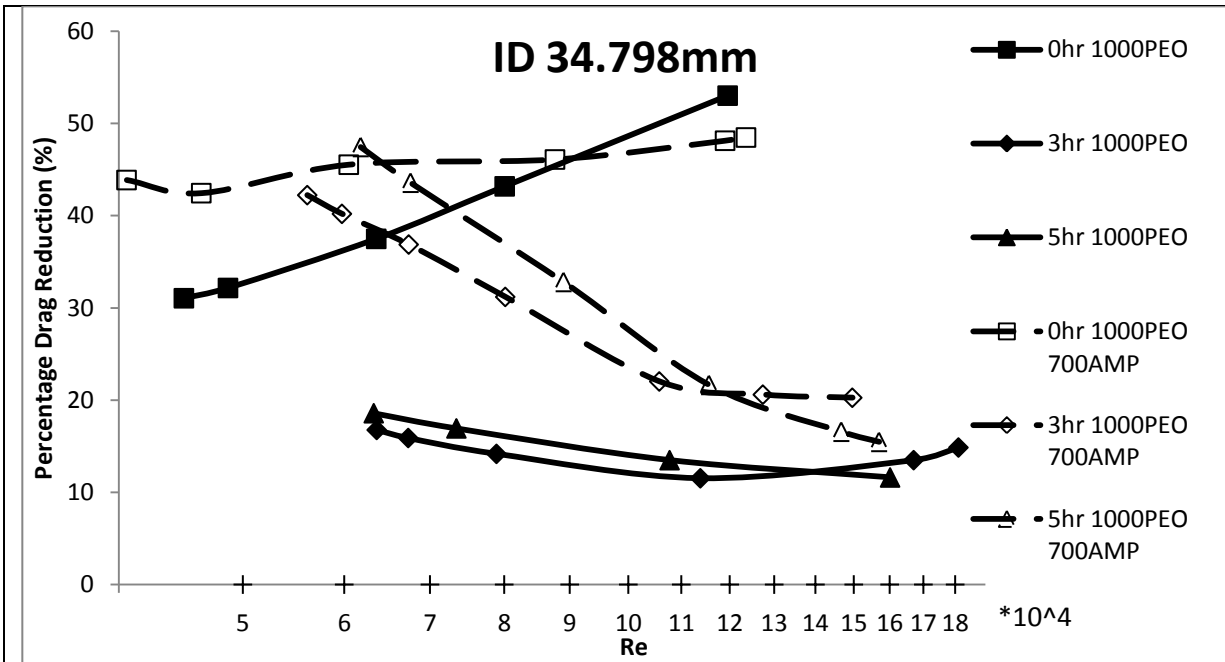
Figure 5.6 a) Percent Drag Reduction vs. Reynolds number for 1000ppm PEO and 1000ppm PEO/700 ppm Amphosol Solution at Different Degradation times in a 34.798mm Internal Diameter Pipe
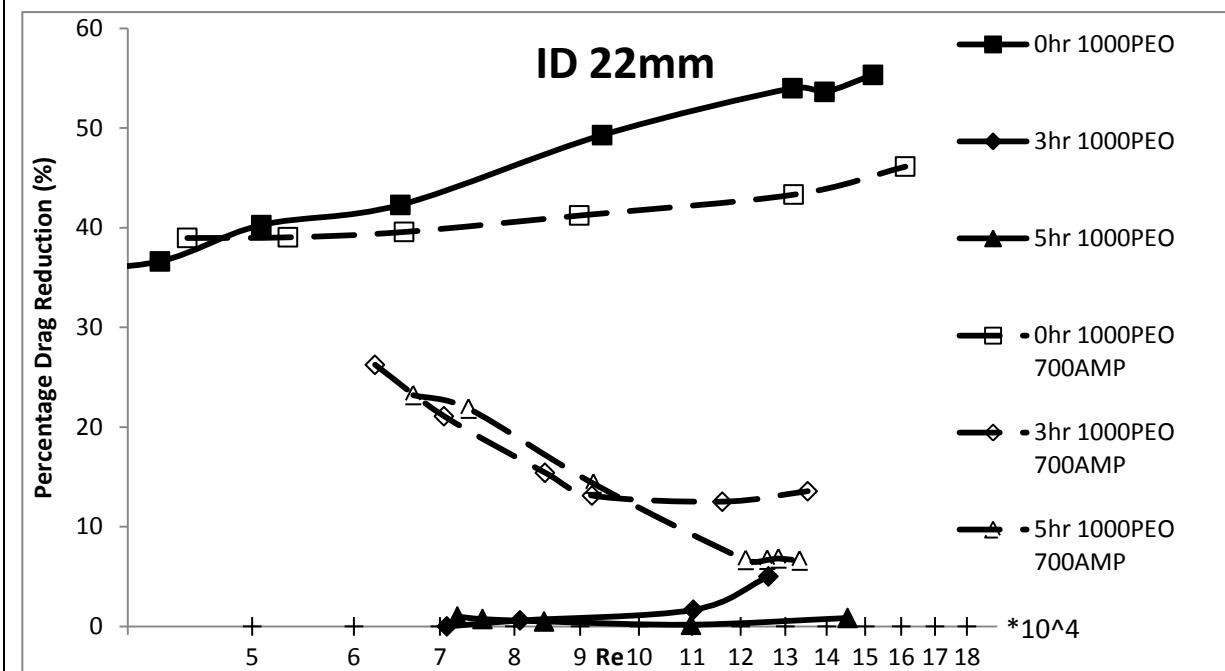


Figure 5.6 b) Percent Drag Reduction vs. Reynolds number for 1000ppm PEO and 1000ppm PEO/700 ppm Amphosol Solution at Different Degradation times in a 22mm Internal Diameter Pipe

Figure 5.6 Percent Drag Reduction vs. Reynolds number for 1000ppm PEO and 1000ppm PEO/700 ppm Amphosol Solution at Different Degradation times for 2 Pipe Sizes

As before we see that when there is no degradation both the pure polymer and the polymer/surfactant mixture show similar drag reduction profiles but a clear difference

appears after 3 hours of degradation. This suggests that at the start the PEO is primarily responsible for drag reduction in both cases but as PEO is rapidly degraded the influence of Amphosol on drag reduction plays an increasingly important role. After degradation Amphosol is the primary drag reducing agent especially at low Reynolds numbers where the micelles are still intact.

Since the interaction between PEO and Amphosol is weak the discrepancy in %DR cannot be attributed to an interaction but is instead credited to the Amphosol drag reduction acting alone and independent of PEO. This is further supported by the fact that initially when no PEO degradation has taken place there is little difference in %DR values between the pure polymer and the polymer/surfactant mixture, differences in %DR occur after degradation of the polymer allowing surfactant micelles to play a larger role in drag reduction. At 700ppm Amphosol the surfactant micelles are large enough to cause drag reduction unlike the previously seen 100ppm concentration of Amphosol in the previous chapter. For pure PEO %DR is observed to increase with Reynolds number when there is no degradation and is approximately constant once degradation has occurred. An increase in drag reduction with increasing Reynolds number suggests PEO expands with the increasing stress and causes an increase in drag reduction, but after degradation occurs the polymer chains have been scissioned into smaller chains which are already fully extended in the Reynolds range tested.

Surfactant micelles can break apart in high shear zones (such as within the pump) but reassemble thus they experience reversible degradation. Notice that for the PEO/Amphosol mixture as the Reynolds number increases the percentage drag reduction decreases dramatically and approaches the %DR of pure PEO solution for similar degradation times. This is attributed to the breakup of the micelles in high shear zones as the Reynolds number increases. After PEO degradation we observe a distinct profile for the PEO/Amphosol mixture. The PEO/Amphosol %DR vs. Reynolds number profile appears to be fit by 2 separate lines. A possible explanation for this is that at low Reynolds numbers the surfactant micelles are causing drag reduction but past the critical shear stress the micelle breaks apart and the polymer takes over as the drag reducing agent. Thus the first line fit describes the surfactant drag reducing section while the second line describes the degraded polymer drag reducing section after the surfactant micelles have broken apart. In figure 5.7 below the points where these changes occur are marked with red data points. Through this method we can determine the critical shear stress required to break apart the surfactant micelle.
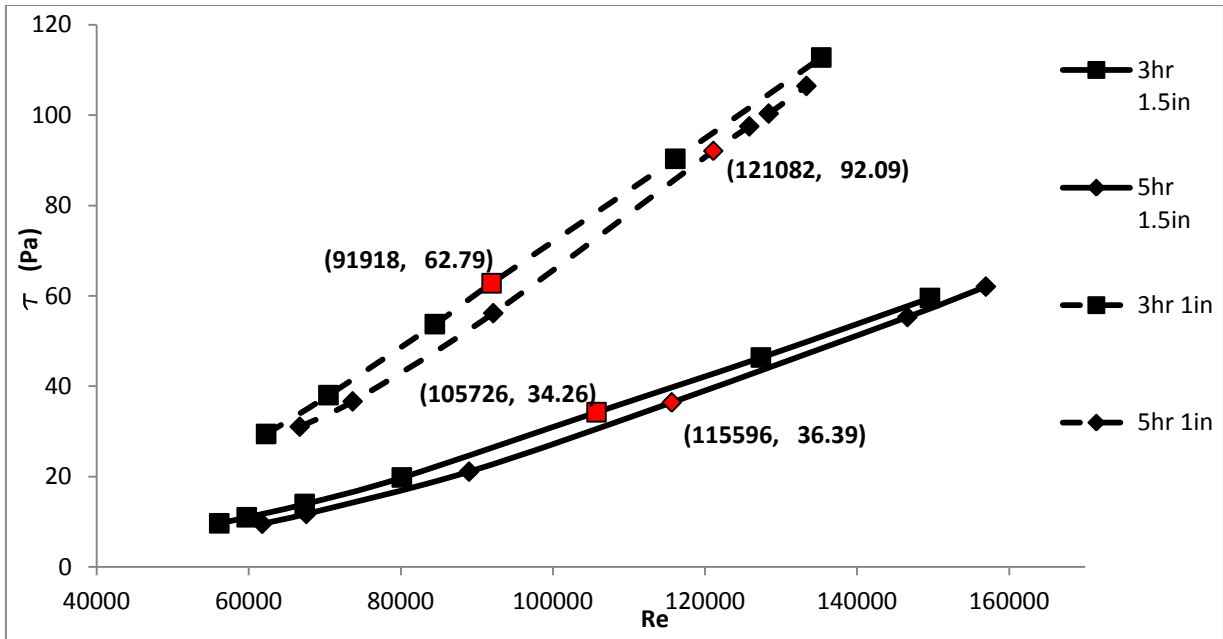
Figure 5.7 Shear Stress vs. Reynolds number for 1000ppm PEO/700ppm Amphosol solution after 3 hours and 5 hours of degradation for the 34.8mm internal diameter and the 22mm internal diameter pipes

Figure 5.7 above marks the Reynolds numbers where the slope changes appear for %DR vs. Reynolds number and shows the associated critical shear stress values. For the 1.5 inch pipe we observe that the critical shear stress is approximately constant and independent of degradation time. This suggests that the drag reduction observed is surfactant produced and independent of the polymer. The 1 inch pipes data points are spaced out too far apart to draw the same conclusion.

## 5.3 Conclusions

- Viscosity measurements show increased PEO/Amphosol interaction at overlap concentration 1550ppm PEO
- Undegraded PEO molecules undergo extension under increased stress with increasing Reynolds number leading to an increase in percent drag reduction
- PEO undergoes the largest amount of degradation and subsequently the largest drag reduction drop in the first hour when the chains are longest
- Presence of 700ppm Amphosol in 1000ppm PEO slows down degradation and increases percent drag reduction after polymer degradation has occurred, this is particularly evident at low Reynolds numbers
- At high Reynolds numbers the Amphosol surfactant micelle deteriorates and percent drag reduction approaches that of the pure polymer

# Chapter 6   PAM/PEO Results and Discussion:

## 6.1 Bench-Scale of PAM/PEO Results

Surface tension, conductivity and relative viscosity measurements were taken to determine the concentrations at which PAM and PEO had strong interaction levels. Typically surface tension and conductivity are not used to detect polymer-polymer interaction but as PEO is a surface active polymer and the version of PAM used is anionic an exploitive opportunity is present. Experiments were carried out on solutions of 100ppm and 200ppm PAM with varying PEO concentration.

### 6.1.1 Surface Tension

Surface tension measurements were taken to determine the concentrations of PEO and PAM at which the strongest interaction occurs. The PAM polymer concentration was held constant at 100ppm and 200ppm while varying the PEO concentration. PEO is a surface active polymer with a minimum surface tension of 62 dyne/cm which allows for the possibility of measuring polymer-polymer interaction if the interaction occurs before the minimum surface tension is reached. The results are presented below:
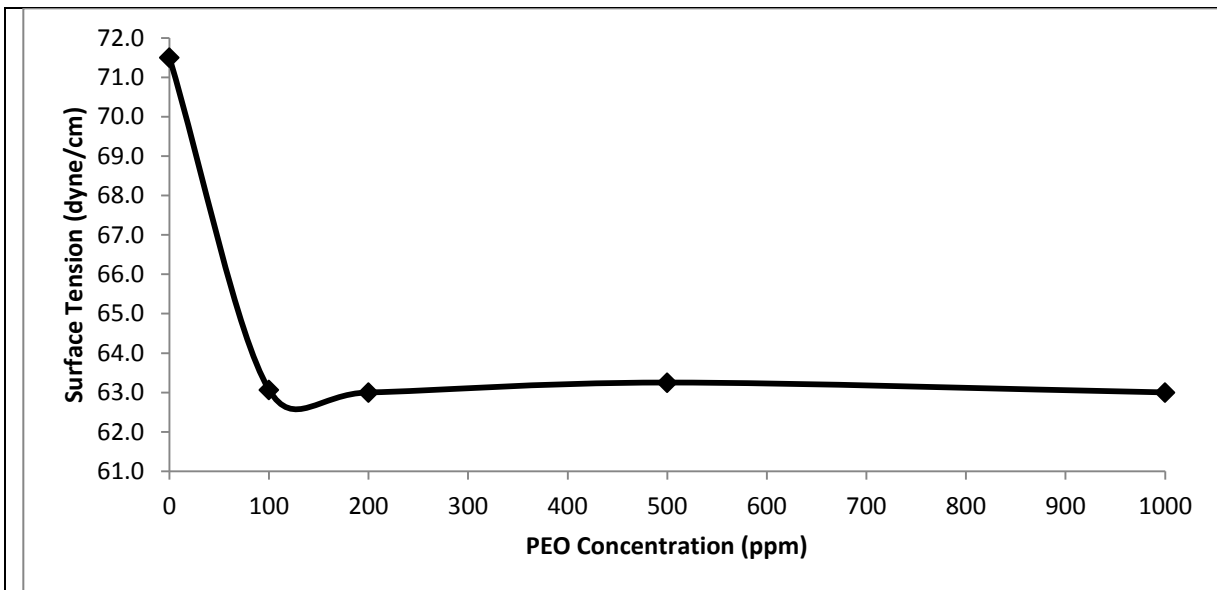
Figure 6.1 a) Surface Tension vs. PEO Concentration for 100 ppm PAM solution
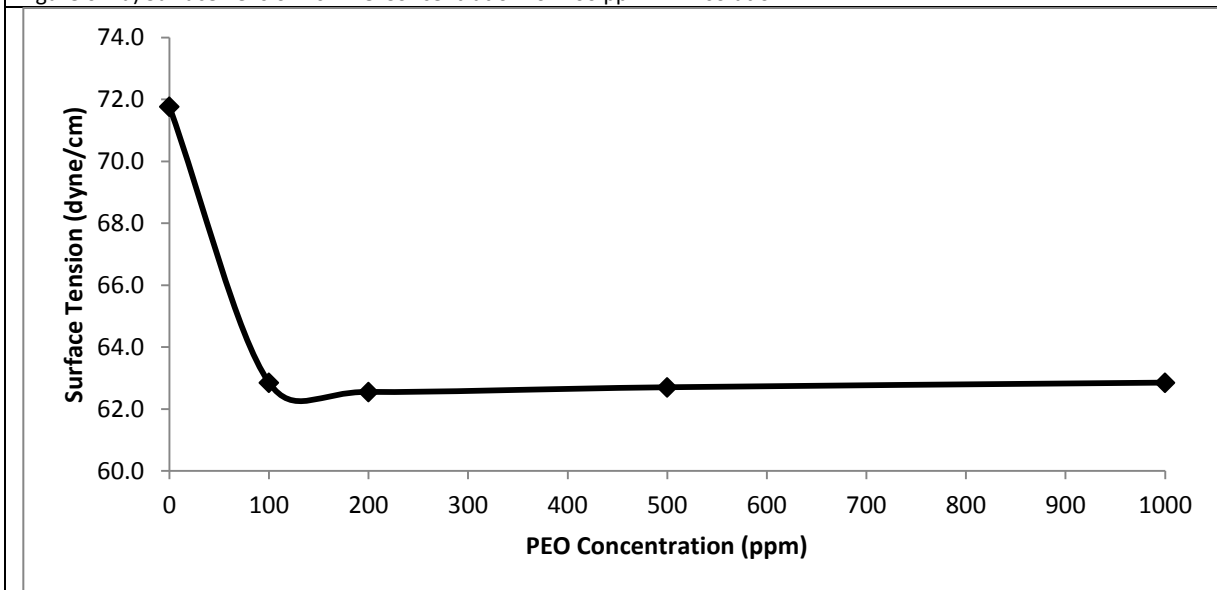


Figure 6.1 b) Surface Tension vs. PEO Concentration for 200 ppm PAM solution

Figure 6.1 Surface Tension Plots for 100ppm and 200ppm PAM under varying PEO Concentrations

PAM is not a surface active molecule and does not cause a decrease in surface tension with increasing polymer concentration. However PEO is surface active and drops the surface tension to approximately 63 dyne/cm after which no further decrease is observed. This minimum surface tension is achieved at 100ppm PEO and thus any PAM/PEO interaction that occurs past this point is not detectable by this method. No interaction can be observed from the surface tension measurements taken. Surface tension measurement is rarely used to detect polymer-polymer interactions.

## 6.1.2 Relative Viscosity

Relative viscosity is defined as the ratio of the time taken by the tested solution to pass through a marked section of the Ubbelohde Viscometer to time it take pure water to pass through the same section of the viscometer. Presented below are the relative viscosities of PAM/PEO mixtures at various PEO concentrations along with the relative viscosity of pure PEO.
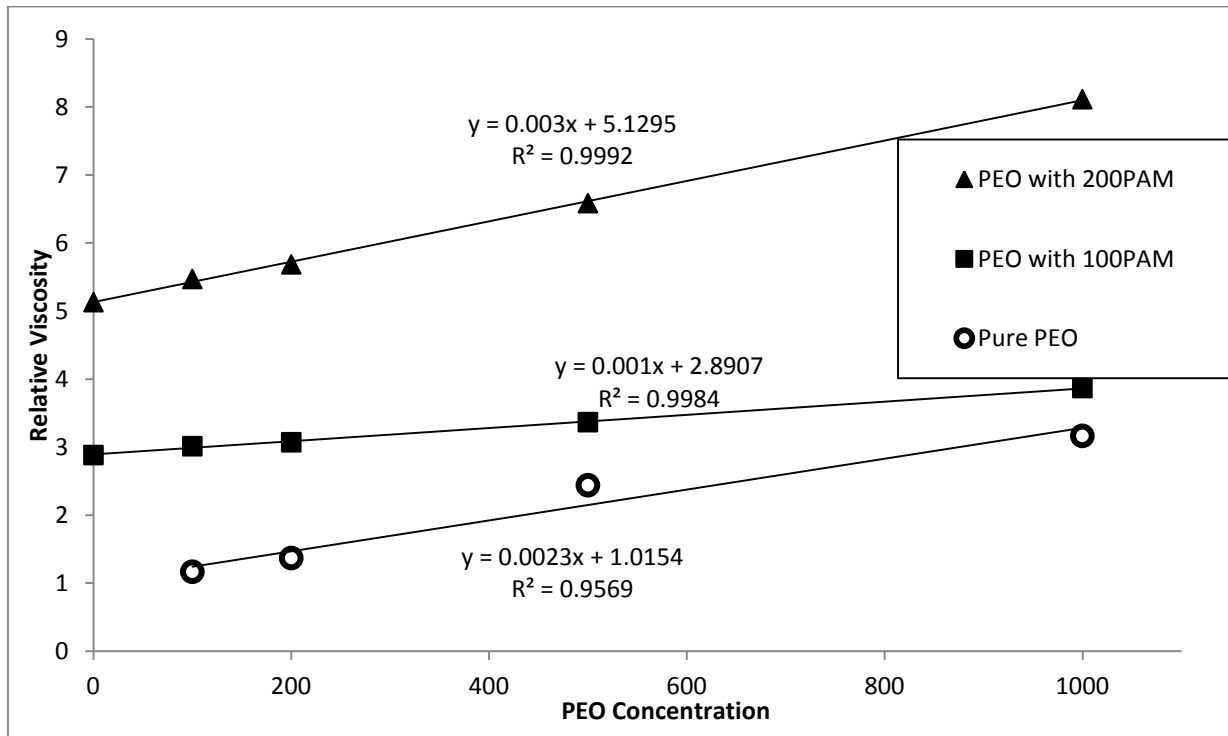


Figure 6.2 Relative Viscosity for 100ppm PAM and 200ppm PAM with varying PEO concentration

Figure 6.2 shows that as PEO concentration increases so does the relative viscosity. By fitting trendlines to the various solutions and comparing the slopes it is also evident that an interaction between PEO and PAM takes place. The slope for the pure PEO system is steeper than that of the 100ppm PAM/PEO mixture though the overall viscosity for the mixture is higher. This reduced slope indicates that the PEO molecules are not causing as large an increase in viscosity per amount of polymer added. At a concentration of 200 ppm PAM the slope closely resembles that of the pure polymer and is merely offset by the initial PAM concentration. The change in slope strongly suggests an interaction between PEO and PAM takes place and the increase in viscosity indicates a potential positive effect on drag reduction which is seen to be the case in the pilot plant experiments.

### 6.1.3 Conductivity

We note that the version of PAM used is anionic and that the PEO is nonionic. Previous experimental measurements have shown a slight increase in conductivity with increasing PEO concentration and a large increase with increasing PAM concentration. In the figures below PAM/PEO mixtures conductivities are measured against increasing PEO concentration to determine if any interaction takes place between the two.
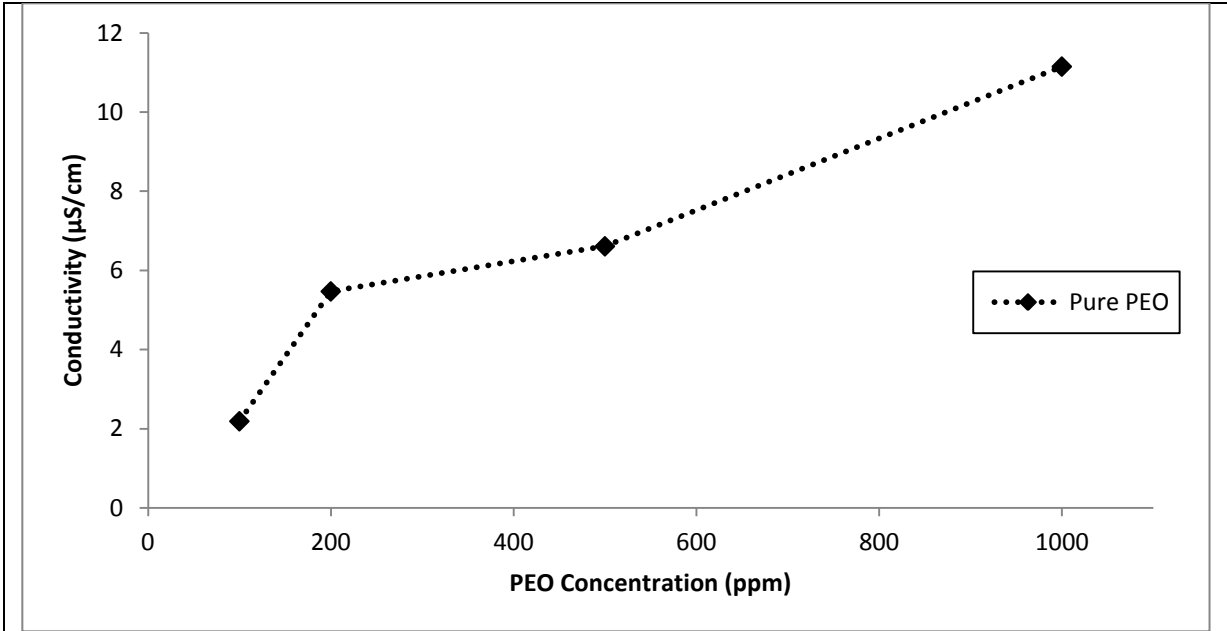
Figure 6.3 a) Conductivity of Pure PEO solution at various concentrations
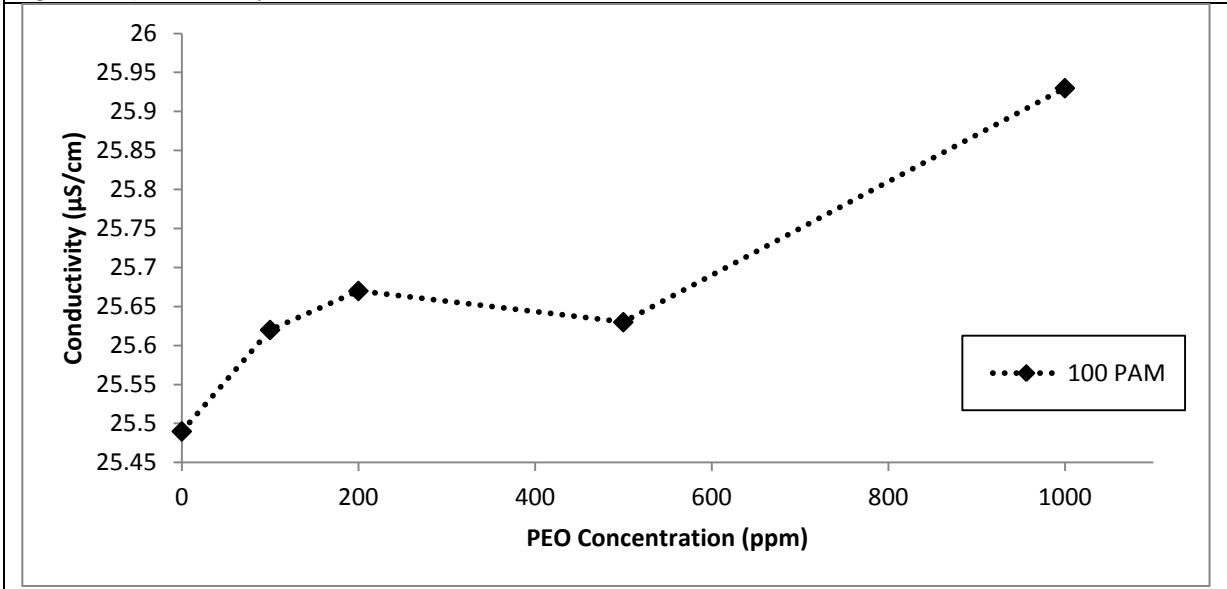


Figure 6.3 b) Conductivity of 100 ppm PAM with varying PEO concentration
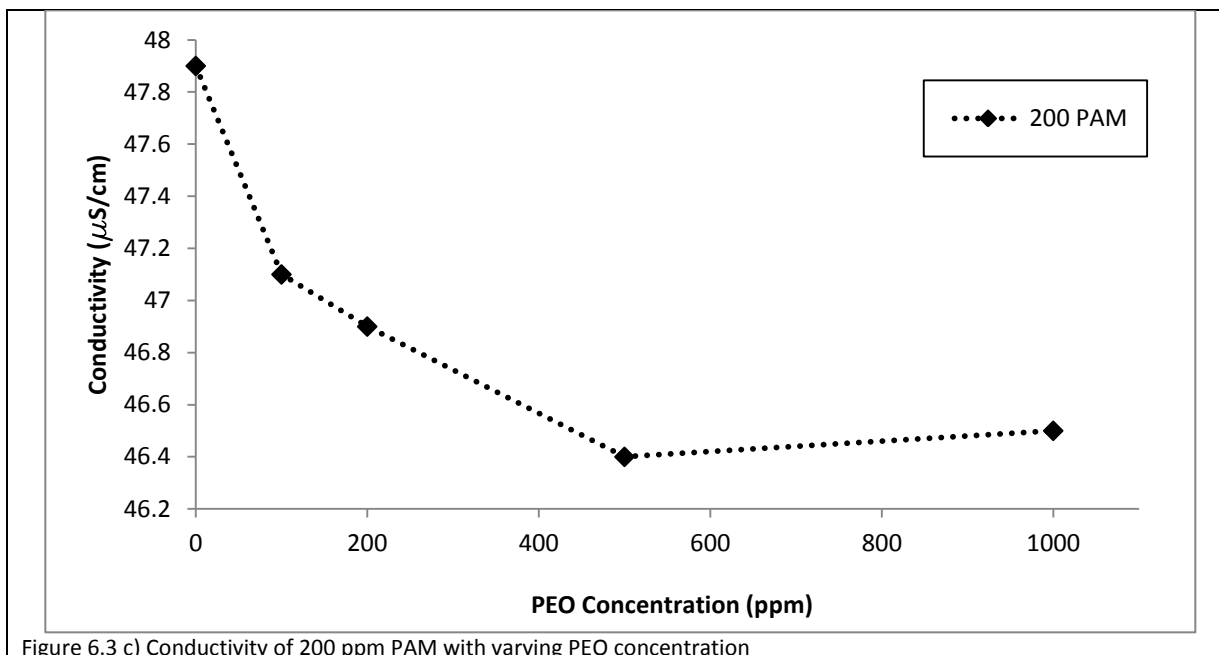
Figure 6.3 c) Conductivity of 200 ppm PAM with varying PEO concentration

Figure 6.3 Conductivity of PAM/PEO mixtures and pure PEO solution at various PEO concentrations

We note that PEO is a non ionic polymer and the change in PEO concentration from 100ppm to 1000 ppm is only associated with an 8.96 μS/cm increase in conductivity. PAM is highly conductive and doubles in conductivity displaying a 22.41 μS/cm increase from 100ppm to 200ppm. Thus we expect to see a slight increase in conductivity with the addition of PEO to PAM solution. Instead for 100 ppm PAM we observe a 0.44μS/cm increase from 0 to 1000ppm PEO and at 200 ppm we observe a decrease of 1.4μS/cm from 0 to 1000 ppm PEO increase. The conductivity is determined by the charge and electrical mobility of solution, thus the less than expected conductivity values are attributed to decreased electrical mobility of PAM molecules due to complexation with PEO. In figure 6.3c we observe a decrease in conductivity far from the overlap concentration indicating that the decrease in PAM mobility is due to complexation and not due to PEO network formation. Further evidence that the decrease in conductivity is due to PAM/PEO complexation is that the minimum values in solution conductivity occur before 1000ppm PEO and not at the highest solution viscosity. A dip is seen at 500ppm PEO with a conductivity increase at 1000ppm. The increased PAM concentration of 200ppm compared to 100 ppm allows for more opportunities for PEO/PAM complexation and this results in a decreased conductivity. Conductivity is observed to decrease up to a point passed which there is an increase in conductivity, this could be due to initially polymer-polymer complexation occurs and decreases the mobility followed by free uncomplexed PEO in solution which increases conductivity.

83

## 6.2 Drag Reduction for PAM/PEO Results

In the following section concentrations that showed possible positive interaction based off bench-scale results were run through the flow-loop. In the first section we only consider the pure polymers PAM and PEO. The drag reduction data for 1000 ppm PEO and 200ppm PAM solutions for 2 hours of degradation are presented in this first section. In the second section the drag reduction data for 100ppm PAM/500ppm PEO mixture degraded for 5 hours is shown and compared to relevant pure polymer drag reduction data.

### 6.2.1 Pure Polymer Drag Reduction Comparison between PAM and PEO

In figure 6.4 we compare between the pure polymers PEO and PAM. Figure 6.4a shows the fanning friction factor against generalized Reynolds number for 200ppm PAM and 1000ppm PEO solutions at 2 pipe sizes. In figures 6.4 b,c the percentage drag reduction is plotted against the Reynolds number for 2 hours of degradation.
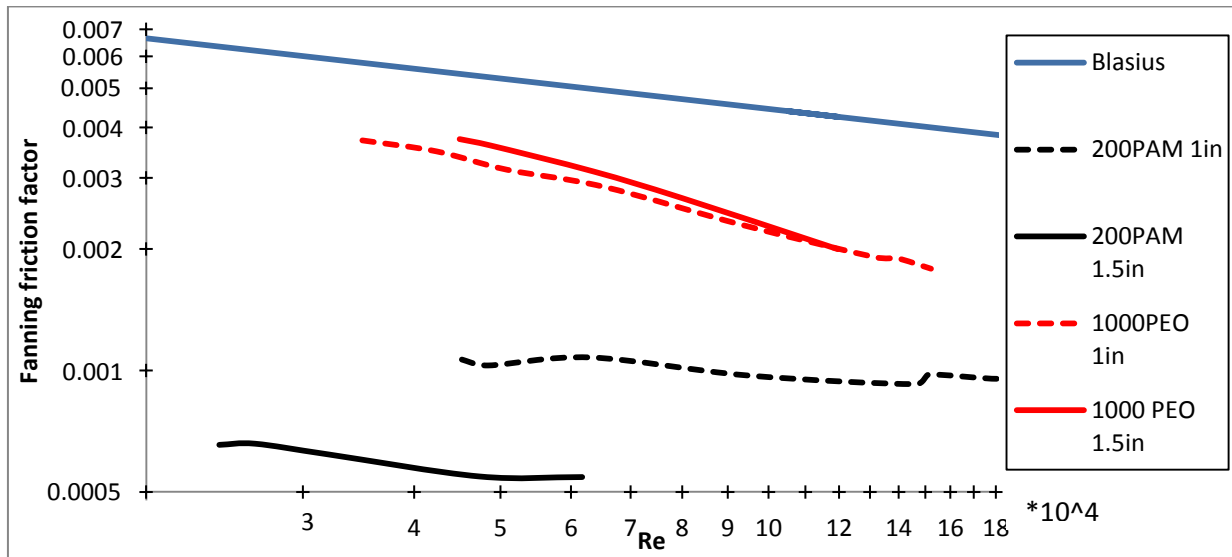


Figure 6.4 a) 200 ppm PAM and 1000ppm PEO Drag Reduction Comparison in 34.8mm and 22mm Internal Diameter Pipes
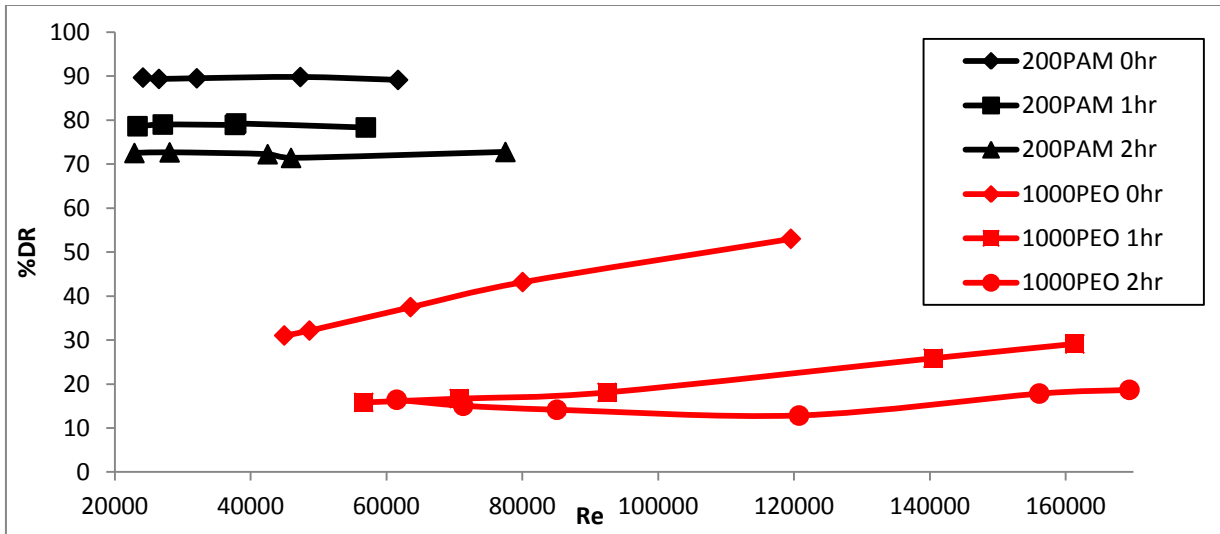
Figure 6.4 b) PAM and PEO %DR values vs. Reynolds number in 34.8mm ID Pipe for selected concentrations and degradation times
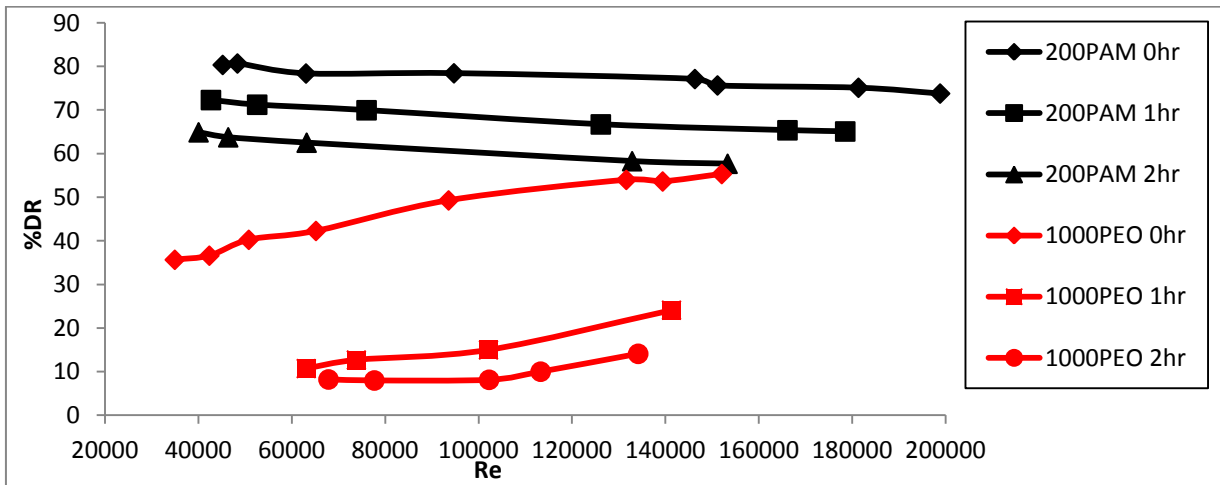


Figure 6.4 c) PAM and PEO %DR values vs. Reynolds number in 22mm ID Pipe for selected concentrations and degradation times

Figure 6.4 Drag Reduction comparisons of pure polymer systems consisting of 200 ppm PAM and 1000 ppm PEO in 1.5 in and 1 in pipes

Figure 6.4 shows 200ppm PAM solution achieves more drag reduction than the 1000 ppm PEO solution. We also observe that pipe diameter has a more pronounced affect on PAM than PEO with PAM achieving higher drag reduction in the larger 1.5 inch pipe over the 1 inch pipe.  While %DR of PAM is independent of the Reynolds number the %DR of PEO is dependent on the Reynolds number. This suggests that PAM molecules are fully extended from the start of the tested Reynolds range while PEO molecules undergo extension under the increased shear stress at high Reynolds number leading to an increase in drag reduction.

We also note that PAM molecules undergo less degradation than PEO in the same 2 hour interval.

Polymer Degradation is influenced by polymer concentration, solvent quality, flow geometry and turbulence intensity. High molar mass polymers break preferentially over lower molar mass polymers and scission predominately occurs at the midpoint. With regards to figure 6.4 b and c we observe that PAM molecules are more resistant to degradation than PEO. The PAM solution's rate of degradation appears to be constant with respect to time with a drop of approximately 10% per hour while the rate of PEO degradation is strongly time dependent. In the first hour of degradation PEO undergoes a decrease of approximately 30% per hour while in the next hour only a 7% drop is observed. Note that degraded PEO with a shorter chain length after polymer scission has a %DR value less affected by the Reynolds number. (Vanapalli, Islam et al. 2005) have shown that the critical shear rate for scission $\dot{\gamma}_w \propto M^{-2.2}$ for PEO and $\dot{\gamma}_w \propto M^{-2.73}$ for PAM. This shows that for the same molar mass PEO is more susceptible to polymer scission than PAM under similar flow conditions.

We also note the previous finding (Mohsenipour 2011) that for both PAM and PEO there is an increase in drag reduction with polymer concentration up to the overlap concentration, past which drag reduction is negligibly effected by increasing polymer concentration.

Overall PAM appears to be a better drag reducing agent with higher percentage drag reduction values achieved at lower concentrations and with a slower degradation time. Studies have shown that PEO is less affected by the presence of counter ions in solution (Mohsenipour 2011) and this poses a possible exploitive opportunity.

## 6.2.2 PAM/PEO Mixture Drag Reduction

In figure 6.5 below the Fanning Friction Factor is plotted against the Generalized Reynolds number for 100ppm PAM/500ppm PEO solution at various degradation times. The values for pure PEO and PAM along with the Blasius line are included for comparison.
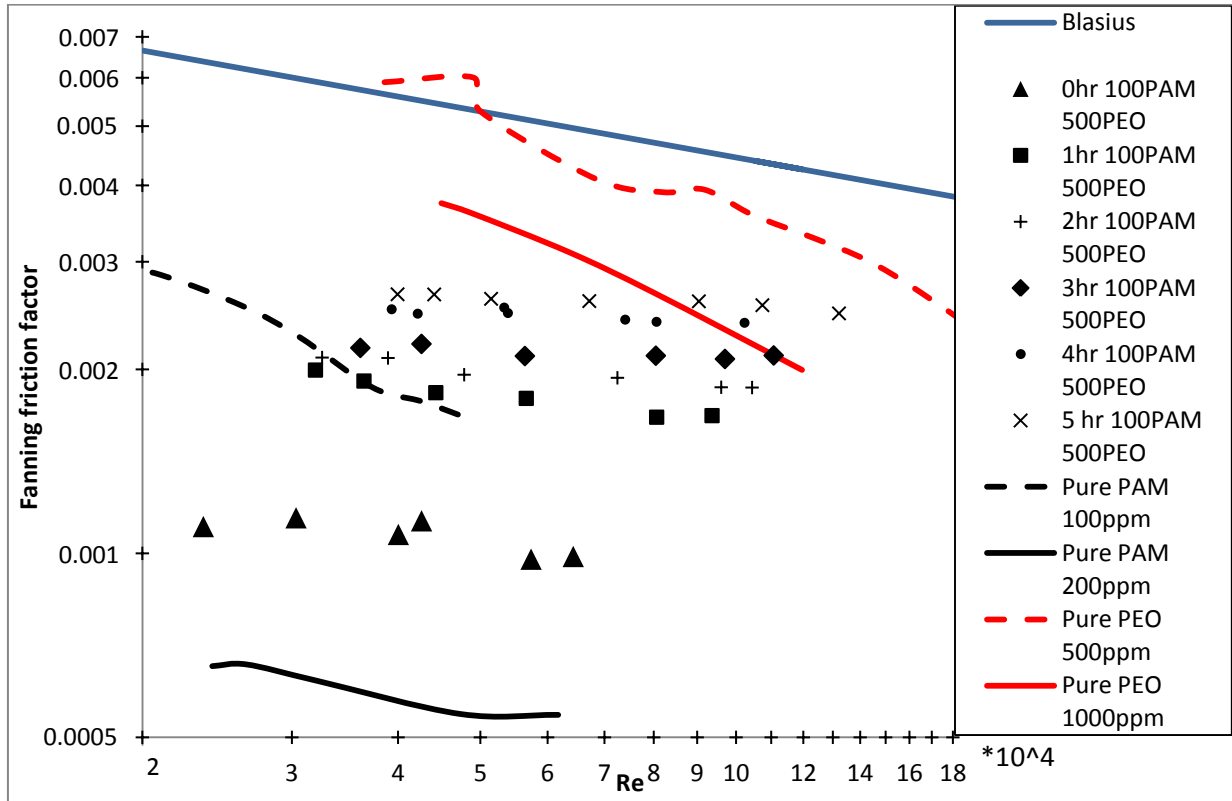


Figure 6.5 a) Fanning Friction factor vs. Reynolds Number for 500ppm PEO with 100ppm PAM mixture at different degradation times with various pure polymer data included for 1.5 inch pipe (Data for pure 500ppm PEO and pure 100ppm PAM provided by (Mohsenipour 2011))
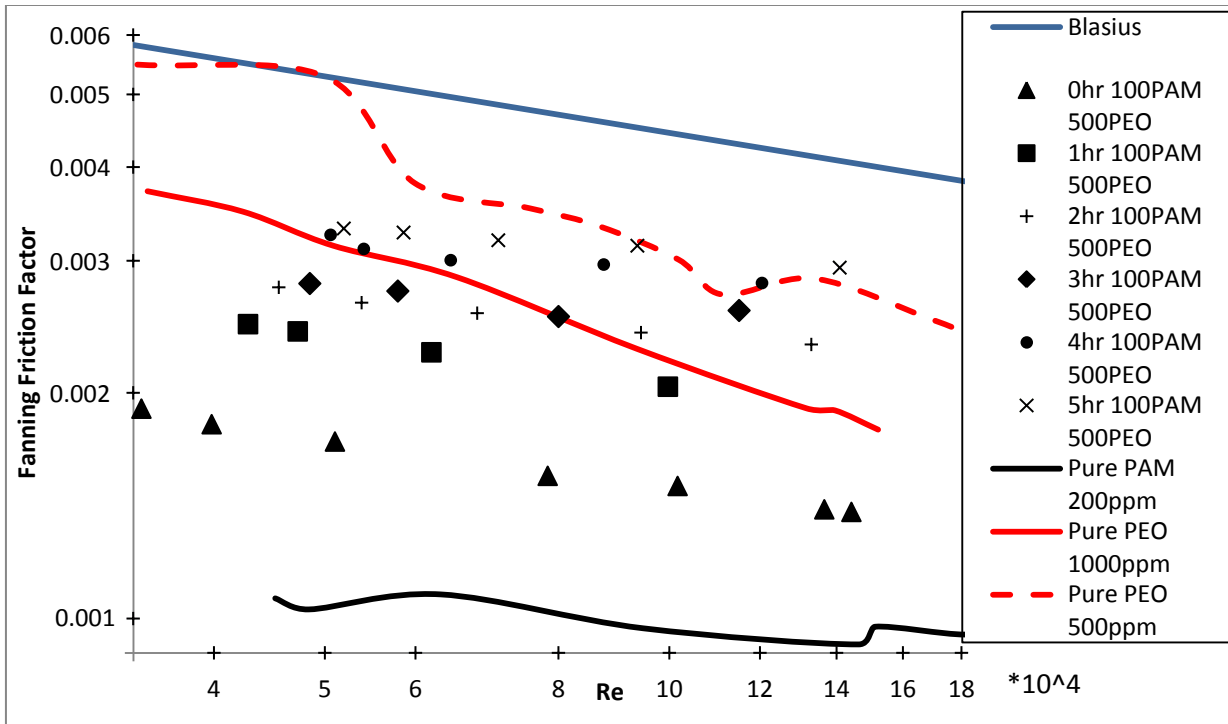
Figure 6.5 b) Fanning Friction factor vs. Reynolds Number for 500ppm PEO with 100ppm PAM mixture at different degradation times with various pure polymer data included for 1 inch pipe (Data for pure 500ppm provided by (Mohsenipour 2011))

Figure 6.5 above shows the drag reduction achieved for a 100 ppm PAM and 500 ppm PEO mixture in 1 inch and 1.5 inch diameter pipes at different degradation times with various pure polymer concentrations included for comparison. The PAM/PEO mixture achieves higher levels of drag reduction than either of the polymers achieve independently. In addition the 100ppm PAM/ 500ppm PEO mixture achieves a higher level of drag reduction than 1000ppm PEO solution but not as much as the 200ppm PAM solution.

We also note that the mixture's drag reduction level is not merely the addition of the pure polymers drag reduction levels but instead the improved drag reduction is due to polymer-polymer interaction. This is evident from the fact that even at Reynolds numbers where 500ppm PEO displays no departure from the blasius line when in mixture with 100ppm PAM we observe an increase in drag reduction over the pure 100ppm PAM solution. This increase in drag reduction must be due to PEO-PAM interaction.

We also observe that the largest jump in drag reduction occurs in the first hour of degradation especially in the 1.5 inch pipe. Further degradation leads to a steady decline in drag reduction with over 5 hours of degradation we still observe more drag reduction in the PAM/PEO mixture than for 500ppm undegraded PEO alone. This highlights some of the possible benefits of the PAM/PEO mixture over the pure components alone.

The mixture shows higher drag reduction level at smaller concentrations than PEO alone and with slower degradation times than PEO. Further studies need to be performed on PAM/PEO mixture in tap water as PEO molecules conformation is not significantly affected by the presence of counterions unlike PAM and this poses a possible advantage of the mixture over PAM solution alone.

## 6.3 Conclusions

- Relative Viscosity plot show change in slope compared to pure PEO plot for 100ppm PAM/varying PEO concentration mixture
- 200ppm PAM solution experiences slight decrease in conductivity with increasing PEO concentration indicating polymer-polymer complexation
- PAM has higher percentage drag reduction and slower degradation times at lower concentrations than PEO
- Percentage Drag Reduction of PAM is independent of Reynolds number while Percentage Drag Reduction of PEO is dependent on Reynolds number in the 40000-190000 Reynolds Range
- Rate of Degradation is strongly time dependent for PEO
- 100ppm PAM/500ppm PEO mixture shows increased drag reduction compared to pure polymer at the same concentration
- The observed increase in drag reduction occurs before the onset Reynolds number for pure PEO alone at the same concentration implying a polymer-polymer interaction induced increase

# Chapter 7   Conclusions and Future Recommendations

## 7.1 Conclusions

- The critical aggregation concentration for PAM/Amphosol is independent of polymer concentration
- The point of free micellization formation is strongly dependent on polymer concentration and the polymer concentration's effect decreases past the overlap concentration
- 200ppm PAM/100ppm Amphosol shows no increase in degradation time or achieved drag reduction level when compared to pure 200ppm PAM solution
- PAM and PAM/Amphosol mixtures experience larger drop in drag reduction during the first hour of degradation compared to the subsequent hour
- 250ppm PAM in tap water shows less drag reduction than 200ppm PAM in DI water.

- Viscosity measurements show increased PEO/Amphosol interaction at overlap concentration 1550ppm PEO
- Undegraded PEO molecules undergo extension under increased stress with increasing Reynolds number leading to an increase in percent drag reduction
- PEO undergoes the largest amount of degradation and subsequently the largest drag reduction drop in the first hour when the chains are longest
- Presence of 700ppm Amphosol in 1000ppm PEO slows down degradation and increases percent drag reduction after polymer degradation has occurred, this is particularly evident at low Reynolds numbers
- At high Reynolds numbers the Amphosol surfactant micelle deteriorates and percent drag reduction approaches that of the pure polymer

- Relative Viscosity plots show change in slope compared to pure PEO plot for 100ppm PAM/varying PEO concentration mixture
- 200ppm PAM solution experiences slight decrease in conductivity with increasing PEO concentration indicating polymer-polymer complexation
- PAM has higher percentage drag reduction and slower degradation times at lower concentrations than PEO

- Percentage Drag Reduction of PAM is independent of Reynolds number while Percentage Drag Reduction of PEO is dependent on Reynolds number in the 40000-190000 Reynolds Range
- The rate of Degradation is strongly time dependent for PEO
- 100ppm PAM/500ppm PEO mixture shows increased drag reduction compared to pure polymers at the same concentration
- The observed increase in drag reduction occurs before the onset Reynolds number for pure PEO alone at the same concentration implying a polymer-polymer interaction induced increase

## 7.2 Recommendations for Future Work

The drag reduction of Amphosol alone should be studied and the factors that affect it such as temperature and concentration. The critical shear rate should be found for all pipes, concentrations and temperatures.

PAM/PEO mixtures should be run through the loop in tap water with the mixtures resultant drag reduction compared to that of pure PAM in tap water and pure PEO in tap water as well as studying the effect of counterions on rate of degradation.

The drop in drag reduction should be modeled as a function of time and shear rate. In addition to this the onset Reynolds number for drag reduction to occur can be found for various concentrations of PAM and PEO and then related back to a Weissenburg number of one giving us an estimate of the polymer relaxation time as a function of concentration for PAM and PEO.

# Appendix A: PAM/Amphosol Data

Relevant Excel Files can be found at:

https://drive.google.com/folderview?id=0B1oHKhn79y6eeWxXM0VlTmxyekk&usp=sharing

## A.1 Bench-Scale Data

Pure Amphosol

| Surfactant concentration ppm | Shear Rate (RPM) | |
|---|---|---|
| | 300 | 600 |
| | Dial Reading | |
| 0 | 10 | 16 |
| 100 | 9.5 | 15 |
| 200 | 10 | 15 |
| 400 | 10 | 15 |
| 600 | 9.5 | 15 |
| 800 | 10 | 15.5 |
| 1000 | 10 | 14.5 |
| 1500 | 11 | 19 |
| 2000 | 10 | 15 |
| 3000 | 9.5 | 15 |
| 4000 | 10 | 15 |
| 5000 | 10 | 15 |

Equation 3.3 page 43 is used to convert the Dial Reading to Shear Stress reading in Pascals

Equation 3.4-3.5 page43 and 44 is used to convert shear rate from RPM to inverse Seconds

| Surfactant concentration ppm | Shear Rate (1/s) | |
|---|---|---|
| | 512.7412374 | 1025.482475 |
| | Shear Stress (Pa) | |
| 0 | 0.5116 | 1.0402 |
| 100 | 0.46755 | 0.9521 |
| 200 | 0.5116 | 0.9521 |
| 400 | 0.5116 | 0.9521 |
| 600 | 0.46755 | 0.9521 |
| 800 | 0.5116 | 0.99615 |
| 1000 | 0.5116 | 0.90805 |
| 1500 | 0.5997 | 1.3045 |

| | | | |
|---|---|---|---|
| 2000 | 0.5116 | 0.9521 |
| 3000 | 0.46755 | 0.9521 |
| 4000 | 0.5116 | 0.9521 |
| 5000 | 0.5116 | 0.9521 |

50ppm PAM

| Surfactant concentration ppm | Shear Rate (RPM) | | | | |
|---|---|---|---|---|---|
| | 100 | 180 | 200 | 300 | 600 |
| | Shear Stress Dial Reading | | | | |
| 0 | 9 | 12 | 12.5 | 15.5 | 23.5 |
| 50 | 8 | 11 | 11 | 14 | 21.5 |
| 100 | 8 | 10.5 | 11 | 13 | 21 |
| 150 | 8 | 10.5 | 11 | 14 | 21.5 |
| 200 | 8.5 | 10 | 11 | 13.5 | 20.5 |
| 400 | 7.5 | 10 | 10.5 | 13.5 | 20 |
| 600 | 8 | 10 | 10.5 | 13.5 | 20.5 |
| 800 | 7.5 | 10 | 10 | 13.5 | 20 |
| 1000 | 7.5 | 9.5 | 10.5 | 13 | 20 |
| 1500 | 7 | 9.5 | 10 | 12.5 | 20 |
| 2000 | 7 | 9 | 10 | 12.5 | 19 |
| 3000 | 6.5 | 8.5 | 9 | 11.5 | 18.5 |
| 4000 | 6.5 | 9 | 9.5 | 12 | 19 |

| Surfactant concentration ppm | Shear Rate(1/s) | | | | |
|---|---|---|---|---|---|
| | 170.9137458 | 307.6447425 | 341.8274916 | 512.7412374 | 1025.482475 |
| | Shear Stress (Pa) | | | | |
| 0 | 0.4235 | 0.6878 | 0.73185 | 0.99615 | 1.70095 |
| 50 | | 0.5997 | 0.5997 | 0.864 | 1.52475 |
| 100 | | 0.55565 | 0.5997 | 0.7759 | 1.4807 |
| 150 | | 0.55565 | 0.5997 | 0.864 | 1.52475 |
| 200 | | 0.5116 | 0.5997 | 0.81995 | 1.43665 |
| 400 | | 0.5116 | 0.55565 | 0.81995 | 1.3926 |
| 600 | | 0.5116 | 0.55565 | 0.81995 | 1.43665 |
| 800 | | 0.5116 | 0.5116 | 0.81995 | 1.3926 |
| 1000 | | 0.46755 | 0.55565 | 0.7759 | 1.3926 |
| 1500 | | 0.46755 | 0.5116 | 0.73185 | 1.3926 |

| | 2000 | | 0.4235 | 0.5116 | 0.73185 | 1.3045 |
|---|---|---|---|---|---|---|
| | 3000 | | | 0.4235 | 0.64375 | 1.26045 |
| | 4000 | | 0.4235 | 0.46755 | 0.6878 | 1.3045 |

100ppm PAM

| Surfactant concentration ppm | Shear Rate (RPM) | | | | | | |
|---|---|---|---|---|---|---|---|
| | 60 | 90 | 100 | 180 | 200 | 300 | 600 |
| | Dial Reading | | | | | | |
| 0 | 9 | 11 | 11.5 | 15 | 16 | 20 | 30 |
| 50 | 9 | 10.5 | 10.5 | 14.5 | 15 | 19 | 27 |
| 100 | | 10 | 10.5 | 13.5 | 14.5 | 18 | 26.5 |
| 150 | | 9.5 | 10 | 13.5 | 14.5 | 17.5 | 26.5 |
| 200 | | 9.5 | 10 | 13.5 | 14 | 17.5 | 25.5 |
| 400 | | 9 | 10 | 12.5 | 13.5 | 17 | 25 |
| 600 | | | 9 | 12 | 12.5 | 16.5 | 24.5 |
| 800 | | | 9 | 12 | 12.5 | 16.5 | 24.5 |
| 1000 | | | 8.5 | 11.5 | 12.5 | 15.5 | 23.5 |
| 1500 | | | 8.5 | 11 | 12.5 | 15 | 24 |
| 2000 | | | | 11 | 11.5 | 15 | 23 |
| 3000 | | | | 10.5 | 11 | 14.5 | 22.5 |

200ppm PAM

| Surfactant concentration ppm | Shear Viscosity | | | | | | | |
|---|---|---|---|---|---|---|---|---|
| | 30 | 60 | 90 | 100 | 180 | 200 | 300 | 600 |
| | Dial Reading | | | | | | | |
| 0 | 12 | 13.5 | 15.5 | 16 | 21 | 22.5 | 27 | 40 |
| 50 | 10 | 11.5 | 14 | 15 | 19 | 20 | 25 | 36 |
| 100 | 10 | 11.5 | 14 | 14.5 | 19.5 | 20.5 | 25 | 36.5 |
| 150 | 9 | 11.5 | 13.5 | 14.5 | 18.5 | 19.5 | 24.5 | 35 |
| 200 | 9.5 | 12.5 | 13.5 | 14 | 18.5 | 19.5 | 24 | 35 |
| 400 | | 10.5 | 12.5 | 13.5 | 17.5 | 18.5 | 23 | 33.5 |
| 600 | | 9.5 | 12 | 12.5 | 16.5 | 17.5 | 22.5 | 32.5 |
| 800 | | 9.5 | 11.5 | 12 | 16 | 17.5 | 21.5 | 32 |
| 1000 | | 9.5 | 11 | 11.5 | 15.5 | 16.5 | 21 | 31.5 |
| 1500 | | | 11 | 11 | 15 | 15.5 | 19.5 | 29.5 |
| 2000 | | | 10 | 10.5 | 15 | 15.5 | 19.5 | 30 |
| 3000 | | | 9.5 | 9.5 | 13.5 | 13.5 | 17.5 | 27.5 |
| 4000 | | | 9 | 9.5 | 12.5 | 13.5 | 17 | 26.5 |

500ppm PAM

| Surfactant concentration ppm | Shear Rate (RPM) | | | | | | | | | | | |
|---|---|---|---|---|---|---|---|---|---|---|---|---|
| | 0.9 | 1.8 | 3 | 6 | 30 | 60 | 90 | 100 | 180 | 200 | 300 | 600 |
| | Dial Reading | | | | | | | | | | | |
| 0 | 9 | 9.5 | 10.5 | 12 | 17.5 | 21 | 28 | 25.5 | 34 | 36.5 | 43.5 | 65 |
| 50 | | 9 | 10 | 11.5 | 16 | 20.5 | 25.5 | 26 | 33.5 | 35.5 | 42.5 | 61.5 |
| 100 | | 9.5 | 10.5 | 12.5 | 16.5 | 22 | 26 | 26 | 34 | 35.5 | 42.5 | 60 |
| 150 | | | 9.5 | 11 | 16 | 20 | 25 | 24 | 32 | 33.5 | 41 | 62 |
| 200 | | | | 10.5 | 16.5 | 20.5 | 25 | 25.5 | 34 | 35.5 | 43 | 59 |
| 400 | | | | 10 | 15 | 19 | 22..5 | 23.5 | 30.5 | 32 | 38.5 | 55.5 |
| 600 | | | | | 13 | 17 | 20.5 | 21.5 | 28.5 | 30.5 | 37 | 54 |
| 800 | | | | | 11.5 | 15.5 | 20 | 20.5 | 28.5 | 30 | 37 | 53 |
| 1000 | | | | | 12 | 16.5 | 19.5 | 20 | 26.5 | 28.5 | 35 | 51 |
| 1500 | | | | | 11 | 15 | 17.5 | 18.5 | 25 | 26.5 | 32.5 | 47.5 |
| 2000 | | | | | 10 | 13.5 | 16 | 17.5 | 23.5 | 25 | 31 | 46 |
| 3000 | | | | | 9.5 | 12.5 | 15.5 | 16.5 | 22.5 | 23.5 | 29.5 | 44.5 |
| 4000 | | | | | | 11 | 14 | 14.5 | 20.5 | 21.5 | 27.5 | 42 |

| Surfactant concentration ppm | Conductivity #1 microS/cm | Avg. Surface Tension (Dyne/cm) | Flow Time (sec) | Relative Viscosity |
|---|---|---|---|---|
| 0 | 1.97 | 69.33333333 | 111.6666667 | 1 |
| 50 | 23.61 | 34.33333333 | x | |
| 100 | 43.3 | 37.26666667 | 108.3333333 | 0.970149254 |
| 150 | 59.5 | 31 | x | |
| 200 | 78.1 | 32.36666667 | 112.3333333 | 1.005970149 |
| 400 | 149.2 | 29.63333333 | 114.3333333 | 1.023880597 |
| 600 | 221.9 | 33 | 115.3333333 | 1.032835821 |
| 800 | 287.2 | 30.1 | 113.3333333 | 1.014925373 |
| 1000 | 357 | 31.73333333 | 114.3333333 | 1.023880597 |
| 1500 | 531 | 32.23333333 | 113 | 1.011940299 |
| 2000 | 708 | 31.93333333 | 112.6666667 | 1.008955224 |
| 3000 | 1049 | 31.53333333 | 116.3333333 | 1.041791045 |
| 4000 | 1376 | 33.46666667 | 115.3333333 | 1.032835821 |
| 5000 | 1724 | 32.56666667 | 115.3333333 | 1.032835821 |
| | | | | |
| | | | | |
| 50 ppm PAM | | | | |
| Surfactant concentration ppm | Conductivity microS/cm | Avg. Surface Tension (Dyne/cm) | Flow Time (sec) | Relative Viscosity |
| 0 | 15.18 | 71.33333333 | 203.8333333 | 1.825373134 |
| 50 | 36.9 | 39.4 | 171.6666667 | 1.537313433 |
| 100 | 53.9 | 35.5 | 185 | 1.656716418 |
| 150 | 71.7 | 33.43333333 | 183.3333333 | 1.641791045 |
| 200 | 87.8 | 33.56666667 | 174 | 1.558208955 |
| 400 | 161.5 | 32.96666667 | 175.6666667 | 1.573134328 |
| 600 | 234.6 | 33.53333333 | 167.8333333 | 1.502985075 |
| 800 | 306 | 33.3 | 161.6666667 | 1.447761194 |

| Surfactant concentration ppm | Conductivity microS/cm | Avg. Surface Tension (Dyne/cm) | Flow Time (sec) | Relative Viscosity |
|---|---|---|---|---|
| 1000 | 383 | 34.3 | 157.6666667 | 1.411940299 |
| 1500 | 552 | 33.3 | 154.6666667 | 1.385074627 |
| 2000 | 733 | 32.9 | 153 | 1.370149254 |
| 3000 | 1068 | 33.2 | 148.6666667 | 1.331343284 |
| 4000 | 1400 | 32.85 | 147 | 1.31641791 |
| | | | | |
| | | | | |
| 100 ppm PAM | | | | |
| Surfactant concentration ppm | Conductivity microS/cm | Avg. Surface Tension (Dyne/cm) | Flow Time (sec) | Relative Viscosity |
| 0 | 25.94 | 70.8 | 265 | 2.373134328 |
| 50 | 43.8 | 43.66666667 | 273 | 2.444776119 |
| 100 | 61.5 | 38.13333333 | 265 | 2.373134328 |
| 150 | 78.1 | 36.06666667 | 250 | 2.23880597 |
| 200 | 96.4 | 34.06666667 | 244 | 2.185074627 |
| 400 | 166.4 | 32.76666667 | 233 | 2.086567164 |
| 600 | 238.7 | 32.86666667 | 224.5 | 2.010447761 |
| 800 | 311 | 32.66666667 | 200 | 1.791044776 |
| 1000 | 383 | 32.93333333 | 207 | 1.853731343 |
| 1500 | 554 | 32.9 | 199.3333333 | 1.785074627 |
| 2000 | 726 | 33 | 189.5 | 1.697014925 |
| 3000 | 1069 | 33 | 179 | 1.602985075 |
| 4000 | | | | |
| | | | | |
| | | | | |
| 200 ppm PAM | | | | |
| Surfactant concentration ppm | Conductivity microS/cm | Avg. Surface Tension (Dyne/cm) | Flow Time (sec) | Relative Viscosity |
| 0 | 15.02 | 71.3 | 544.6666667 | 4.87761194 |
| 50 | 64.5 | 44.66666667 | 666.3333333 | 5.967164179 |
| 100 | 90.8 | 38.53333333 | 441.5 | 3.953731343 |
| 150 | 105.6 | 39.1 | 432.6666667 | 3.874626866 |
| 200 | 130.5 | 38.55 | 405 | 3.626865672 |
| 400 | 194.2 | 35.5 | 379 | 3.394029851 |
| 600 | 268.6 | 34.1 | 353 | 3.16119403 |
| 800 | 332 | 34.26666667 | 346.3333333 | 3.101492537 |

| | | | | |
|---|---|---|---|---|
| 1000 | 417 | 34.3 | 340 | 3.044776119 |
| 1500 | 595 | 34.03333333 | 300 | 2.686567164 |
| 2000 | 763 | 33.75 | 289.6666667 | 2.594029851 |
| | | | | |
| | | | | |
| 500 ppm PAM | | | | |
| Surfactant concentration ppm | Conductivity microS/cm | Avg. Surface Tension (Dyne/cm) | Flow Time (sec) | Relative Viscosity |
| 0 | 121.5 | 71.46666667 | 1963.333333 | 17.58208955 |
| 50 | 140.8 | 46.93333333 | 1801 | 16.12835821 |
| 100 | 148.1 | 41.96666667 | 1627 | 14.57014925 |
| 150 | 208.1 | 40.85 | 1315.666667 | 11.78208955 |
| 200 | 166.3 | 39.1 | 1168.666667 | 10.46567164 |
| 400 | 248.4 | 36.5 | 1127 | 10.09253731 |
| 600 | 318 | 35.9 | 1058 | 9.474626866 |
| 800 | 412 | 34.7 | 900.5 | 8.064179104 |
| 1000 | 456 | 35.4 | 712.5 | 6.380597015 |
| 1500 | 626 | 34.65 | 712.6666667 | 6.382089552 |
| 2000 | 800 | 34.9 | 623.5 | 5.58358209 |
| 3000 | 1126 | 34.45 | 565 | 5.059701493 |
| 4000 | 1503 | 34.86666667 | 494 | 4.423880597 |

## A.2 Pilot Plant Data

The Generalized Reynold number from Equation 3.7 (page 45) is calculated from a power-law fit of the Shear Stress to Shear Rate Data shown below

Shear Stress in Pascals on Y-Axis and Shear rate in inverse seconds on X-axis

200ppm PAM
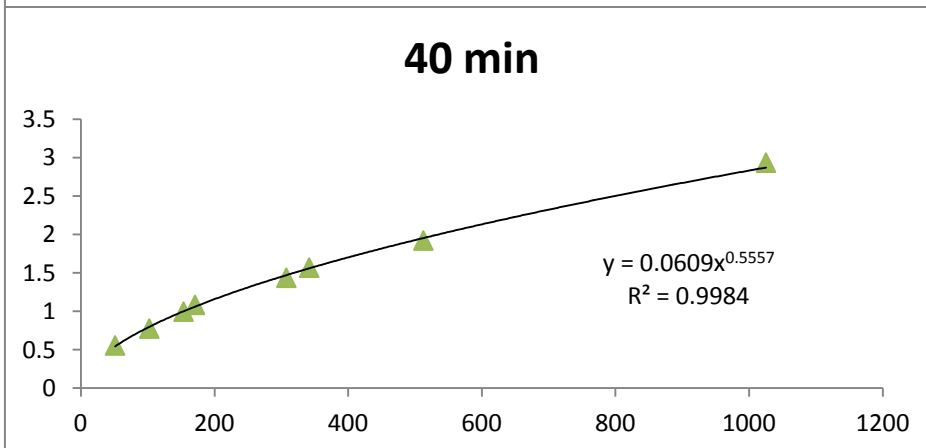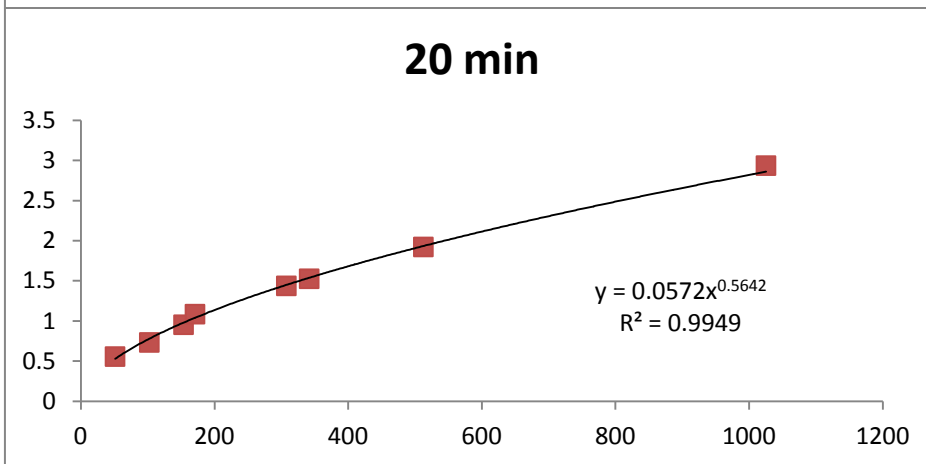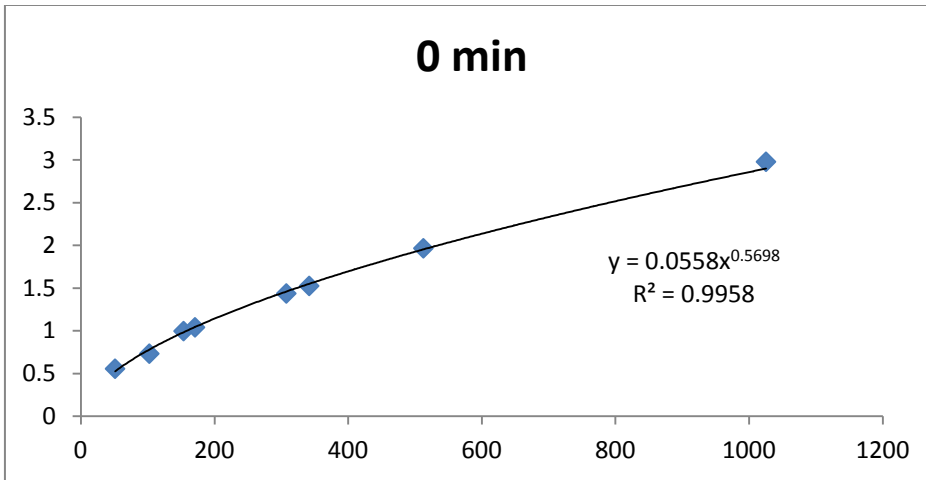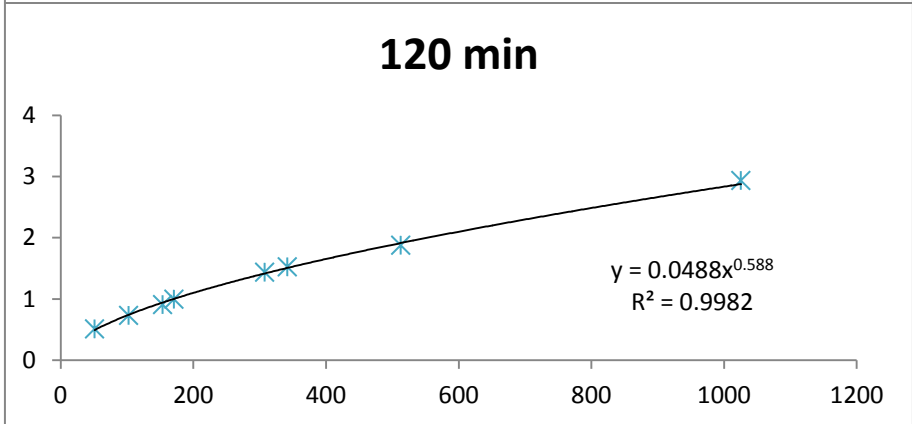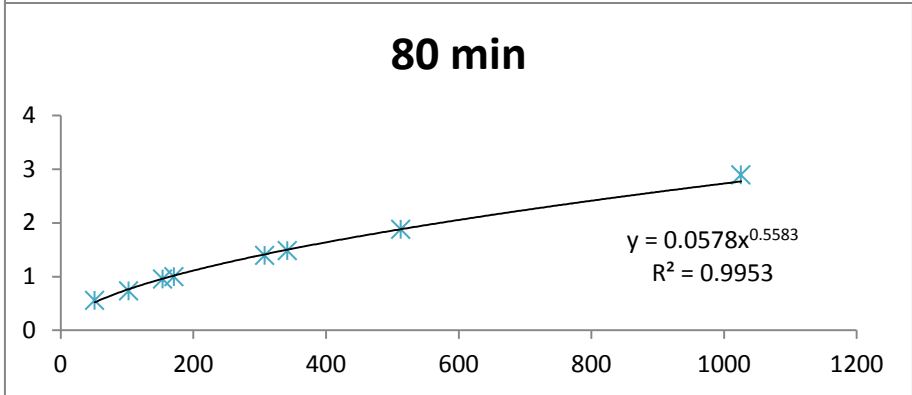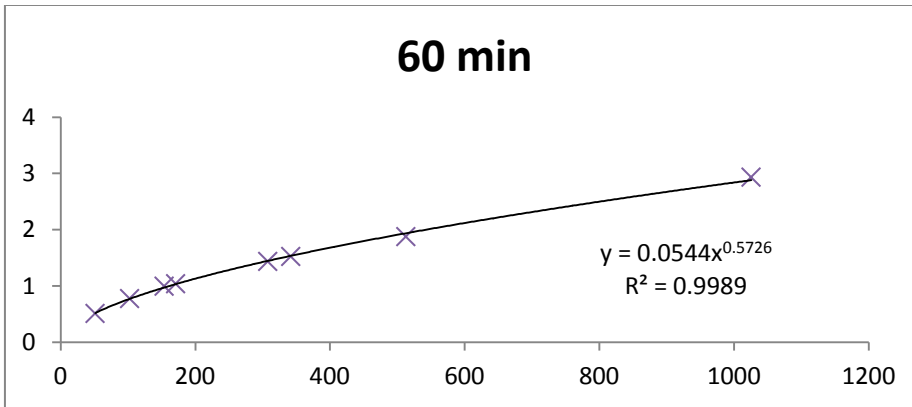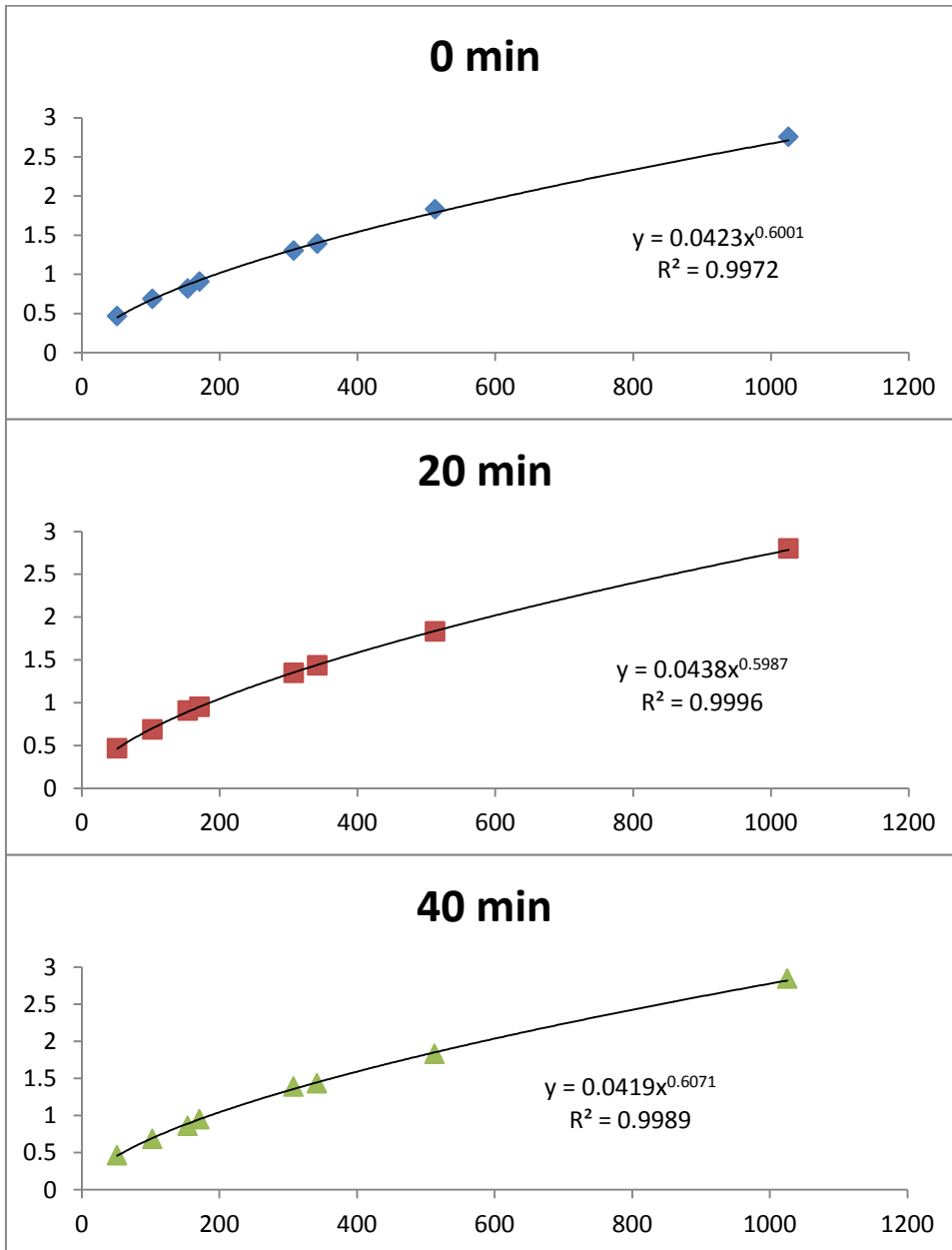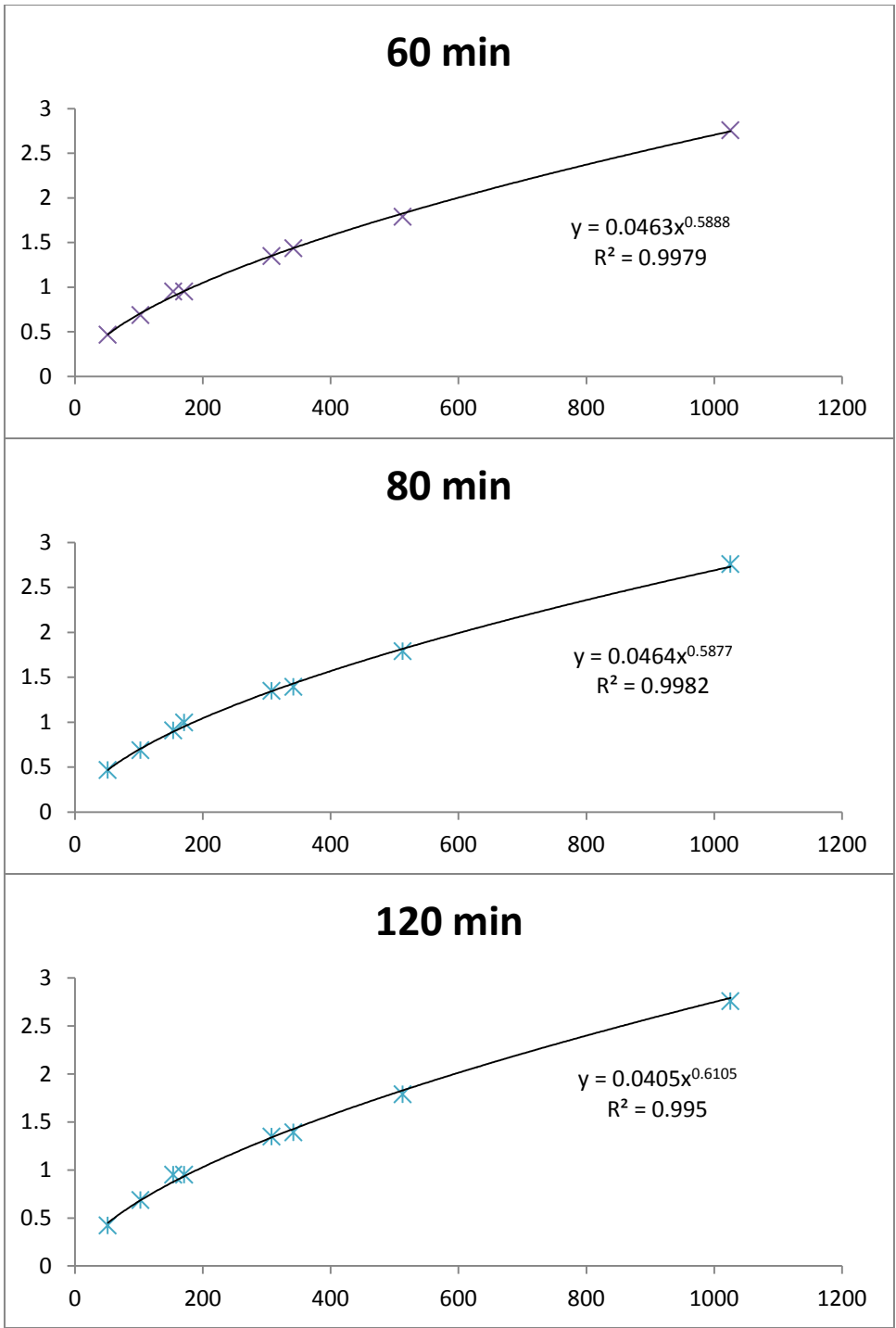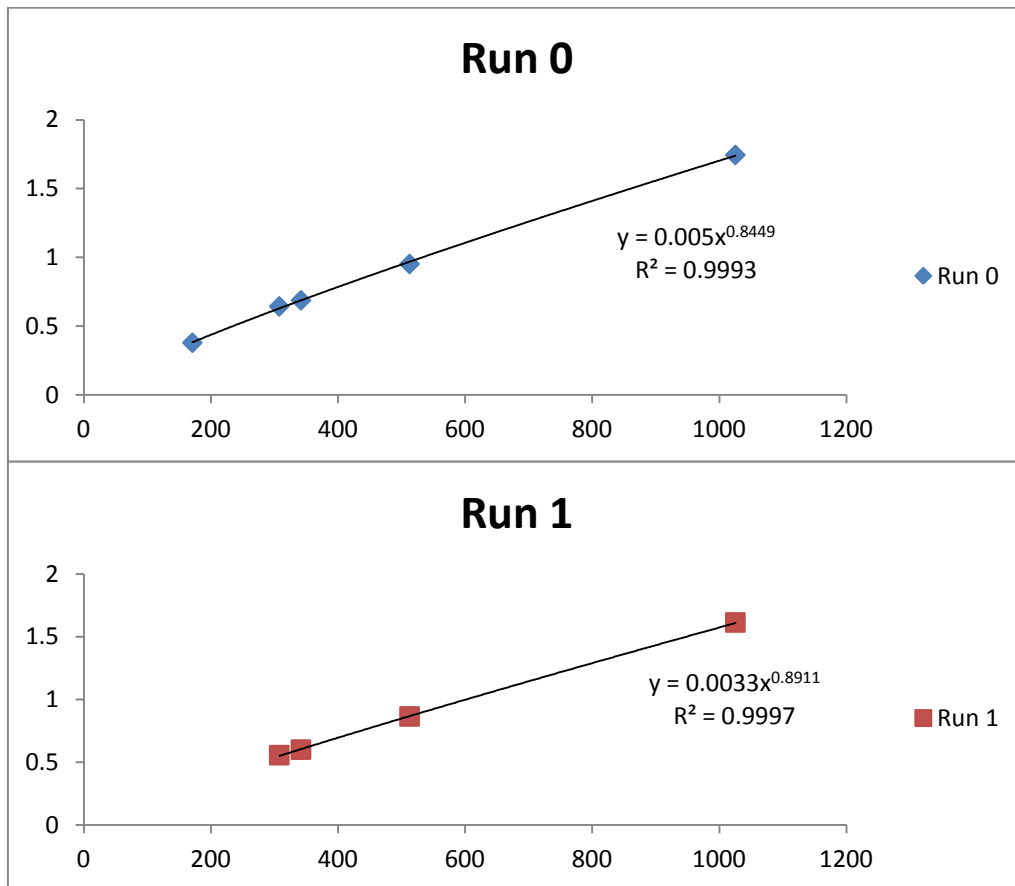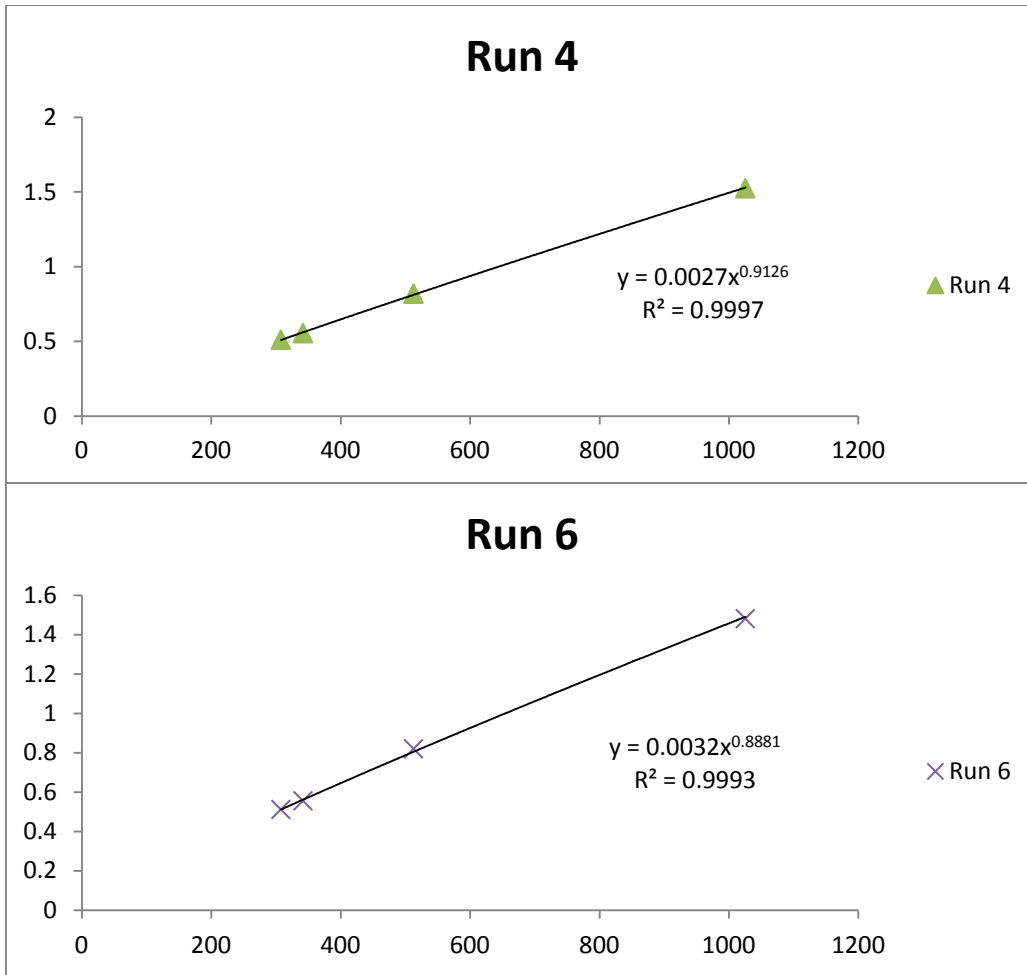
**0 min**

$y = 0.0558x^{0.5698}$
$R^2 = 0.9958$

**20 min**

$y = 0.0572x^{0.5642}$
$R^2 = 0.9949$

**40 min**

$y = 0.0609x^{0.5557}$
$R^2 = 0.9984$

**60 min**

$y = 0.0544x^{0.5726}$
$R^2 = 0.9989$

**80 min**

$y = 0.0578x^{0.5583}$
$R^2 = 0.9953$

**120 min**

$y = 0.0488x^{0.588}$
$R^2 = 0.9982$

200ppm PAM/ 100ppm Amphosol



## 0 min

$y = 0.0423x^{0.6001}$
$R^2 = 0.9972$

## 20 min

$y = 0.0438x^{0.5987}$
$R^2 = 0.9996$

## 40 min

$y = 0.0419x^{0.6071}$
$R^2 = 0.9989$

## 60 min

$y = 0.0463x^{0.5888}$
$R^2 = 0.9979$

## 80 min

$y = 0.0464x^{0.5877}$
$R^2 = 0.9982$

## 120 min

$y = 0.0405x^{0.6105}$
$R^2 = 0.995$

250ppm PAM Tap water



**Run 0**

$y = 0.005x^{0.8449}$
$R^2 = 0.9993$

◆ Run 0

**Run 1**

$y = 0.0033x^{0.8911}$
$R^2 = 0.9997$

■ Run 1

## Run 4

$y = 0.0027x^{0.9126}$
$R^2 = 0.9997$

▲ Run 4

## Run 6

$y = 0.0032x^{0.8881}$
$R^2 = 0.9993$

✕ Run 6

From this Data the Generalized Reynolds Number is calculated. The dimensions of the setup are found in Table 3.5. Included below is the Raw Data from the setup:

1inch

| 200PAM 0 min | | | 200 PAM 60 min | | | 200 PAM 120 min | |
|---|---|---|---|---|---|---|---|
| Channel 1(V) | Channel 3(V) | | Channel 1(V) | Channel 3(V) | | Channel 1(V) | Channel 3(V) |
| 2.663 | 1.115 | | 2.615 | 1.208 | | 2.578 | 1.252 |
| 2.775 | 1.129 | | 2.792 | 1.239 | | 2.824 | 1.313 |
| 3.029 | 1.154 | | 3.268 | 1.339 | | 3.448 | 1.503 |
| 3.664 | 1.224 | | 4.02 | 1.553 | | 4.748 | 1.976 |
| 4.208 | 1.315 | | 3.26 | 1.342 | | 3.587 | 1.565 |

1.5inch

| 200PAM 0 min | | | 200PAM 60 min | | | 200PAM 120 min | | |
|---|---|---|---|---|---|---|---|---|
| Channel 0(V) | Channel 1(V) | Channel 3(V) | Channel 0(V) | Channel 1(V) | Channel 3(V) | Channel 0(V) | Channel 1(V) | Channel 3(V) |
| | 2.238 | 1.872 | | 2.185 | 2.137 | | 2.135 | 2.34 |
| | 2.298 | 1.925 | | 2.372 | 2.495 | | 2.26 | 2.638 |
| | 2.563 | 2.393 | | 2.777 | 3.373 | | 2.569 | 3.419 |
| | 3.079 | 3.207 | 3.335 | 3.536 | | 4.172 | 3.659 | |
| | 3.819 | 4.843 | 4.33 | 4.076 | | 4.799 | 3.943 | |
| 3.112 | 3.884 | | 4.645 | 4.235 | | | | |
| 3.657 | 4.276 | | | | | | | |
| 4.109 | 4.494 | | | | | | | |

1.5Inch

| 200PAM/100AMP 0 min | | 60 min | | 120 min | |
|---|---|---|---|---|---|
| Channel 1 | Channel 3 | Channel 1 | Channel 3 | Channel 1 | Channel 3 |
| 2.431 | 1.11 | 2.52 | 1.188 | 2.548 | 1.208 |
| 2.596 | 1.136 | 2.682 | 1.209 | 2.771 | 1.263 |
| 2.997 | 1.173 | 3.031 | 1.279 | 3.369 | 1.436 |
| 4.162 | 1.302 | 3.88 | 1.499 | 4.438 | 1.812 |
| 4.616 | 1.382 | 4.484 | 1.692 | 4.711 | 1.938 |
| | | 4.784 | 1.79 | 3.417 | 1.431 |

1Inch

| 200PAM/100AMP 0 min | | | 60 min | | | 120 min | | |
|---|---|---|---|---|---|---|---|---|
| Channel 0 | Channel 1 | Channel 3 | Channel 0 | Channel 1 | Channel 3 | Channel 0 | Channel 1 | Channel 3 |
|  | 2.238 | 1.872 |  | 2.185 | 2.137 |  |  |  |
|  | 2.298 | 1.925 |  | 2.372 | 2.495 |  | 2.135 | 2.34 |
|  | 2.563 | 2.393 |  | 2.777 | 3.373 |  | 2.26 | 2.638 |
|  | 3.079 | 3.207 | 3.335 | 3.536 |  |  | 2.569 | 3.419 |
|  | 3.819 | 4.843 | 4.33 | 4.076 |  | 4.172 | 3.659 |  |
| 3.112 | 3.884 |  | 4.645 | 4.235 |  | 4.799 | 3.943 |  |
| 3.657 | 4.276 |  |  |  |  |  |  |  |
| 4.109 | 4.494 |  |  |  |  |  |  |  |

Equation 3.9 is used to convert channel1 reading to mass flowrate, Table3.6 shows the conversion for channel0 and channel3 respectively

# Appendix B: PEO/Amphosol Data

Relevant Excel Files can be found at:

https://drive.google.com/folderview?id=0B1oHKhn79y6eeWxXM0VlTmxyekk&usp=sharing

## B.1 Bench-Scale Data

**100 ppm PEO**

| Surfactant concentration ppm | Conductivity microS/cm | Avg. Surface Tension (Dyne/cm) | Flow Time in sec | Relative Viscosity |
|---|---|---|---|---|
| 0 | 2.19 | 62.7 | 130.5 | 1.16865672 |
| 200 | 76.8 | 32.0 | 128.5 | 1.15074627 |
| 400 | 150.6 | 31.3 | 129.5 | 1.15970149 |
| 1000 | 374 | 32.2 | 130.5 | 1.16865672 |

| **200 ppm PEO** | **Discrepancy in conductivity due to DI difference in days not interaction 50 to 125 on one day rest on another** | | | |
|---|---|---|---|---|
| Surfactant concentration ppm | Conductivity microS/cm | Avg. Surface Tension (Dyne/cm) | Flow Time in sec | Relative Viscosity |
| 0 | 5.47 | 61.9 | 153 | 1.37014925 |
| 50 | 24.87 | 40.2 | | |
| 100 | 44 | 36.4 | 165.5 | 1.48208955 |
| 125 | 50.8 | 34.4 | | |
| 150 | 73.7 | 35.3 | 168.5 | 1.50895522 |
| 200 | 89.4 | 33.9 | 166.5 | 1.49104478 |
| 300 | 117.8 | 34.1 | 167.5 | 1.5 |
| 400 | 159.6 | 33.6 | 162 | 1.45074627 |
| 500 | 189.2 | 32.4 | 169 | 1.51343284 |
| 700 | 260 | 32.8 | 169 | 1.51343284 |
| 1000 | 369 | 32.9 | 168.5 | 1.50895522 |

| 500 ppm PEO | | | | |
|---|---|---|---|---|
| Surfactant concentration ppm | Conductivity microS/cm | Avg. Surface Tension (Dyne/cm) | Flow Time in sec | Relative Viscosity |
| 0 | 6.61 | 63.8 | 272.5 | 2.44029851 |
| 100 | 45.4 | 37.6 | 273 | 2.44477612 |
| 300 | 117.7 | 35.2 | 268 | 2.4 |
| 500 | 190.8 | 33.9 | 264 | 2.3641791 |
| 700 | 267.9 | 33.7 | 269.5 | 2.41343284 |
| 1000 | 369 | 33.6 | 266.5 | 2.38656716 |
| 5000 | 1725 | 33.6 | 265.5 | 2.37761194 |

| 1000 ppm PEO | | | | |
|---|---|---|---|---|
| Surfactant concentration ppm | Conductivity microS/cm | Avg. Surface Tension (Dyne/cm) | Flow Time in sec | Relative Viscosity |
| 0 | 11.15 | 63.0 | 353.5 | 3.16567164 |
| 300 | 122 | 35.3 | 392 | 3.51044776 |
| 500 | 192.1 | 34.4 | 371 | 3.32238806 |
| 700 | 262.6 | 34.2 | 443 | 3.96716418 |
| 1000 | 366 | 34.7 | 425.5 | 3.81044776 |
| 5000 | 1711 | 33.8 | 429.5 | 3.84626866 |
| 10000 | 3320 | 33.8 | 437.5 | 3.91791045 |

## B.2 Pilot-Plant Data

The Generalized Reynold number from Equation 3.7 (page 45) is calculated from a power-law fit of the Shear Stress to Shear Rate Data shown below

Shear Stress in Pascals on Y-Axis and Shear rate in inverse seconds on X-axis

1000ppm PEO
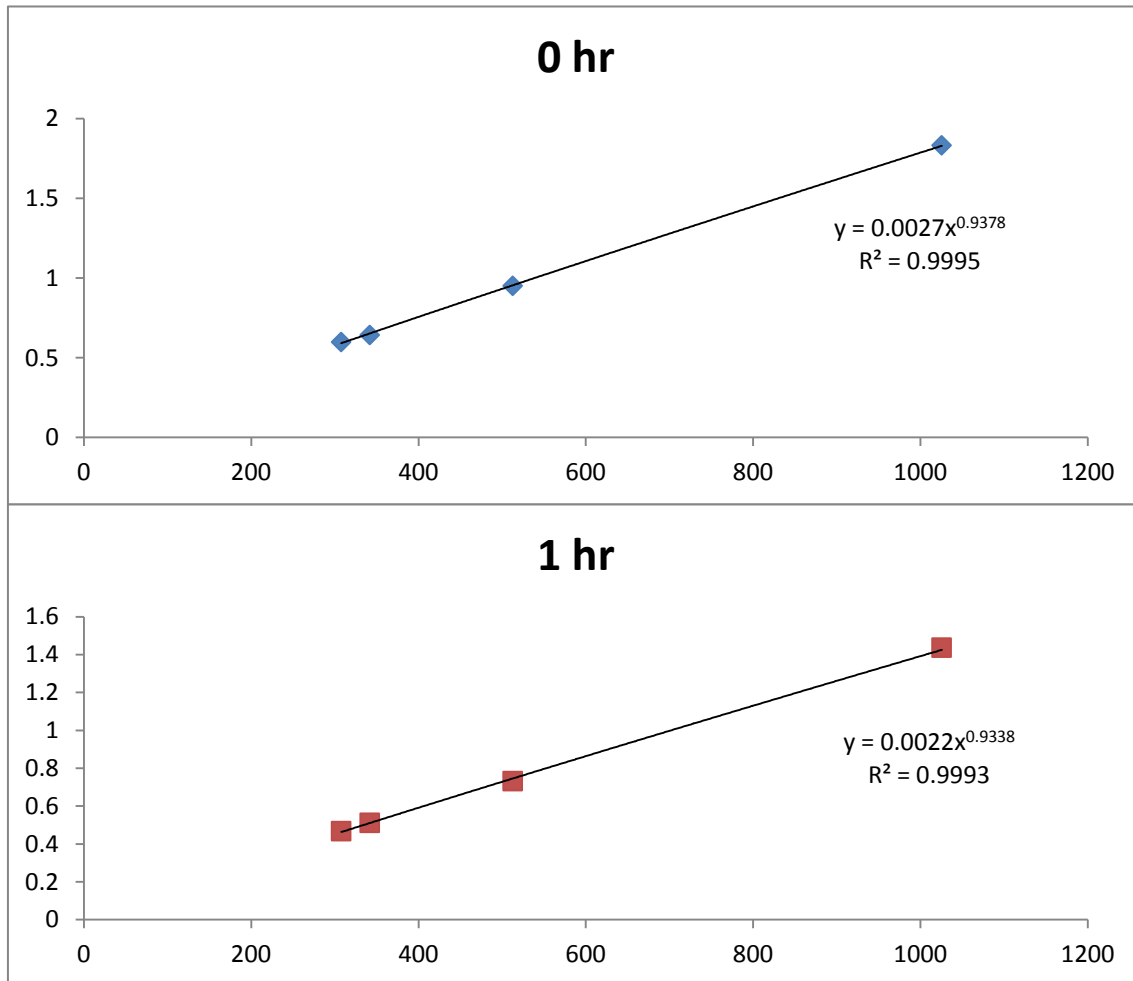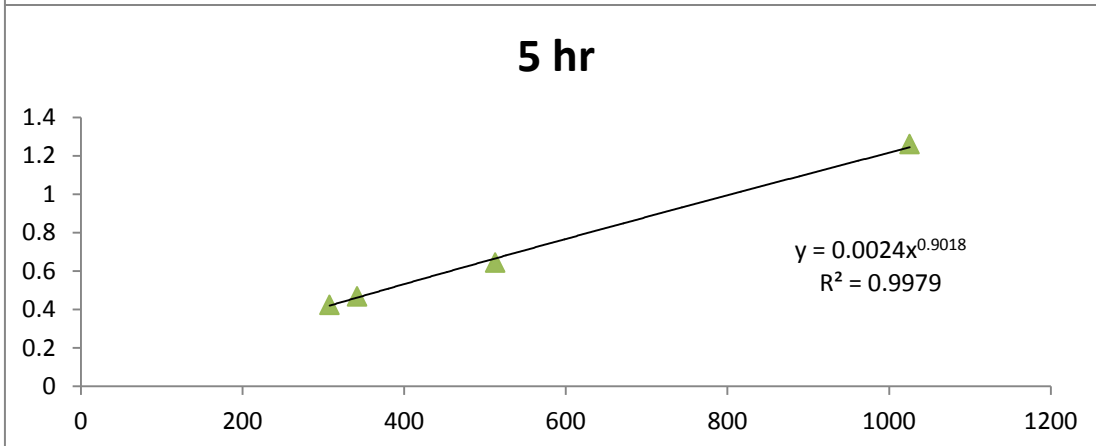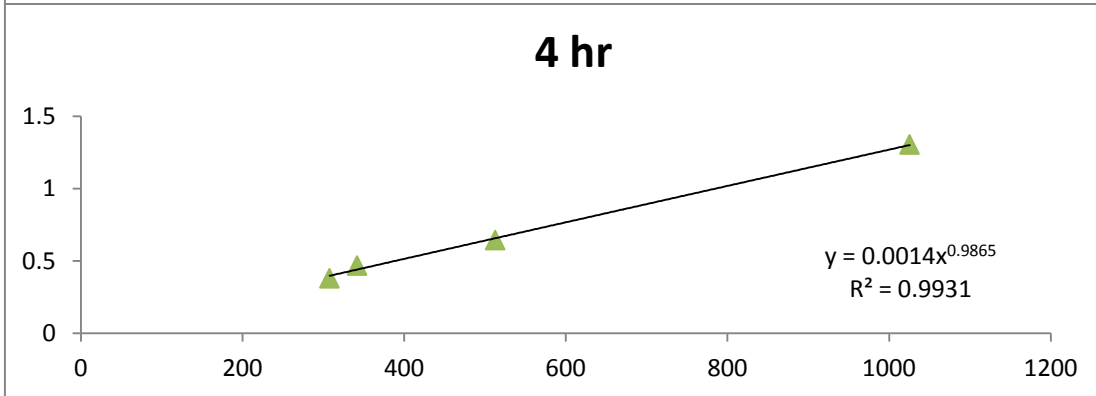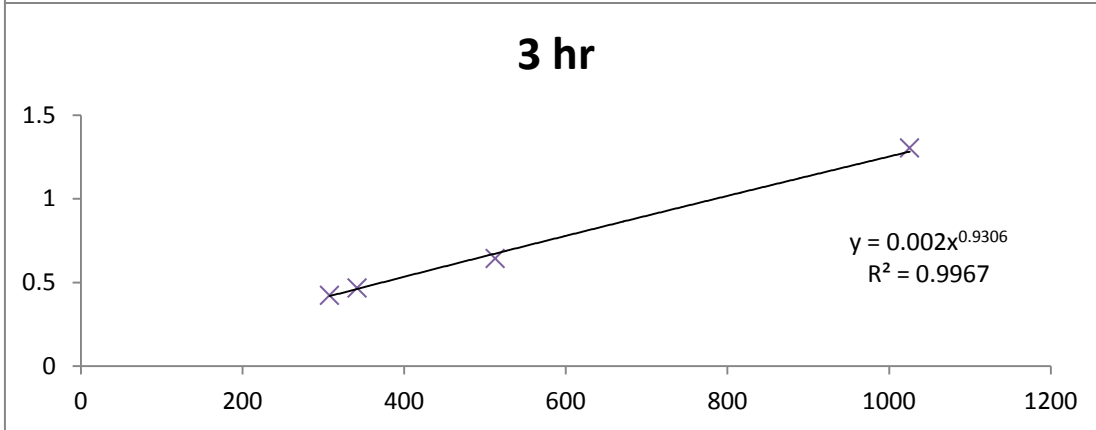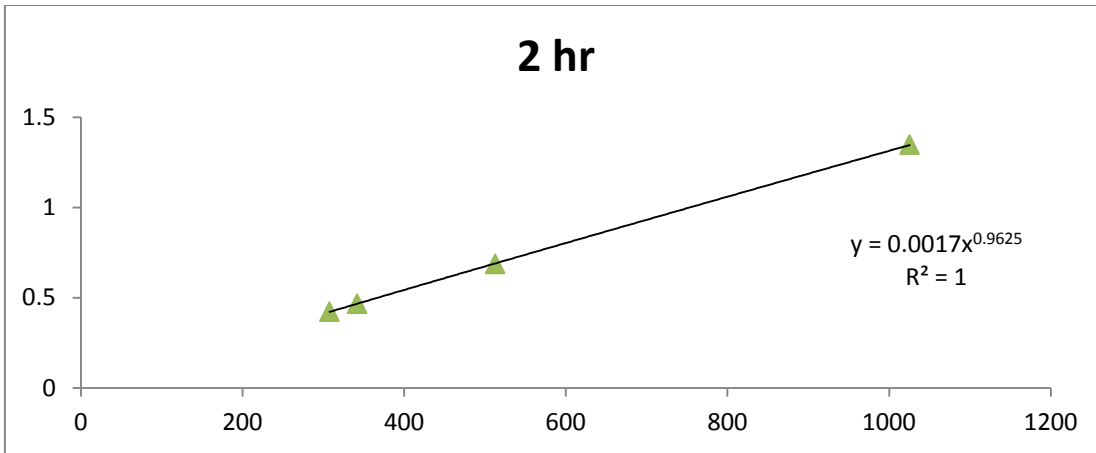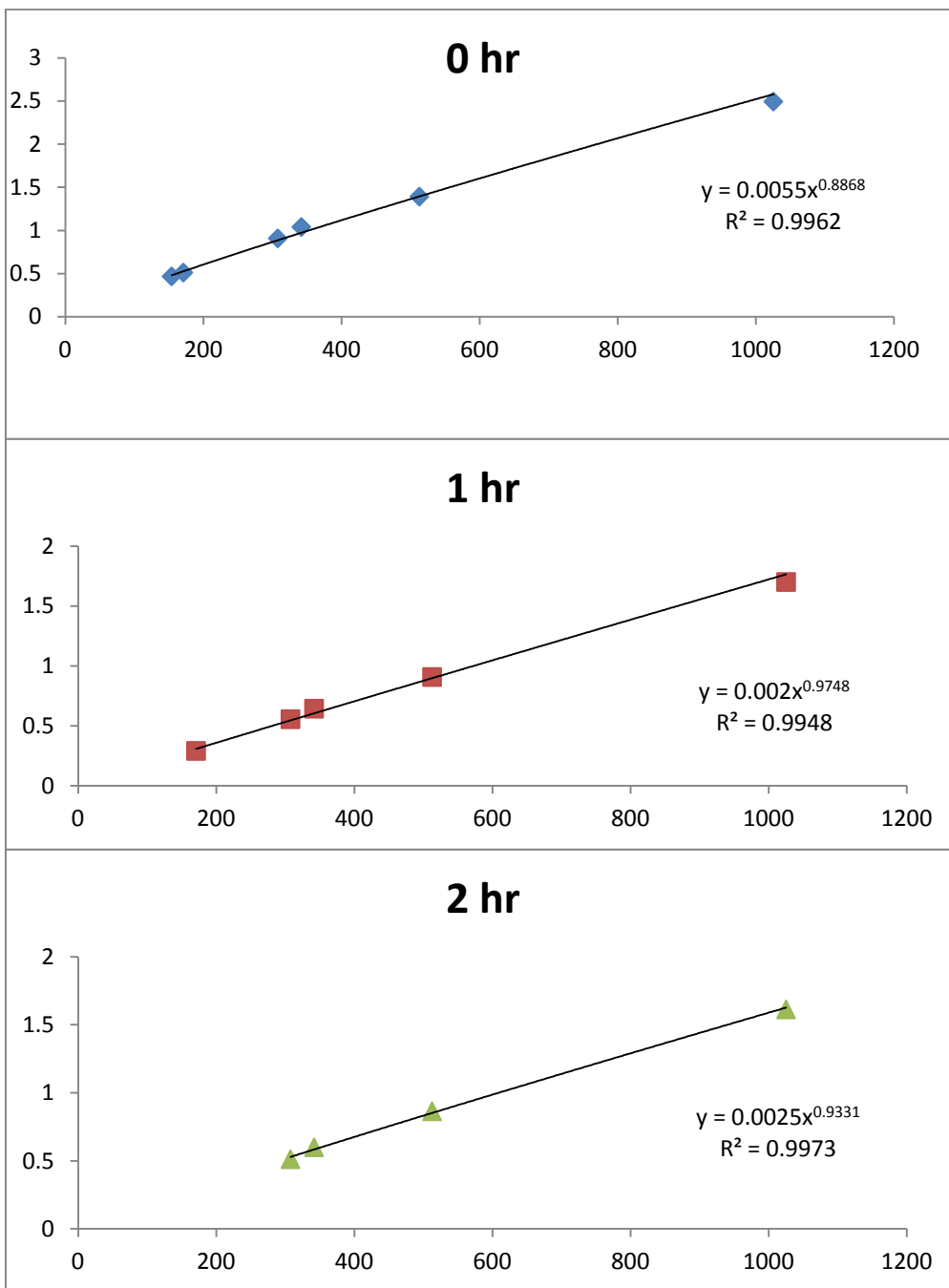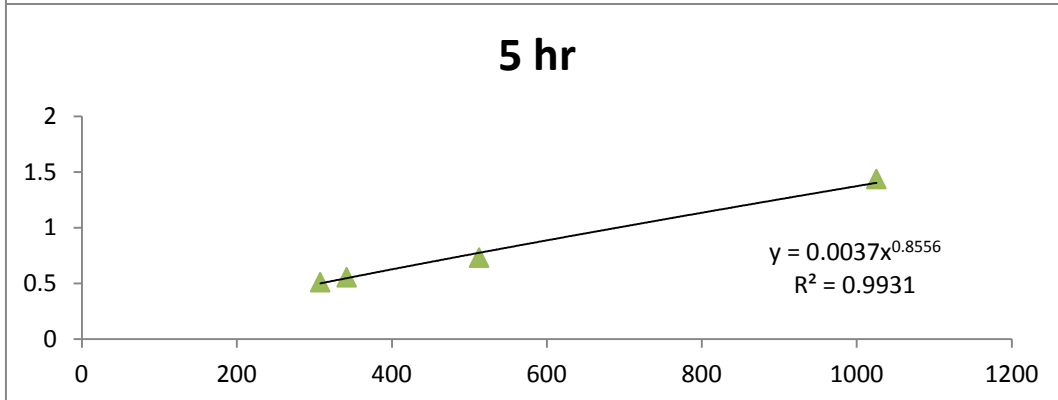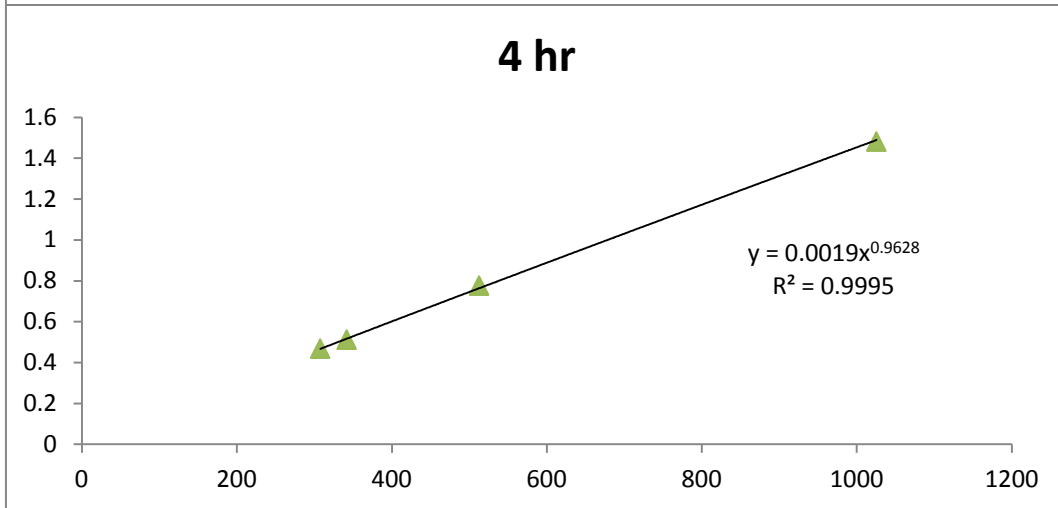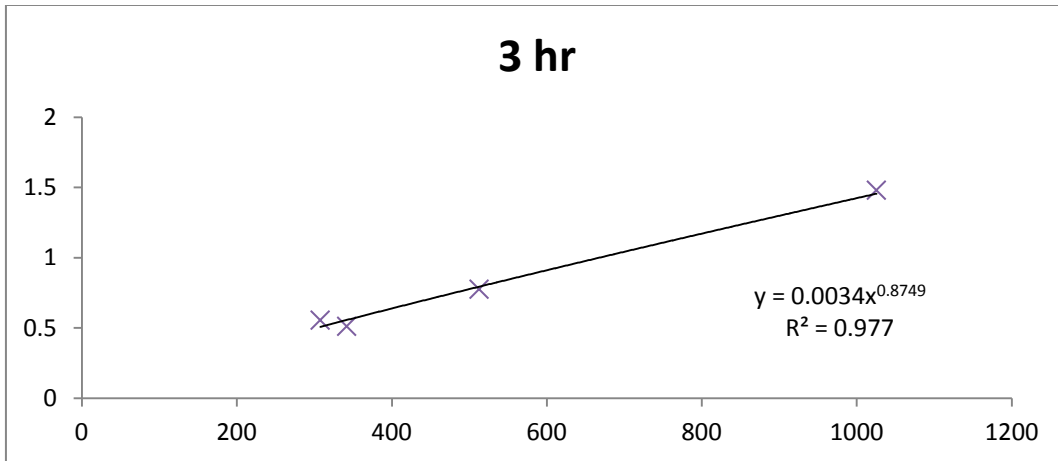


**0 hr**

$y = 0.0027x^{0.9378}$
$R^2 = 0.9995$

**1 hr**

$y = 0.0022x^{0.9338}$
$R^2 = 0.9993$

**2 hr**

$y = 0.0017x^{0.9625}$
$R^2 = 1$

**3 hr**

$y = 0.002x^{0.9306}$
$R^2 = 0.9967$

**4 hr**

$y = 0.0014x^{0.9865}$
$R^2 = 0.9931$

**5 hr**

$y = 0.0024x^{0.9018}$
$R^2 = 0.9979$

1000ppm PEO/700ppm Amphosol



0 hr

$y = 0.0055x^{0.8868}$
$R^2 = 0.9962$

1 hr

$y = 0.002x^{0.9748}$
$R^2 = 0.9948$

2 hr

$y = 0.0025x^{0.9331}$
$R^2 = 0.9973$

# 3 hr

$y = 0.0034x^{0.8749}$
$R^2 = 0.977$

# 4 hr

$y = 0.0019x^{0.9628}$
$R^2 = 0.9995$

# 5 hr

$y = 0.0037x^{0.8556}$
$R^2 = 0.9931$

From this Data the Generalized Reynolds Number is calculated. The dimensions of the setup are found in Table 3.5. Included below is the Raw Data from the setup:

1.5Inch

| 1000PEO 0min | | 3hr | | 4hr | | 5hr | |
|---|---|---|---|---|---|---|---|
| Channel 1 | Channel 3 | Channel 1 | Channel 3 | Channel 1 | Channel 3 | Channel 1 | Channel 3 |
| 2.479 | 1.453 | 2.483 | 1.502 | 2.488 | 1.415 | 2.486 | 1.494 |
| 2.594 | 1.505 | 2.564 | 1.554 | 2.65 | 1.541 | 2.702 | 1.631 |
| 3.05 | 1.711 | 2.815 | 1.725 | 2.898 | 1.74 | 3.415 | 2.183 |
| 3.549 | 1.936 | 3.559 | 2.337 | 3.526 | 2.242 | 4.467 | 3.236 |
| 4.72 | 2.478 | 4.665 | 3.418 | 4.66 | 3.43 | | |
| | | 4.952 | 3.709 | | | | |

1Inch

| 1000PEO 0 min | | | 3hr | | 4hr | | | 5hr | |
|---|---|---|---|---|---|---|---|---|---|
| Channel 0 | Channel 1 | Channel 3 | Channel 0 | Channel 1 | Channel 0 | Channel 1 | Channel 3 | Channel 0 | Channel 1 |
| | 1.698 | 1.971 | 2.215 | 1.977 | | 1.986 | 3.26 | 2.195 | 1.976 |
| | 1.837 | 2.302 | 2.491 | 2.105 | | 2.037 | 3.467 | 2.285 | 2.017 |
| | 1.994 | 2.646 | 3.433 | 2.479 | 3.202 | 2.402 | | 2.53 | 2.125 |
| | 2.258 | 3.38 | 3.921 | 2.678 | 4.141 | 2.723 | | 3.316 | 2.431 |
| | 2.77 | 4.763 | | | | 2.592 | | | |
| | | | | | 3.74 | | 4.569 | 2.849 | |
| 3.959 | 3.442 | | | | | | | | |
| 4.275 | 3.578 | | | | | | | | |
| 4.634 | 3.798 | | | | | | | | |

1.5Inch

| 1000PEO/700AMP 0min | | 3hr | | 4hr | | 5hr | |
|---|---|---|---|---|---|---|---|
| Channel 1 | Channel 3 | Channel 1 | Channel 3 | Channel 1 | Channel 3 | Channel 1 | Channel 3 |
| 2.108 | 1.223 | 2.575 | 1.409 | 2.681 | 1.391 | 2.663 | 1.405 |
| 2.257 | 1.279 | 2.665 | 1.463 | 2.753 | 1.443 | 2.799 | 1.493 |
| 2.612 | 1.397 | 2.853 | 1.582 | 3.261 | 1.822 | 3.289 | 1.871 |
| 3.282 | 1.701 | 3.163 | 1.819 | 3.603 | 2.19 | 3.878 | 2.489 |
| 4.039 | 2.096 | 3.768 | 2.403 | 3.953 | 2.567 | 4.544 | 3.254 |
| 4.148 | 2.156 | 4.267 | 2.892 | 4.716 | 3.491 | 4.761 | 3.526 |
| | | 4.77 | 3.424 | 4.07 | 2.705 | | |

1Inch

| 0 min | | | 3hr | | 4hr | | 5hr | |
|---|---|---|---|---|---|---|---|---|
| Channel 0 | Channel 1 | Channel 3 | Channel 0 | Channel 1 | Channel 0 | Channel 1 | Channel 0 | Channel 1 |
| | 1.719 | 1.921 | 1.945 | 1.986 | 1.953 | 2.027 | 1.996 | 2.001 |
| | 1.852 | 2.226 | 2.218 | 2.101 | 2.217 | 2.145 | 2.174 | 2.092 |
| | 2.036 | 2.695 | 2.717 | 2.294 | 3.298 | 2.497 | 2.794 | 2.329 |
| | 2.391 | 3.73 | 3.879 | 2.718 | 4.437 | 2.854 | 3.934 | 2.688 |
| 3.433 | 2.994 | | 3.004 | 2.395 | 3.763 | 2.644 | 4.107 | 2.746 |
| 4.194 | 3.405 | | 4.591 | 2.969 | | | 4.197 | 2.777 |
| | | | | | | | 4.391 | 2.837 |

Equation 3.9 is used to convert channel1 reading to mass flowrate, Table3.6 shows the conversion for channel0 and channel3 respectively

# Appendix C: PAM/PEO Data

Relevant Excel Files can be found at:
https://drive.google.com/folderview?id=0B1oHKhn79y6eeWxXM0VlTmxyekk&usp=sharing

## C.1 Bench-Scale Data

## 100 ppm PAM

| PEO concentration ppm | Conductivity microS/cm | Avg. Surface Tension (Dyne/cm) | Flow Time (seconds) | Relative Viscosity |
|---|---|---|---|---|
| 0 | 25.49 | 71.5 | 322 | 2.88358209 |
| 100 | 25.62 | 63.1 | 336.5 | 3.013432836 |
| 200 | 25.67 | 63.0 | 343 | 3.071641791 |
| 500 | 25.63 | 63.3 | 376 | 3.367164179 |
| 1000 | 25.93 | 63.0 | 432 | 3.868656716 |

## 200 ppm PAM

| PEO concentration ppm | Conductivity microS/cm | Avg. Surface Tension (Dyne/cm) | Flow Time (sec) | Relative Viscosity |
|---|---|---|---|---|
| 0 | 47.9 | 71.8 | 573 | 5.131343284 |
| 100 | 47.1 | 62.9 | 611 | 5.471641791 |
| 200 | 46.9 | 62.6 | 635 | 5.686567164 |
| 500 | 46.4 | 62.7 | 735.5 | 6.586567164 |
| 1000 | 46.5 | 62.9 | 906 | 8.113432836 |

## C.2 Pilot-Plant Data

The Generalized Reynold number from Equation 3.7 (page 45) is calculated from a power-law fit of the Shear Stress to Shear Rate Data shown below

Shear Stress in Pascals on Y-Axis and Shear rate in inverse seconds on X-axis

**0 hr**

$y = 0.0235x^{0.7001}$
$R^2 = 0.9996$

- Series1
- Power (Series1)

**1 hr**

$y = 0.0109x^{0.7657}$
$R^2 = 0.9995$

- Run 1
- Power (Run 1)

**2 hr**

$y = 0.0149x^{0.7113}$
$R^2 = 0.9994$

▲ Run 4

**3 hr**

$y = 0.0135x^{0.7133}$
$R^2 = 0.9974$

✕ Run 6

**4 hr**

$y = 0.0088x^{0.7688}$
$R^2 = 0.9981$

Series3

**5 hr**

$y = 0.0112x^{0.7275}$
$R^2 = 0.9994$

Series3
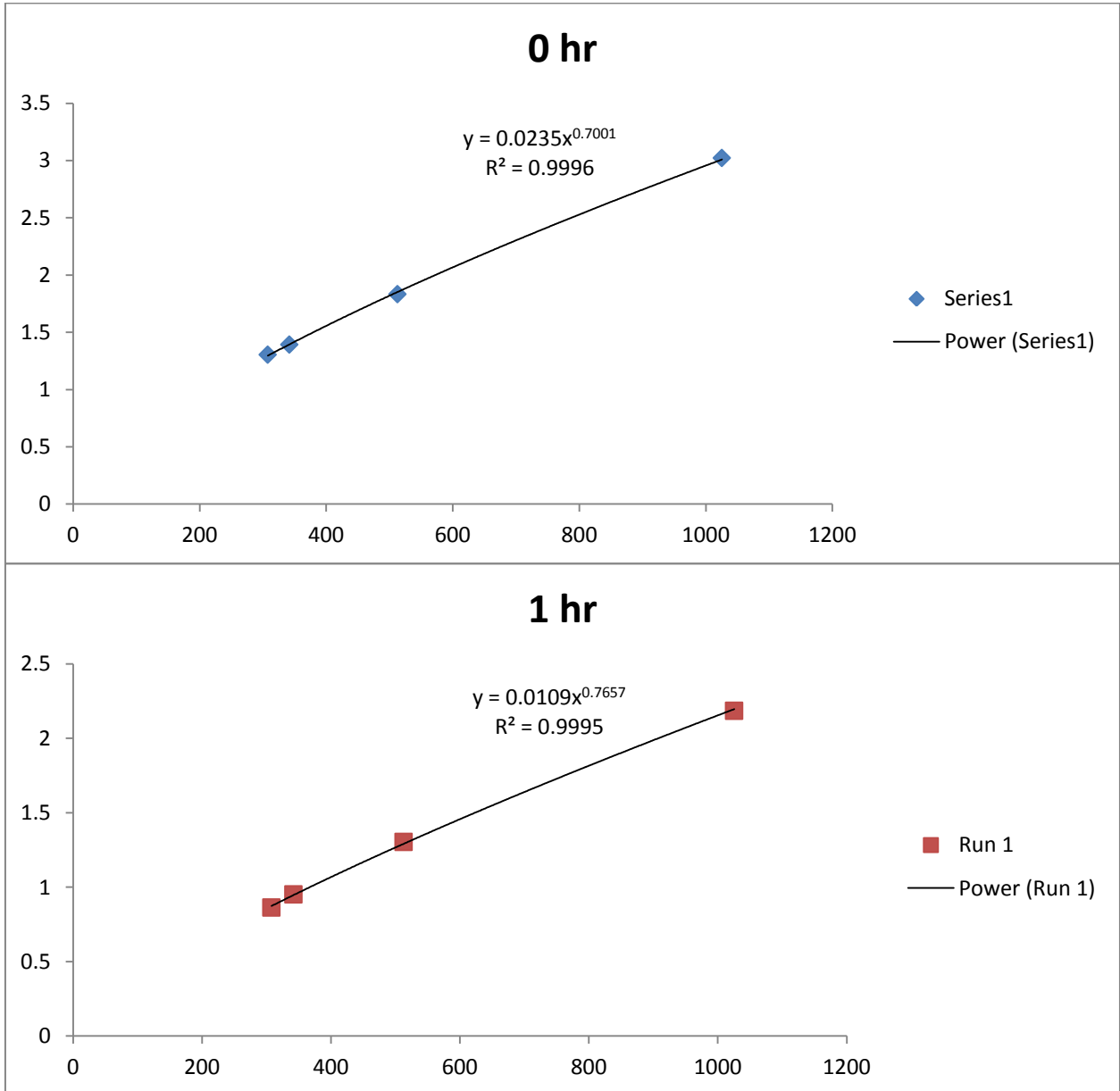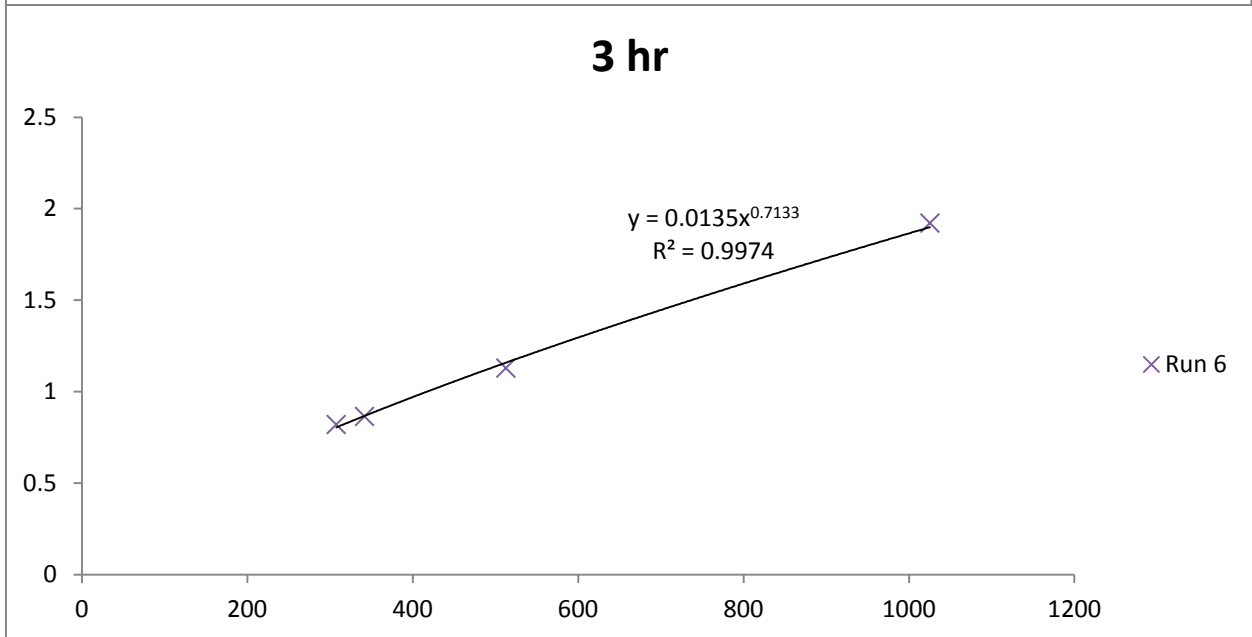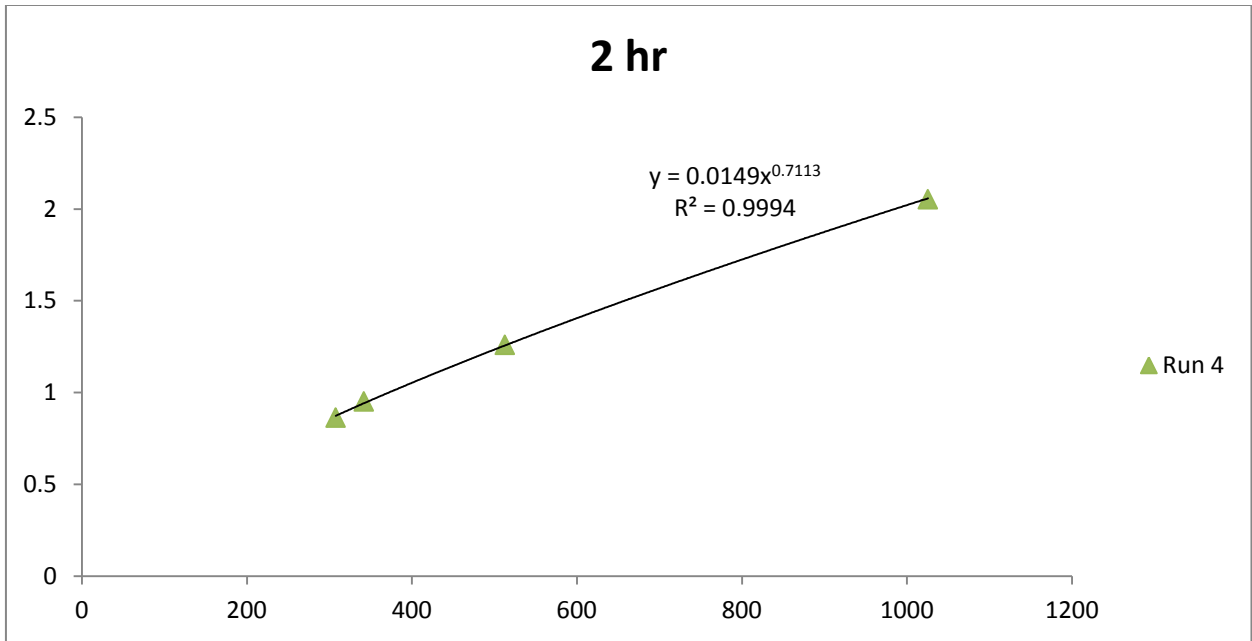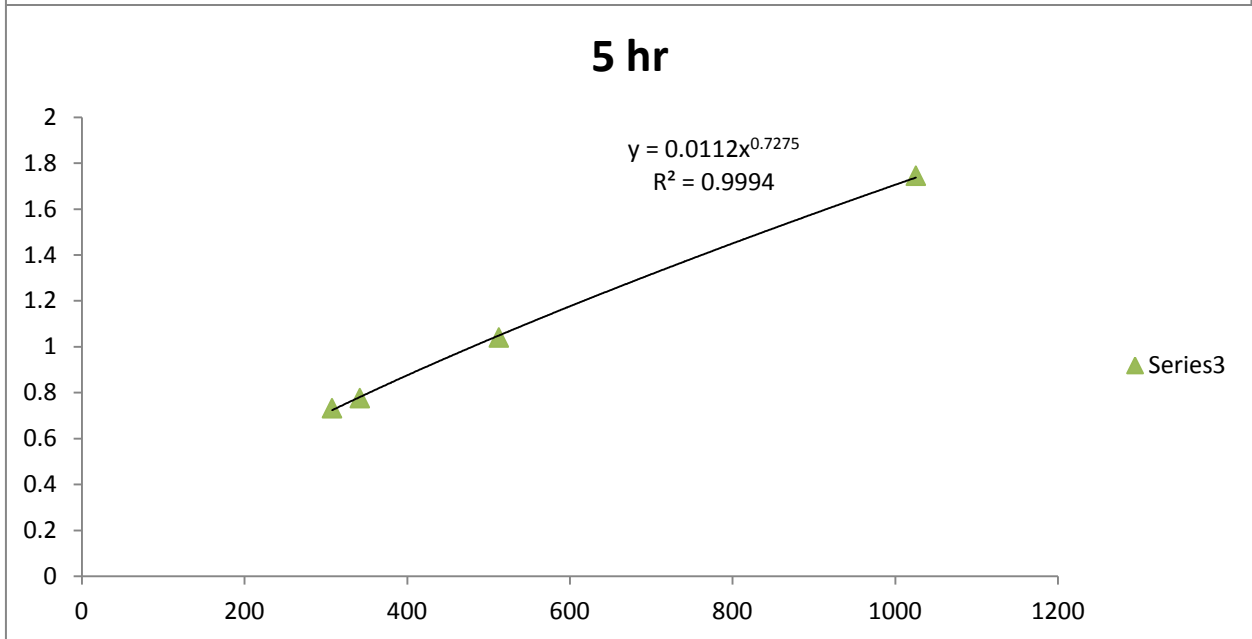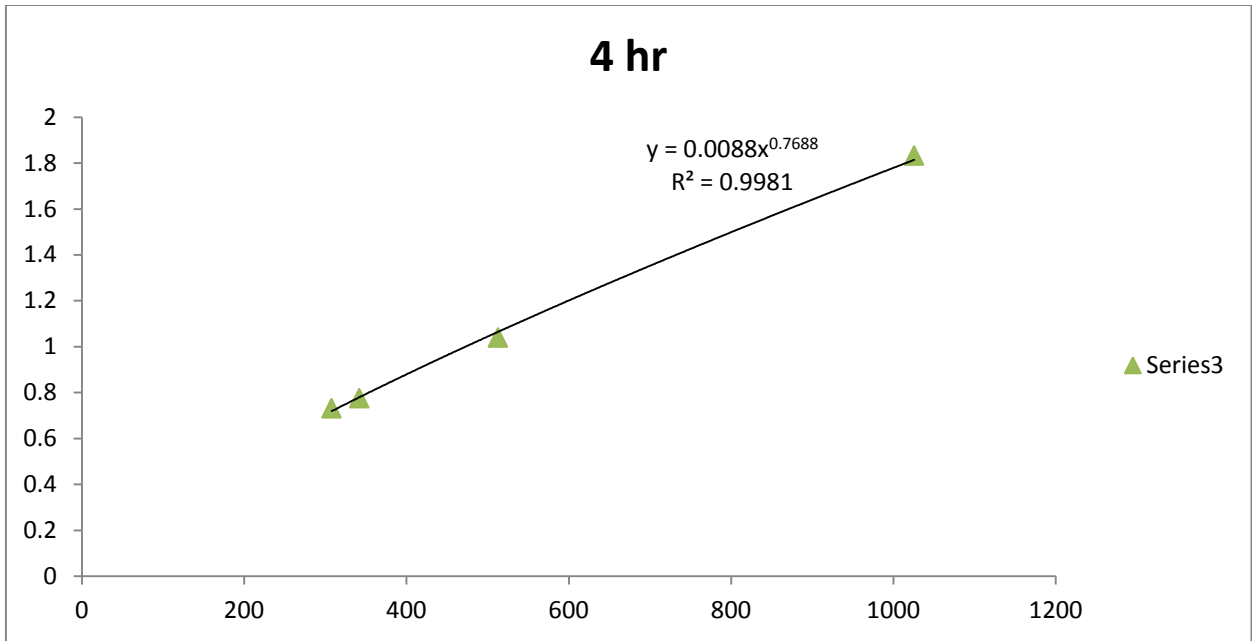
From this Data the Generalized Reynolds Number is calculated. The dimensions of the setup are found in Table 3.5. Included below is the Raw Data from the setup:

1.5Inch

| 100PAM/500PEO 0min | | 1hr | | 2hr | | 3hr | | 4hr | |
|---|---|---|---|---|---|---|---|---|---|
| Channel 1 | Channel 3 | Channe l 1 | Channe l 3 | Channe l 1 | Channe l 3 | Channe l 1 | Channe l 3 | Channe l 1 | Channe l 3 |
| 2.566 | 1.163 | 2.49 | 1.254 | 2.489 | 1.265 | 2.509 | 1.281 | 2.504 | 1.32 |
| 2.901 | 1.238 | 2.658 | 1.298 | 2.711 | 1.343 | 2.717 | 1.363 | 2.593 | 1.351 |
| 3.354 | 1.334 | 2.942 | 1.385 | 3.009 | 1.438 | 3.136 | 1.527 | 2.944 | 1.514 |
| 4.106 | 1.518 | 3.37 | 1.552 | 3.775 | 1.808 | 3.816 | 1.902 | 3.518 | 1.828 |
| 4.392 | 1.62 | 4.157 | 1.899 | 4.453 | 2.197 | 4.258 | 2.186 | 2.928 | 1.516 |
| 3.471 | 1.3843 | 4.566 | 2.148 | 4.685 | 2.359 | 4.611 | 2.471 | 3.698 | 1.94 |
| | | | | | | | | 4.276 | 2.371 |

| 5hr | |
|---|---|
| Channel 1 | Channel 3 |
| 2.51 | 1.34 |
| 2.633 | 1.394 |
| 2.844 | 1.489 |
| 3.274 | 1.727 |
| 3.873 | 2.147 |
| 4.29 | 2.476 |
| 4.874 | 2.977 |

1Inch

| 100PAM / 500PEO 0 min | | 1hr | | 2hr | | 3hr | | 4hr | |
|---|---|---|---|---|---|---|---|---|---|
| Channel 0 | Channel 1 | Channel 0 | Channe l 1 | Channe l 0 | Channe l 1 | Channe l 0 | Channe l 1 | Channe l 0 | Channe l 1 |
| 1.584 | 2.075 | 1.658 | 2.003 | 1.724 | 1.995 | 1.708 | 1.978 | 1.827 | 1.982 |
| 1.69 | 2.199 | 1.755 | 2.088 | 1.892 | 2.133 | 1.908 | 2.123 | 1.882 | 2.037 |
| 1.954 | 2.452 | 2.09 | 2.354 | 2.235 | 2.358 | 2.382 | 2.445 | 2.129 | 2.196 |
| 2.651 | 3.02 | 3.11 | 2.993 | 2.934 | 2.755 | 3.468 | 2.918 | 2.83 | 2.537 |
| 3.388 | 3.471 | 3.964 | 3.371 | 4.167 | 3.291 | 4.554 | 3.345 | 3.894 | 2.992 |

| 4.495 | 4.102 | 3.243 | 3.027 | 3.799 | 3.138 | 2.125 | 2.247 | 3.549 | 2.831 |
| 4.77 | 4.235 | 4.118 | 3.447 | | | | | | |

| 5hr | |
| --- | --- |
| Channel 0 | Channel 1 |
| 1.813 | 1.964 |
| 1.968 | 2.06 |
| 2.272 | 2.232 |
| 2.936 | 2.536 |
| 4.424 | 3.117 |
| 2.862 | 2.503 |
| 3.415 | 2.734 |

Equation 3.9 is used to convert channel1 reading to mass flowrate, Table3.6 shows the conversion for channel0 and channel3 respectively

## *Bibliography*

BELLARE, J.R., KANEKO, T. and EVANS, D.F., 1988. Seeing Micelles. *Langmuir,* **4**(4), pp. 1066-1067.

BEWERSDORFF, H.W., DOHMANN, J., LANGOWSKI, J., LINDNER, P., MAACK, A., OBERTHUR, R. and THIEL, H., 1989. Sans-Studies and Ls-Studies on Drag-Reducing Surfactant Solutions. *Physica B,* **156**, pp. 508-511.

BEWERSDORFF, H.W., GYR, A., HOYER, K. and TSINOBER, A., 1993. An Investigation of Possible Mechanisms of Heterogeneous Drag Reduction in Pipe and Channel Flows. *Rheologica Acta,* **32**(2), pp. 140-149.

BEWERSDORFF, H.W. and OHLENDORF, D., 1988. The Behavior of Drag-Reducing Cationic Surfactant Solutions. *Colloid and Polymer Science,* **266**(10), pp. 941-953.

BEWERSDORFF, H.W. and THIEL, H., 1993. Turbulence Structure of Dilute Polymer and Surfactant Solutions in Artificially Roughened Pipes. *Applied Scientific Research,* **50**(3-4), pp. 347-368.

BEWERSDORFF, H., 1986. Heterogeneous Drag Reduction in Turbulent Pipe Flow. In: B. GAMPERT, ed, Springer Berlin Heidelberg, pp. 337-348.

CHARA, Z., ZAKIN, J., SEVERA, M. and MYSKA, J., 1993. Turbulence Measurements of Drag-Reducing Surfactant Systems. *Experiments in Fluids,* **16**(1), pp. 36-41.

CHOU, L.C. AND J.L. ZAKIN, 1991. Use of Mixed Cations and Mixed Counter-Ion to Extend the Effective Temperature Range for Drag Reducing Surfactant Additives, *Proc. International Symposium on Fluis for District Heatring, Copenhagen, Denmark* 1991, pp. 75-86.

CHRISTENSEN, R.N. AND J.L. ZAKIN, June 1991. Drag and Heat Transfer Reduction in Circular Tubes and Plate Fin Heat Exchangers, *Proc. 82nd Int. District Heating and Cooling Assoc.* June 1991, pp. 182-202.

DEROUSSEL, P., 1993. *Nonionic Surfactant Drag Reduction*, The Ohio State University, Columbus, OH.

DOI, M. and EDWARDS, S.F., 1978. Dynamics of Rod-Like Macromolecules in Concentrated-Solution .1. *Journal of the Chemical Society-Faraday Transactions Ii,* **74**, pp. 560-570.

DOI, M. and EDWARDS, S.F., 1978. Dynamics of Rod-Like Macromolecules in Concentrated-Solution .2. *Journal of the Chemical Society-Faraday Transactions Ii,* **74**, pp. 918-932.

ELSON, T.P. and GARSIDE, J., 1983. Drag Reduction in Aqueous Cationic Soap Solutions. *Journal of Non-Newtonian Fluid Mechanics,* **12**(2), pp. 121-133.

GASLJEVIC, K. AMD E.F. MATTHYS, 1995. On the Diameter Effect for Turbulent Flow of Drag-Reducing Surfactant Solutions. *Development and Application of Non-Newtonian Flows III, IMECE, San Francisco ASME Pub.,* **231**, pp. 237-243.

GILLISSEN, J.J.J., 2008. Polymer flexibility and turbulent drag reduction. *Physical Review E,* **78**(4), pp. 046311.

GRAVSHOLT, S., 1976. Viscoelasticity in Highly Dilute Aqueous-Solutions of Pure Cationic Detergents. *Journal of colloid and interface science,* **57**(3), pp. 575-577.

HARDER, K. and TIEDERMAN, W., 1991. Drag Reduction and Turbulent Structure in 2-Dimensional Channel Flows. *Philosophical Transactions of the Royal Society of London Series A-Mathematical Physical and Engineering Sciences,* **336**(1640), pp. 19-34.

HERSHEY, H.C. and ZAKIN, J.L., 1967. A Molecular Approach to Predicting Onset of Drag Reduction in Turbulent Flow of Dilute Polymer Solutions. *Chemical Engineering Science,* **22**(12), pp. 1847-&.

HERSHEY, H., KUO, J. and MCMILLAN, M., 1975. Drag Reduction of Straight and Branched-Chain Aluminum Disoaps. *Industrial & Engineering Chemistry Product Research and Development,* **14**(3), pp. 192-199.

HOFFMANN, H. and M. LOBYL AND H. REHAGE, 1985. Flow Birefringence and Rheological Measurements on Viscoelastic Detergent Solutions. *Physics of Amphiphiles: Micells, Vesicles and Microemulsions V. Degiorgio and M.Corti, eds. North Holland, Amsterdam,* , pp. 237-260.

HOYT, J.W. and SELLIN, R.H.J., 1991. Polymer Threads and Drag Reduction. *Rheologica Acta,* **30**(4), pp. 307-315.

HOYT, J., 1991. Negative Roughness and Polymer Drag Reduction. *Experiments in Fluids,* **11**(2-3), pp. 142-146.

LANDAHL, M.T., 1977. Dynamics of Boundary-Layer Turbulence and Mechanism of Drag Reduction. *Physics of Fluids,* **20**(10), pp. S55-S63.

LINDER, P., H.W. BEWERSDORDD, R. HEEN, P. SITTART, H. THIEL, J. LANGOWSKI AND R, OBERTHUR, 1990. *Program Colloidal Polymer Science,* **81**, pp. 107-112.

LU, B., 1997. *Ph.D Dissertation*, The Ohio State University, Columbus, Ohio.

LU, B., Y. TALMON AND J.L. ZAKIN, June 9-13 1996. The Effect of Counterion Chemical Structure Variations on the MicroStructure, Drag Reduction and Rheological Behavior of Cationinc Surfactants, *presented at 11th International Symposium on Surfactants in Solution, Jerusalem, Israel* June 9-13 1996.

LU, B., Y. TALMON AND J.L. ZAKIN, 1996. Effect of Counterion to Surfactant Ratio on Drag Reduction and Rheology of Cationic Surfactant Systems in. *Turbulence Modification and Drag Reduction, ASME Pub.,* **FED-Vol 237**, pp. 169-175.

LU, B.,X. LI, Y. TALMON AND J.L. ZAKIN, Novermber 10-15 1996. Extensional and Shear Rheometric Flow Studies, Drag Reduction and Microstructure of Cationic Surfactant Solutions, *AIChe 1996 Annual Meeting, paper 990, Chicago* Novermber 10-15 1996.

LU, B.,X. LI, Y. TALMON AND J.L. ZAKIN, 1996. Influence of Chemical Structures of Cationic Surfactants on Their Drag Reduction and Rheological Behaviors, *Proc. XIIth International Congress on Rheology, Quebec, Canada* 1996.

LU, B., LI, X., ZAKIN, J.L. and TALMON, Y., 1997. A non-viscoelastic drag reducing cationic surfactant system. *Journal of Non-Newtonian Fluid Mechanics,* **71**(1-2), pp. 59-72.

MATRAS, Z., MALCHER, T. and GZYL-MALCHER, B., 2008. The influence of polymer-surfactant aggregates on drag reduction. *Thin Solid Films,* **516**(24), pp. 8848-8851.

MATTHYS, E.F., 1991. Heat-Transfer, Drag Reduction, and Fluid Characterization for Turbulent-Flow of Polymer-Solutions - Recent Results and Research Needs. *Journal of Non-Newtonian Fluid Mechanics,* **38**(2-3), pp. 313-342.

MCCOMB, W.D. and RABIE, L.H., 1982. Local Drag Reduction due to Injection of Polymer-Solutions into Turbulent-Flow in a Pipe .1. Dependence on Local Polymer Concentration. *AICHE Journal,* **28**(4), pp. 547-557.

MCMILLAN, M.L., 1970. *Ph.D. Dissertation*, The Ohio State Universtiy, Columbus, OH.

MOHSENIPOUR, A.A., 2011. *Turbulent Drag Reduction by Polymers, Surfactants and their Mixtures in Pipeline Flow* , University of Waterloo.

MONTI, R., 1972. Heat Transfer in Drag Reducing Solutions. *Progress in Heat and Mass Transfer,* **5**, pp. 239-261.

OHLENDORF, D., INTERTHAL, W. and HOFFMANN, H., 1986. Surfactant Systems for Drag Reduction - Physicochemical Properties and Rheological Behavior. *Rheologica Acta,* **25**(5), pp. 468-486.

PARK, S.P., H.S. SUH, S.H. MOON AND H.K. YOON, 1996. Pump and Temperature Effects on and Flow Characteristics of Drag Reducing Surfactants, *Turbulence Modification and Drag Reduction* 1996, pp. 177-182.

PINHO, F.T. and WHITELAW, J.H., 1990. Flow of Non-Newtonian Fluids in a Pipe. *Journal of Non-Newtonian Fluid Mechanics,* **34**(2), pp. 129-144.

POLLERT, J., P. KOMRZY, K. SVEJKOVSKY, J. POLLERT JUN, B. LU AND J.L. ZAKIN, 1996. Drag Reduction and Heat Transfer of Cationic Surfactant Solutions, *"Turbulence Modification and Drag Reduction," Proc. ASME Fluids Engineering Division Summer Meeting* 1996, pp. 31-36.

PORTE, G., J. APPELL AND Y. POGGI, 1980. *J.Phys.Chem.,* **84**, pp. 3105-3110.

REHAGE, H. and HOFFMANN, H., 1991. Viscoelastic Surfactant Solutions - Model Systems for Rheological Research. *Molecular Physics,* **74**(5), pp. 933-973.

REHAGE, H., HOFFMANN, H. and WUNDERLICH, I., 1986. A Rheological Switch - Shear Induced Phase-Transitions in Aqueous Surfactant Solutions. *Berichte Der Bunsen-Gesellschaft-Physical Chemistry Chemical Physics,* **90**(11), pp. 1071-1075.

ROSE, G.D., K.L. FOSTER, V.L., SLOCUM AND J.G, LENHART, July 1984. Drag Reduction and Heat Transfer Characteristics of Viscoelastic Surfactant Formulations, *"Drag Reduction in Fluids Flow," Proc. 3rd Int, Conf, on Drag Reduction, R.H.J. Sellin and R.T. Moses, eds.* July 1984.

SASAKI, S., 1991. Drag Reduction Effect of Rod-Like Polymer-Solutions .1. Influences of Polymer Concentration and Rigidity of Skeletal Back Bone. *Journal of the Physical Society of Japan,* **60**(3), pp. 868-878.

SASAKI, S., 1991. Drag Reduction Effect of Rod-Like Polymer-Solutions .2. Comparison between Microgel and Linear Type Polyions. *Journal of the Physical Society of Japan,* **60**(8), pp. 2613-2618.

SAVINS, J.G., 1967. *Rheologica Acta,* **6**, pp. 323-330.

SMITH, R.E. and TIEDERMAN, W.G., 1991. The Mechanism of Polymer Thread Drag Reduction. *Rheologica Acta,* **30**(2), pp. 103-113.

TANFORD, C., 1972. Micelle Shape and Size. *Journal of Physical Chemistry,* **76**(21), pp. 3020-&.

TIEDERMAN, W.G., LUCHIK, T.S. and BOGARD, D.G., 1985. Wall-Layer Structure and Drag Reduction. *Journal of Fluid Mechanics,* **156**(JUL), pp. 419-437.

TRABELSI, S., RASPAUD, E. and LANGEVIN, D., 2007. Aggregate formation in aqueous solutions of carboxymethylcellulose and cationic surfactants. *Langmuir,* **23**(20), pp. 10053-10062.

VANAPALLI, S.A., ISLAM, M.T. and SOLOMON, M.J., 2005. Scission-induced bounds on maximum polymer drag reduction in turbulent flow. *Physics of Fluids,* **17**(9), pp. 095108.

VIRK, P.S., 1975. Drag Reduction Fundamentals. *AICHE Journal,* **21**(4), pp. 625-656.

VIRK, P.S. and  WAGGER, D.L., 1990. Aspects of Mechanisms in Type B Drag Reduction. In: A. GYR, ed, Springer Berlin Heidelberg, pp. 201-213.

VIRK, P., MERRILL, E., MICKLEY, H., SMITH, K. and MOLLOCHR.EL, 1967. Toms Phenomenon - Turbulent Pipe Flow of Dilute Polymer Solutions. *Journal of Fluid Mechanics,* **30**, pp. 305-&.

VISSMANN, K. and BEWERSDORFF, H.W., 1990. The Influence of Pre-Shearing on the Elongational Behavior of Dilute Polymer and Surfactant Solutions. *Journal of Non-Newtonian Fluid Mechanics,* **34**(3), pp. 289-317.

VLEGGAAR, J., & TELS, M., 1973. Drag reduction by polymer threads. *Chem. Eng. Sc.,* **28**, pp. 965-968.

WEI, T. and WILLMARTH, W., 1992. Modifying Turbulent Structure with Drag-Reducing Polymer Additives in Turbulent Channel Flows. *Journal of Fluid Mechanics,* **245**, pp. 619-641.

WHITE, C.M. and MUNGAL, M.G., 2008. Mechanics and prediction of turbulent drag reduction with polymer additives. *Annual Review of Fluid Mechanics,* **40**, pp. 235-256.

ZAKIN, J.L. and LUI, H., 1983. Variables Affecting Drag Reduction by Nonionic Surfactant Additives. *Chemical Engineering Communications,* **23**(1-3), pp. 77-88.

ZAKIN, J. and BEWERSDORFF, H., 1998. Surfactant drag reduction. *Reviews in Chemical Engineering,* **14**(4-5), pp. 253-320.

ZAKIN, J., MYSKA, J. and CHARA, Z., 1996. New limiting drag reduction and velocity profile asymptotes for nonpolymeric additives systems. *AICHE Journal,* **42**(12), pp. 3544-3546.